

# Final Report, July, 2000

## Earthquake Hazard of the Santa Barbara Fold Belt, California

NEHRP Award #99HQGR0081

SCEC Award #572726

E. A. Keller (PI) [keller@magic.ucsb.edu](mailto:keller@magic.ucsb.edu)

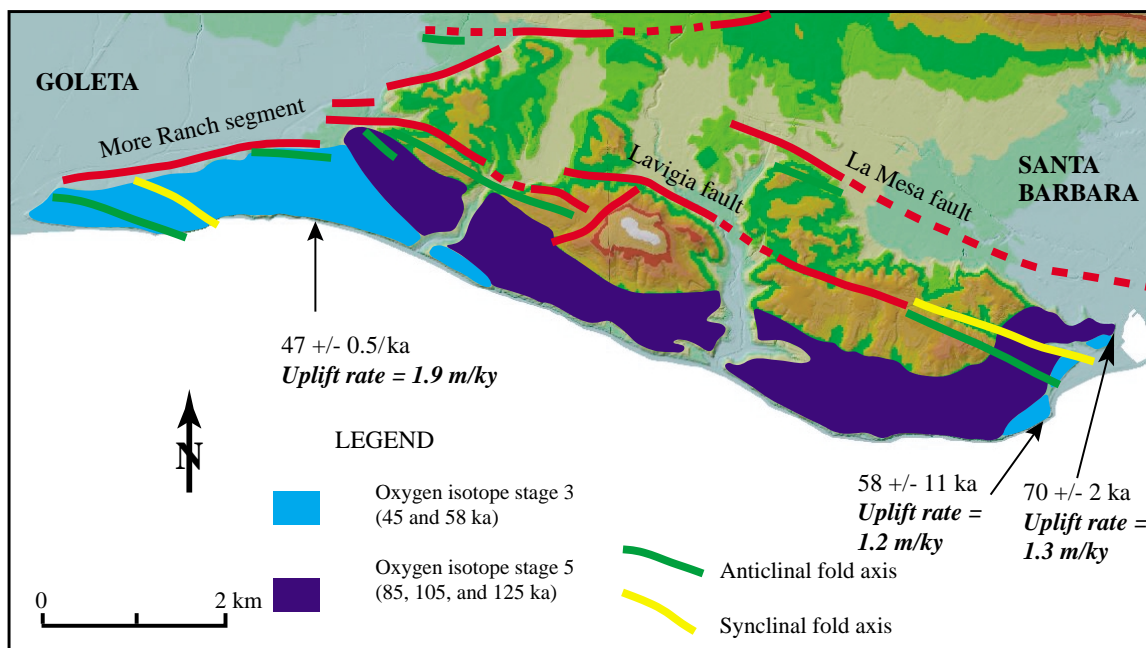
L. D. Gurrola

Institute for Crustal Studies

UC Santa Barbara

Santa Barbara, California 93106

(805) 893-4207



Research supported by the U.S. Geological Survey (USGS), Department of Interior, under USGS award 1434-HQ-GR-02978. The views and conclusions contained in this document are those of the authors and should not be interpreted as necessarily representing the official policies, either expressed or implied, of the U.S. government. Parts of this report are from papers and abstracts published as part of the work for the project, and parts are from the Ph.D. dissertation of Larry Gurrola, in preparation.

## TABLE OF CONTENTS

	<u>Page</u>
Technical Abstract	4
Non-Technical Abstract	6
1.0 Introduction	7
1.1 Objectives	8
1.2 Methods Of Study	8
2.0 Tectonic Setting of the Western Transverse Ranges	11
3.0 Tectonic Framework	12
4.0 Historic Seismicity	13
5.0 Stratigraphy	15
5.1 Pre-Quaternary Stratigraphy	15
5.2 Quaternary Stratigraphy	16
5.21 Santa Barbara Formation	16
5.22 Casitas Formation	17
5.23 Late Pleistocene Marine Terrace Deposit	18
5.24 Late Pleistocene Alluvial and Fanglomerate Units	18
5.25 Holocene Alluvial, Fluvial and Colluvial Units	19
6.0 Tectonic Geomorphology of Marine Terraces	19
6.1 Marine Terraces	19
6.2 Marine Terrace Morphology	21
6.3 Marine Terrace Chronology and Rates of Uplift	21
6.4 Emergent Marine Terraces	23
6.41 UCSB Terrace	23
6.42 Ellwood Terraces	25
6.43 More Mesa Terraces	27
6.44 La Mesa Terraces	29
6.45 Montecito Terraces	33
6.46 Summerland Marine Terraces	33
7.0 Tectonic Geomorphology and Paleoseismicity of Folds and Faults	35
7.1 Fault Segmentation	36
7.2 Mission Ridge Fault System (MRFS)	37
7.21 More Ranch Segment	39
7.211 Ellwood Fold	40
7.212 UC Santa Barbara-Isla Vista	47
7.213 More Mesa-Hope Ranch Anticlines	49
7.22 Mission Ridge Segment	49
7.221 Mission Ridge	49
7.222 Montecito Anticline	50
7.3 Northwest-Striking Faults	50
7.31 Goleta Valley Anticline	51
7.32 La Mesa Anticlines	51
7.33 Santa Barbara Cemetery (Zoo) Anticline	53

7.34 Ortega Hill Anticline	53
7.35 Loon Point Fault and Propagation Fold	54
7.351 Paleoseismic Evaluation	56
8.0 Style of Quaternary Folding	57
9.0 Lateral Propagation of Folds: Geomorphic Analysis	58
10.0 Hypothesis of Tectonic Extrusion	60
11.0 Earthquake Magnitudes	64
12.0 Conclusions	66
13.0 Acknowledgments	67
14.0 Bibliography	68
15.0 References Cited	70
Tables 1-5	following text
Figure 1-25	following tables

## TECHNICAL ABSTRACT

The Santa Barbara Fold Belt (SBFB) is a linear zone of active folds and (mostly) blind faults on the coastal piedmont and in the Santa Barbara Channel. The fold belt is characterized by several flights of emergent late Pleistocene marine terraces uplifted and preserved on the flanks of active, anticlinal folds. At several locations along the fold belt, the first emergent marine terrace is age-dated through methods that include uranium-series analysis of sampled terrace corals,  $^{14}\text{C}$  ages of terrace shells and detrital charcoal, optically stimulated luminescence of terrace sands, and oxygen isotopic signatures of terrace mollusks. These age results are integrated to establish terrace chronology and estimate rates of surface uplift.

The first emergent marine terraces in the western SBFB are approximately 45 ka and correlated to the oxygen isotope stage 3 sea level highstand. Rates of local surface uplift are estimated to be approximately 2 m/ky. Marine terraces preserved in the eastern fold belt range in age from 70 ka to 105 ka and correlate to the oxygen isotope stage 5 sea level highstands. Rates of local surface uplift are estimated to be approximately 1 m/ky.

The onshore portion of the SBFB contains a number of active folds with buried reverse faults. The largest structure is the Mission Ridge Fault System (MRFS) with a vertical slip rate of approximately 0.3 m/ky. Paleoseismic studies of the MRFS at Ellwood Mesa suggest there have been several earthquakes during the late Pleistocene. We expect that the MRFS has an average return period of approximately 3 ky. Reverse faults in the onshore portion of the SBFB are capable

of producing earthquakes of **M<sub>W</sub>** 6 to 6.5. If several segments of the MRFS were to rupture simultaneously, an earthquake of approximately 7.0 is possible. A repeat of the 1925 **M<sub>W</sub>** 6.8 Santa Barbara earthquake would likely inflict several hundred million to a billion or more dollars of property damage while inflicting several to several tens of deaths.

## **NON-TECHNICAL ABSTRACT**

The Santa Barbara area exhibits characteristic hills that are formed as the result of faulting. These hills along the coastal area have numerous ancient, raised beaches preserved on them. These beaches contain shells that are used to determine the age of the beach deposit. The estimated ages are used to determine the rate of uplift of the Santa Barbara coastal area.

The Santa Barbara area has ancient beaches that occur above the modern beach that range in age from 45,000 to 105,000 years. The uplift rate of the Santa Barbara area is approximately 1 to 2 **m/ky**. This rate is ten times greater than previously estimated.

The Santa Barbara urban corridor is in an area of known seismicity with an earthquake hazard similar to that of the cities of Ventura and Los Angeles. Faults on the onshore portion of the Santa Barbara Fold Belt are capable of producing earthquakes with magnitudes 6 to 6.5 and some faults offshore may produce earthquakes with magnitudes in excess of 7. Damages from an earthquake similar to the 1925 event which devastated downtown Santa Barbara would today cause several hundred million to a billion or more dollars of property damage with several to several tens of deaths.

## **1.0 INTRODUCTION**

The east-west trending Santa Barbara Fold Belt (SBFB) is a linear belt of active folds located on the south flank of the western Transverse Ranges on the coastal piedmont and offshore in the Santa Barbara Channel (Figure 1). Topographically well-expressed folds are the result of mostly blind, active reverse and thrust faulting. Faulted anticlines form linear hills. Intervening low areas such as the sites of the City of Santa Barbara and Goleta Valley are faulted synclines. Coastal erosion has exposed the stratigraphy at several of the anticlines. From Carpinteria west to Ellwood a prominent sea cliff characterizes locations of anticlines and synclines are areas where prominent sea cliffs are not present. Thus the gross geomorphology of the Santa Barbara area is clear; where linear hills are encountered, these landforms are actively growing anticlines being uplifted in response to reverse faulting, often buried. On the other hand, low lying areas that comprise salt marshes and sloughs are faulted synclines, characterized by subsidence. This morphology is clearly shown on the digital elevation models used as the base map for Figures 1 and 2.

The onshore fold belt contains about 12 active and potentially active blind faults with associated surficial folds termed seismic sources (Figure 2 and Table 1). About 10 potential seismic sources were discovered as part of this seismic hazard assessment. Active folding due to blind reverse or thrust faulting in the SBFB presents a significant earthquake hazard to the 200,000 people living in Santa Barbara area (Figure 3).

## ***1.1 OBJECTIVES***

Objectives of the tectonic geomorphic study of marine terraces are to: 1) map the distribution of emergent marine terraces and associated paleo-shoreline landforms; 2) estimate the elevation of shoreline angles; 3) develop an understanding of terrace stratigraphy in order to identify fossil sites and collect samples including fossil solitary corals and mollusks for chronological analysis; 4) establish late Pleistocene chronology by independent analyses of numerical data through: uranium series analysis of solitary corals; radiocarbon analysis of terrace fossils and organic detritus; optically stimulated luminescence (OSL) of terrace sands, and oxygen isotope signatures of terrace mollusks; and 5) calculate rates of local surface uplift based on terrace chronology.

The objectives of the earthquake hazard assessment of the SBFB are to: 1) identify potential seismic sources; 2) estimate rates of late Pleistocene faulting, folding and uplift; 3) evaluate the style of late Pleistocene deformation; and 4) estimate the earthquake hazard of the SBFB.

## ***1.2 METHODS OF STUDY***

The geomorphic study of late Pleistocene, emergent marine terraces of the SBFB includes photogeologic and geomorphic mapping of marine terrace landforms. The terrace landforms were mapped on 1928 (1:18,000 scale) stereo aerial photographs. Commonly, the associated shoreline angle of a particular wave-cut platform is buried and only overlying deposits are exposed in sea

cliff and trench exposures, allowing for 3-D mapping, estimation of terrace strata thickness, and collection fossil deposits.

Terrace fossils are rare but most often preserved in the basal conglomerate or in overlying fossiliferous units. Terrace fossil deposits are identified in sea cliff exposures at Ellwood, UC Santa Barbara, More Mesa, Santa Barbara Point, and Santa Barbara City College. Fossil deposits were sampled from sea cliff exposures in order to collect solitary corals for uranium series age-dating and mollusks for oxygen isotopic analysis.

Solitary corals (*Balanophyllia elegans*) are believed to be nearly closed systems with respect to input of uranium from ocean waters following the death of the organism, and therefore provide opportunity for age estimation using uranium-series dating. Fossil mollusks, specifically *Olivella biplicata*, record the oxygen isotope signatures of paleo-ocean temperatures for the sea level highstand at which the terrace formed.

Solitary corals were collected from fossil deposits from the first emergent terraces at UC Santa Barbara and Santa Barbara City College. Initial  $^{234}\text{U}/^{238}\text{U}$  ratios of the coral samples from the SBFB were compared to modern day seawater to confirm that there was not an influx of secondary uranium. X-ray diffraction analyses of the samples was used to determine if there was alteration of the original aragonite composition. Terrace corals at both sites were determined to be more than 99% aragonite with no secondary calcite detected. The corals were prepared and analyzed at the Isotope Laboratory, Department of Geological Sciences, California Institute of Technology. The corals provide numerical ages for the first

emergent terraces at UC Santa Barbara (UCSB) and Santa Barbara City College (SBCC) allow the correlation of the terraces to late Pleistocene sea level highstand the terraces are assumed to have formed at.

Terrace fossil deposits rarely contain solitary corals; therefore alternative age-dating methods were employed. These include radiocarbon analyses of terrace fossil mollusks and detrital charcoal.

Additionally, terrace sand samples were collected for optically stimulated luminescence (OSL) measurements of terrace potassium feldspar and quartz grains. The OSL data yield maximum ages of deposition of the sands for the UCSB, More Mesa, Santa Barbara Point, Santa Barbara Cemetery, and Loon Point terraces.

Fossil mollusk shells were collected at the Ellwood, UC Santa Barbara, More Mesa, Santa Barbara Point, and SBCC terraces for oxygen isotope analysis (Trecker, 1999). The isotopic signatures are associated the late Pleistocene oxygen isotopic sea level curve and assist in the correlation of terraces from location to location.

Earthquake hazard assessment of the SBFB includes photogeologic, geologic, and geomorphic mapping of Quaternary strata including emergent, late Pleistocene marine terraces preserved on limbs of uplifting, anticlinal folds. The geology of topographically well-expressed folds are exposed in natural and trench exposures, allowing for 3-D mapping, to determine fold geometry, morphology and style of folding.

Review of geologic and geotechnical data and consulting reports were conducted to incorporate unpublished data. Numerous

reports involved trench pit excavations for geotechnical, environmental remediation, or fault investigations that revealed both deformed and undeformed Quaternary strata including marine terrace units. During the period of this study (mid- to late 1990s), direct observations and data acquisition at trench pit or borehole drilling investigations were completed to evaluate sites for paleoseismic study. Site-specific investigations include fault-trench excavations along the forelimbs of the Ellwood and Loon Point anticlines to evaluate paleoseismicity of the Mission Ridge fault system and Loon Point fault. Characterization of seismic potential is determined for on land faults in the SBFB based on the rates of deformation from paleoseismic study and fault geometry using method of Wells and Coppersmith (1994).

## **2.0 TECTONIC SETTING OF THE WESTERN TRANSVERSE RANGES**

Shortening across the western Transverse Ranges is the result of strain partitioning associated with right-slip convergence at the "Big Bend" of the San Andreas fault (SCEC, 1995). North-south convergence of about 6 m/ky produces surficial folding formed by blind, reverse (and thrust) faulting (Suppe, 1997).

The SBFB is a continuation of the Ventura Fold Belt. The belt is formed on the south limb of the Santa Ynez anticlinorium, and is bounded north and south by the strike-slip Santa Ynez and Santa Cruz Island faults, respectively. Namson and Davis (1992) argue that the anticlinorium is related to a low-angle, north-dipping ramp of a detachment or decollement at 10-12 km depth. If this hypothesis is

correct, then slip on the decollement is transferred to the north-verging structures (backthrusts) on the coastal piedmont (including offshore structures) of the SBFB. Late Pleistocene to Holocene deformation and seismic activity is concentrated on structures south of the Santa Ynez fault on the coastal piedmont and offshore in the Santa Barbara Channel.

### **3.0 TECTONIC FRAMEWORK**

The west-trending Santa Ynez anticlinorium forms the principal topographic feature of the SBFB. The tectonic framework of the fold belt on the coastal piedmont consists of three sets of faults: 1) west-striking, oblique reverse MRFS; 2) northwest-striking oblique reverse faults; and 3) northeast-striking lateral tear faults (Figures 1 and 2).

Segments of the west- and northwest striking faults are defined by geometric, geomorphic and structural characteristics. Segment boundaries of the west and northwest-striking faults are defined by abrupt changes in geometry, geomorphic expression, structural style of deformation, and termination of folds. These segment boundaries coincide with north-east striking faults termed cross faults (Gurrola and Kamerling, 1996). These subtly expressed cross faults may behave as tear faults during coseismic rupture.

Subsurface petroleum data indicates vertical displacement of Tertiary units for the MRFS (Olson, 1982; Jackson and Yeats, 1982). However, the mostly blind MRFS produces folds in the overlying Pleistocene sedimentary units. These sedimentary units deform as fault-propagation folds with hanging wall anticlines (or monoclines)

and footwall synclines. In some cases, subsidiary structures such as bending moment faults have propagated up through the fore- and backlimbs of the anticline or syncline such as the Ellwood and the Mission Ridge anticlines.

#### **4.0 HISTORIC SEISMICITY**

Historic seismicity in the SBFB is shown on Table 2; most seismic activity is located south of the Santa Ynez Range. A seismic map of the probability of seismic shaking for southern California, based upon historic seismicity, and produced by the Southern California Earthquake Center suggests the Santa Barbara area can expect 3 to 4 earthquakes per century with shaking that will exceed 0.2 g, the level of activity where damage to older buildings begins.

The historic record of the Santa Barbara area dates back to the establishment of the missions Purisma and Santa Barbara during the late 18th century (Table 2). Since the early 19th century, three large earthquakes have occurred in the SBFB including the 1812, the 1925, and the 1978 events (Sylvester and Mendes, 1981). Seismologic data for the 1812 and 1925 events are scarce as seismograph stations were non-existent for the 1812 rupture and only a few were operating in 1925. Those seismograph stations determine the location of the epicenter for the 1925 rupture within a 60 km radius.

The 1812 earthquake is the earliest of the three earthquakes, and probably had a magnitude of about **M<sub>W</sub>** 7. The 1812 earthquake produced regional damage throughout northern and southern Santa Barbara County. The seismic source was most likely offshore,

perhaps on the offshore Oak Ridge, the North Channel Slope, or the Pitas Point faults.

A large earthquake near the City of Santa Barbara on 26 June, 1925 produced extensive damage to the downtown and surrounding areas (Willis, 1925). Estimated modified Mercalli (MM) intensities were approximately MM VII in the lower, southeast downtown area, whereas maximum intensities were approximately MM VIII-IX at the La Mesa hills (Olsen, 1972).

Preceding the 1925 event, voluminous amounts of petroleum were observed along Santa Barbara beaches and moderate-sized foreshocks began at 3:27 a.m. The main shock followed at 6:42 a.m. and lasted for a duration of about forty seconds (Willis, 1925). Olsen and Sylvester (1975) believe that the intensity of shaking indicates a maximum magnitude of M6.3 for the main earthquake, however, **Stein** and **Hanks** (1998) calculate a moment magnitude of **Mw** 6.8 for the earthquake. The fault that ruptured in 1925 has not been identified, but either offshore or onshore source is possible based on intensity of shaking.

Additional evidence for the estimated **Mw** 6.8 (**Stein** and **Hanks**, 1998) is the presence of liquefaction at Goleta Beach. Large waves from storms in the winter of 1997-98 excavated a 3 m high beach scarp at Goleta Beach. The beach scarp exposed 2 to 3 m of convoluted, artificial fill with pervasive soft sediment deformation. The wavelengths of strata convolutions and spacing of vertical dish (dewatering) structures range from one to three meters. These liquefaction features form the lower 1 to 2 m of the scarp and are truncated by overlying, undeformed 1 m thick artificial fill.

Fragments of a Coca-Cola bottle collected from the deformed artificial fill were established to have been manufactured either between 1916 to 1925 or 1945 to 1960. The undeformed, overlying fill is most likely emplaced after 1945, therefore the bottle was most likely manufactured between 1916 and 1925 indicating a pre-1925 age for the deformed artificial fill. The most likely earthquake that produced shaking intensities to produce liquefaction features is the 1925 Santa Barbara earthquake.

The 1978 **Mw** 5.9 Santa Barbara earthquake produced local, moderate damage in the area of Goleta. Following the 1978 event, numerous seismograph stations were installed throughout the Santa Barbara region to gather aftershock data. However, the location and geometry of the epicenter remain in dispute due to disagreement among seismologists (e.g., Corbett and Johnson, 1982; Yeats and Olson, 1984). Yeats and Olson (1984) believe that the 1978 **Mw** 5.9 Santa Barbara earthquake occurred on a south-dipping reverse fault, whereas Corbett and Johnson (1982) argue for a nearshore, low-angle, north-dipping fault. Localized damage in the UC Santa Barbara campus area supports the epicenter location of Corbett and Johnson (1982).

## **5.0 STRATIGRAPHY**

### **5.1 PRE-QUATERNARY STRATIGRAPHY**

Pre-Quaternary strata of the SBFB consist of a section of Eocene through Pliocene rocks that were deposited in a continental margin setting. These rocks include from oldest to youngest:

Coldwater Sandstone; Sespe Formation; Vaqueros Sandstone; Rincon Formation; Monterey Formation; and Sisquoc Formation (Table 3). The Sespe, the Rincon, the Monterey, and the Sisquoc Formations typically form the rocks of the mountain slopes and basement rocks of the coastal piedmont. In some cases, these rocks are locally uplifted in the core of anticlines and along faults.

## **5.2 QUATERNARY STRATIGRAPHY**

Quaternary strata of the SBFB consist of a sequence of Pleistocene and late Pleistocene marine and non-marine strata. The Pleistocene sequences are deposited on pre-Quaternary strata on the coastal piedmont (Table 3). The Quaternary units from oldest to youngest include: Santa Barbara Formation; Casitas Formation; and late Pleistocene-Holocene marine terrace deposits; fanglomerate deposits; and other alluvium.

### **5.21 *Santa Barbara Formation***

The Santa Barbara Formation is a transgressive marine sandstone with minor units of conglomerates, siltstones and claystones. The Santa Barbara Formation is a basal Quaternary unit with poor age control. However, it overlies the 1.2 ma Bailey Ash in Ventura (Izett et al., 1974; Olson, 1982). Thickness of the Santa Barbara Formation ranges from 150 m to 625 m thick (Olson, 1982; Dibblee, 1988).

Paleomagnetic analyses of the Quaternary Santa Barbara and overlying Casitas Formations were conducted to determine magnetic polarity for relative age-dating and degree of deformation

(rotation). Exposed units in Goleta Valley and La Mesa anticlines were sampled for reconnaissance paleomagnetic analyses to determine remnant magnetization polarization (Gurrola, in preparation).

Based on the maximum age for the Santa Barbara Formation of 1.2 ma, paleomagnetic results indicate if deposition occurred during the Matayama (1.2 ma to 790 ka) or Bruhnes (post 790 ka to late Pleistocene) epoch by determining if polarization is reverse (Matayama) or normal (Bruhnes). Paleomagnetic results yield normally magnetized sediments of the Santa Barbara Formation in both the Goleta Valley and La Mesa folds, and are therefore, younger than 790 ka. Clockwise, rotations range from 0° to approximately 30° and are the result of localized rotational deformation near reverse faults with a minor component of sinistral slip (Gurrola, in preparation).

## **5.22 *Casitas Formation***

The mostly non-marine Casitas Formation is the result of alluvial deposition on the coastal piedmont in the middle to late Pleistocene. The rocks typically range from pebbly sandstones to gravel and boulder conglomerates. The basal Casitas Formation grades into regressive units of nearshore marine sandstones and siltstones and is exposed in the sea cliff Loon Point at Summerland.

Stratigraphic relations suggest the Casitas Formation is younger than the underlying Santa Barbara Formation (Olson, 1982). Paleomagnetic analysis of the basal section of the Casitas Formation sampled from the Loon Point and Ortega Hill folds

indicate normal remnant magnetization. These paleomagnetic results are in agreement with results from the underlying Santa Barbara Formation and confirm Casitas deposition occurred during the Bruhnes epoch (post 790 ka). The Casitas Formation is older than the age of the overlying, late Pleistocene marine terrace and alluvial units and most likely is about 500 to 125 ka, and represents a series of Pleistocene aggradation events.

### ***5.23 Late Pleistocene Marine Terrace Deposits***

Wave-cut platforms in the SBFB are eroded on Pre-Quaternary strata such as the Sisquoc and the Monterey Formations and Pleistocene Santa Barbara and Casitas Formations. Wave-cut platforms are commonly overlain by a thin, basal cobble to pebble conglomerate (boulder line) with overlying terrace deposits ranging from a 2 m to 5 m thick section of marine sands with an aeolian cap.

Terrace fossils preserved in the conglomerate or in locally, fossiliferous units were sampled in order to obtain solitary corals for uranium series age-dating analysis. Two solitary corals from the UC Santa Barbara terrace and the Santa Barbara City College terrace were analyzed and yield estimated ages of 47 +/- 0.5 and 70 +/- 2.0 ky, respectively (Table 4).

### ***5.24 Late Pleistocene Alluvial and Fanglomerate Units***

Late Pleistocene fanglomerate deposits are generally coarse boulder to gravel conglomerates deposited as alluvial fans. Alluvial fan deposition on the coastal piedmont occurred on south-flowing

streams from the Santa Ynez Mountains. Alluvial deposits generally range from silt-sandstone to cobble-gravel conglomerate, which may overlie marine terrace deposits. The ages of late Pleistocene alluvial and fanglomerate units are not known, but are younger than underlying Casitas Formation, and therefore are most likely mid to late Pleistocene in age.

### ***5.25 Holocene Alluvial, Fluvial and Colluvial Units***

Holocene alluvium typically consists of clay rich, silt-sandstone and conglomerate units that cap late Pleistocene marine terrace units. An alluvial unit that caps the Loon Point fault terrace (discussed in a later section) is radiocarbon age-dated at 3,980 +/- 40 RCYBP (Table 4). Holocene colluvial units generally consist of brecciated, matrix- to clast-supported conglomerates and are deposited at the base fold, fault, and sea cliff scarps. Holocene fluvial units typically consist of clay, silt, and sand, and gravel to cobble conglomerate units deposited along active south-flowing stream channels on the coastal piedmont.

## **6.0 TECTONIC GEOMORPHOLOGY OF MARINE TERRACES**

### ***6.1 MARINE TERRACES***

Several flights of terraces are preserved in the SBFB. They are assumed to reflect the formation at interglacial paleo-sea level highstands in conjunction with tectonic uplift (Matthews, 1973; Kern, 1977; Lajoie et al., 1982). Emergent marine terraces originate as eroded, wave-cut platforms forming unconformities on the

underlying bedrock. Commonly, as tectonic uplift occurs, a thin veneer of (regressive) marine sands are preserved on the marine platform producing an unconformity which is subsequently covered by alluvial and colluvial sediments.

Late Pleistocene sea level highstands are times when wave-cut platforms and sea cliffs at landward edges of marine platforms are assumed to form. The intersection of the paleo-sea cliff with the wave-cut abrasion platform defines the terrace shoreline angle (Lajoie et al., 1979). The shoreline angle approximates the position of paleo-sea level within one or two meters of mean (high) sea level for that platform level and is the preferred reference to paleo-sea level. However, the shoreline angle is typically buried beneath beach deposits, sea cliff colluvium, and/or alluvium, and as a result the elevation of the shoreline angle is often an estimate.

Fluctuations in late Pleistocene sea levels are well studied for the last 125 ka, and sea level highstands are correlated to coral reef terraces and deep-sea oxygen isotope records (Bloom et al., 1974; Chappell, 1983; Chappell and Shackleton, 1986; Chappell et al., 1996). First emergent terraces of known age are related to the revised paleo-sea level curve by Chappell et al. (1996). A rate of uplift for a particular site is calculated based on the elevation of the shoreline angle of the platform, and the numerical age of the marine terrace, and the elevation of the paleo-sea level highstand of the assumed age of the platform. Muhs et al. (1994a) believe that paleo-sea levels for substages 5a (80 ka) and 5c (105 ka) were closer to present day sea level. If this is the case, then the surface uplift rates

calculated in this study are maximum with respect to known sea level curves.

## ***6.2 MARINE TERRACE MORPHOLOGY***

Marine terraces are some of the most obvious landforms on the Santa Barbara coastal piedmont. Elevations of wave-cut platform shoreline angles range from approximately 25 m to greater than 200 m. Expression of paleo-shoreline angles are relatively poor, but associated paleo-sea cliffs often form moderate to well-expressed scarps. Paleo-shorelines are often laterally discontinuous across streams that dissect terraces, deformed by folds, and/or buried beneath alluvial fan and colluvial deposits (Figure 4).

A sequence of terraces at a specific site is discussed with respect to the first emergent terrace, which is at the seaward edge. The first emergent terraces at Ellwood, UC Santa Barbara, Santa Barbara Point, Santa Barbara City College, More Mesa, Santa Barbara Cemetery, and Summerland have estimated ages based upon considering several potential chronological methods.

## ***6.3 MARINE TERRACE CHRONOLOGY AND RATES OF UPLIFT***

Establishment of the marine terrace chronology is fundamental in order to estimate the vertical rate of surface uplift. Age dating of terrace fossil fauna directly overlying the abrasion platform determines a minimum age of platform formation. Commonly along the California coast, first emergent marine terraces are formed during stage 5 (80 ka to 125 ka) paleo-sea level highstands. However, terraces formed during the substage 3a (45 ka) paleo-sea

level highstand are present along the Santa Barbara and Ventura coasts (Lajoie et al., 1982; Gurrola et al., 1997a,b; 1996). Presence of isotope stage 3 terraces suggests a relatively high rate of surface uplift exceeding 1 m/ky.

In order to numerically age-date marine terraces, it is preferable to locate terrace fossil sites, collect solitary corals, and date the corals by uranium-series analysis (Muhs et al., 1992 and 1994b). Marine terrace chronology is then established using the TIMS method (Chen et al., 1986) of uranium series analysis.

The estimated minimum age of the marine terrace allows for assignment to an oxygen isotopic stage and determination of the associated paleo-sea level relative to modern day sea level. Mapping and estimation of the elevation of the shoreline angles of terraces of known ages provide the data necessary to calculate amounts of vertical surface uplift and styles of vertical deformation.

Non-marine, colluvium and alluvium often obscure the shoreline angle and the elevation is determined from shallow subsurface data or from sea cliff exposures. Once the elevations of shoreline angles are estimated, correlation of undated, higher (or lower) flights of terraces to oxygen isotopic stage and sea level highstands can be accomplished using the method outlined by Bull (1985). Because terraces are discontinuous in the SBFB, it is necessary to correlate terraces of known age to those of unknown age across changes in topography and change of structure (Figure 4). Adjacent flights of terraces of known and unknown age are correlated by several methods including numerical age (u-series,

carbon 14, OSL) and isotopic signatures of fossils (Trecker et al., 1998).

Solitary coral *Balanophyllum elegans* was analyzed from two marine terraces in the SBFB. A terrace coral was sampled from the Isla Vista terrace and one was obtained from a fossil collection at UC Santa Barbara. The coral from the UC Santa Barbara fossil collection was sampled by Lorenzo Yates from the Santa Barbara City College terrace at a location, immediately east of Point Castillo, formerly named Bathhouse Beach. U-series analyses age-date the Isla Vista (UC Santa Barbara) at  $47 \pm 0.5$  ka and Santa Barbara City College (Bathhouse Beach) at  $70 \pm 2$  ka (Table 4) (Gurrola et al., 1997a; 1998).

Radiocarbon and OSL age-dates compliment the uranium series data for terraces where solitary corals were not found. Radiocarbon and OSL samples were obtained from the Loon Point, Santa Barbara Cemetery, Santa Barbara Point, Santa Barbara City College, and UC Santa Barbara terraces (Table 4).

## ***6.4 EMERGENT MARINE TERRACES***

### ***6.41 UCSB Terrace***

The first emergent marine terrace at UCSB extends from Devereaux Slough to Goleta Slough and is bounded by the More Ranch fault to the north and the Coil Oil Point fault to the south (Figure 5). A terrace fossil assemblage is exposed on the sea cliff at Isla Vista beach on the first emergent UCSB marine terrace (Figure

5). The fossil site was sampled and a solitary coral obtained for uranium series and radiocarbon analyses.

The well-preserved, fossil solitary coral *Balanophyllia elegans* was collected and analyzed by X-ray diffraction. The X-ray diffraction analysis of the coral determined that the shell material was entirely aragonite and was not re-crystallized. The fossil coral was then uranium-series analyzed and determined to have an initial  $^{234}\text{U}/^{238}\text{U}$  ratio similar to that of modern day seawater (Chen et al., 1986). The UCSB terrace coral yielded a uranium-series age of  $47 +/ - 0.5$  ka and a radiocarbon age of  $43,400 +/ - 800$  RCYBP (Table 4).

Terrace sands were sampled at the Isla Vista fossil site to measure potassium feldspar grains for optically simulated luminescence (Spencer and Owen, 1999) (Figure 5). OSL measurements of the terrace sands yield age an estimate of approximately  $40 +/ - 0.3$  ka (Table 4).

Oxygen isotopic signatures of terrace mollusks (*Olivella biplicata*) sampled from the fossil site indicate a cool paleo-ocean temperature (Trecker et al., 1998; Trecker, 1999) which is consistent with the numerical ages from uranium-series, radiocarbon, and OSL analysis. Therefore the UCSB terrace is assigned to the isotope substage 3a paleo-sea level highstand at approximately 45 ka.

The paleo-shoreline associated with the UCSB terrace is buried on the footwall of the More Ranch segment. The maximum observed elevation of the marine platform is approximately  $14.0 +/ - 0.5$  m yields a calculated, minimum total vertical surface uplift of 79 m

and a local vertical surface uplift rate of  $1.7 \pm 0.1$  m/ky (Figure 6). This local uplift rate is the result of folding and faulting on several, adjacent structures including the More Ranch segment to the north and the Coal Oil Point fault to the south (Figure 1).

#### ***6.42 Ellwood Terraces***

The Ellwood Mesa marine terrace is the first emergent terrace west of Devereaux Slough. The terrace forms a continuous surface to the west margin of study (Figure 2). At Devereaux Creek, the marine terrace is anticlinally folded on the hanging-wall of the More Ranch segment, whereas to the west, the terrace is faulted and vertically offset in a sea cliff exposure. Although the Ellwood terrace is deformed across the More Ranch segment of the MRFS, the marine abrasion platform is mappable across the fault.

Presently the Ellwood terrace strandline is poorly preserved north of the More Ranch segment (Figure 5). Early (1928) aerial photographs reveal that the strandline is moderately expressed and is mappable across the Ellwood terrace westward to where it trends offshore, west of the fault exposure.

The strandline elevation of the Ellwood terrace is approximately  $23.5 \pm 1.5$  m. Detrital charcoal sampled from the basal terrace unit yielded a radiocarbon age of  $47 \pm 1.5$  ka and allowed for correlation to the oxygen isotope substage 3a and the UCSB terrace (Figure 6; Table 4). Oxygen isotope signatures of fossil mollusks indicate a cool paleo-ocean water temperature (Trecker et al., 1998) which is consistent with substage 3a. Based on the strandline elevation, the amount of total, vertical uplift for substage

3a is approximately 65 m (Chappell et al., 1996) yielding a calculated local rate of vertical surface uplift of approximately 1.9 +/- 0.1 m/ky (Figure 6).

Higher flights of terraces are preserved at 31 +/- 1.5 m, 39 +/- 1.5 m, 44 +/- 1.5 m, 63 +/- 1.5 m, and 131 +/- 1.5 m and in the Dos Pueblos area of Goleta (Figure 5). The shoreline angles associated with these terraces are moderately to poorly preserved and in places, buried by alluvium. To the west, the highest terrace (131 +/- 2.5 m) caps north-south trending ridges and to the east caps the crests of active folds. As a result this terrace is laterally discontinuous due to numerous deeply incised drainages, but by position appears to be the same marine terrace surface from Goleta Valley to the western study area. The terrace surfaces are mostly stripped with little or no marine terrace sediments preserved.

A prominent shoreline angle and associated paleo-sea cliff delineates the next lower (63 +/- 1.5 m) terrace (Figure 5). The well-preserved, east-west trending, paleo-sea cliff abruptly truncates north-south trending ridges, forming faceted spurs. This paleo-shoreline is mappable in Goleta where it decreases in elevation eastward to approximately 38 m and is buried beneath alluvium .

Based on a calculated uplift rate of 1.9 +/- 0.1 m/ky (Figure 6), and assuming a constant rate of uplift (Bull, 1985), the 44 +/- 1.5 m, 63 +/- 1.5 m, and 131 +/- 1.5 m terraces correlate to oxygen isotope substages 3c (58 ka) and 5a (71 ka or 81 ka). The shoreline angles at elevations of 31 m and 39 m probably result from strong local earthquakes and associated coseismic surface uplifts (2 to 4 m+) of the coastline. Alternatively, these strandlines

may be the result of temporary stabilization or hiatus of sea level fluctuations during sea level transgression or regression.

#### **6.43 More Mesa Terraces**

More Mesa is the most laterally continuous and well-expressed marine terrace in the SBFB (Figure 7). The More Mesa terraces are continuous from Las Positas west to Goleta Slough. More Mesa is located on the hanging wall of the More Ranch fault and the north margin is bounded by the More Ranch segment, which truncates several terrace shorelines.

The first emergent marine terrace is preserved on the axis of a Quaternary syncline and the terrace surface is tilted and down-warped to the north (Figure 7). The terrace forms a 4 km long and nearly 1 km wide surface. The shoreline angle of the first emergent terrace is buried due to the synclinal warping of the terrace and is the least discernible of all terraces.

A fossil locality previously unidentified was discovered on the first emergent terrace in a gully at a sea cliff re-entrant (Figure 7). The age of the terrace is estimated by radiocarbon dating of a pholad shell, optically stimulated luminescence of terrace sand grains, and correlation by isotopic signatures of mollusks.

A fossil pholad shell was sampled and obtained from a rock borehole in growth position. Initial SEM analysis determined that the shell material was unaltered aragonite. The shell yielded a  $^{14}\text{C}$  of 36,830 +/- 330 RCYBP (Table 4), however Voelker and others (1998) report a large fluctuation in the calibration of  $^{14}\text{C}$  ages between 32-34 ka. They determine a  $^{14}\text{C}$  age-offset (correction factor) of

approximately 5 +/- 1 ka for the pholad age which results in a calibrated  $^{14}\text{C}$  age of approximately 41,830 +/- 1,330 RCYBP.

Oxygen isotope signatures of fossil mollusks sampled from the More Mesa terrace indicate a cool paleo-ocean temperature signature correlating to the UCSB site (Trecker et al., 1998). Additionally, terrace sands were sampled at the fossil site for optically stimulated luminescence dating to estimate an age for potassium feldspar grains. The luminescence analysis estimated an age of 53 +/- 7 ka for terrace sands (Table 4). The error range does not differentiate between oxygen isotope substage 3a and oxygen isotope substage 3c. However, calibrated radiocarbon age of the fossil pholad and the isotopic signatures of the fossil mollusks, combined with the OSL age suggest the More Mesa terrace correlates to oxygen isotope substage 3a at 45 ka (Figure 6; Table 4). The estimated age of the More Mesa terrace is consistent with other terraces (i.e., Ellwood and Isla Vista-UCSB) uplifted on the hanging wall of the More Ranch fault.

Elevations of the first emergent and higher terrace strandlines are positioned at approximately 35 +/- 0.5 m, 44 +/- 1.5 m, 50 +/- 1.5 m, 59 +/- 1.5 m, and 75 +/- 1.5 m (Figure 7). Wavecut platforms, often partially stripped of sediment are present at elevations of 104 m and 182 m, capping the Lavigia anticline, and their strandlines are absent. Based on the method by Bull (1985), the 38 m, 44 m, 50 m, and 59 m terrace strandlines correlate to the oxygen isotope substages 3a (36 ka to 52 ka). The fourth terrace strandline (59 m) does not correlate to any paleo-sea level

highstands and most likely is the result of coseismic rupture and uplift of the coastline.

Total vertical surface uplift for the first emergent terrace is 100 m +/- 7 m. A vertical surface uplift rate of 2.2 +/- 0.3 m/ky is estimated based on the age of 45 ka, the elevation of the shoreline angle, and the 45 ka paleo-sea level elevation (Figure 6; Table 4).

#### **6.44 La Mesa Terraces**

East of the More Mesa terraces, the La Mesa terraces and associated strandlines are continuous from Los Positas along the southern flank eastward across the Mesa anticline (Figure 8). The terraces are uplifted along the south limb of the La Mesa and Lavigia anticlinal folds, on the hanging walls of the blind, La Mesa and Lavigia reverse faults, respectively. The terraces and associated strandlines are truncated east of SBCC by the Mesa fault and subsequent erosion from Mission Creek.

Along the south limb of the fold at SBCC, a marine terrace fossil assemblage is exposed in the sea cliff on the first emergent marine terrace at SBCC, formerly known as Bathhouse Beach (Figure 8). A fossil coral was obtained from the paleontology collection at the Department of Geological Sciences at UCSB. The coral was a well-preserved, solitary coral (*Balanophyllia elegans*) sampled from the sea cliff exposure at the Bathhouse Beach fossil site.

X-ray diffraction analysis determined the fossil coral to be composed of original aragonite shell material. Uranium series analysis of the fossil coral yielded a measured initial  $^{234}\text{U}/^{238}\text{U}$  activity of  $1.164 \pm 0.015$  which is within the same range as that for

modern seawater (Gurrola et al., 1997b). The estimated uranium series age is approximately of  $70 \pm 2$  ka (Table 4). The oxygen isotope analyses of fossil mollusks indicate warmer paleo-ocean water signatures than the UCSB site (Trecker et al., 1998; 1999). Chappell et al. (1996) recognize a paleo-sea level highstand associated with oxygen isotope substage 5a at  $73 \pm 2$  ka with an elevation of  $-58.5 \pm 13.5$  m. Therefore, the first emergent marine terrace at SBCC is best correlated to the  $73 \pm 2$  ka paleo-sea level highstand at isotope substage 5a (Figures 6 and 8).

At SBCC there are four uplifted terraces with associated paleo-shorelines, and one abrasion platform with the strandline removed by erosion, preserved in the same terrace flight as the SBCC site. The approximate paleo-shoreline elevations of the terraces and abrasion platform beginning with the first emergent are  $30 \pm 1.5$  m,  $44 \pm 1.5$  m,  $54 \pm 2.0$  m,  $75 \pm 2.0$  m, and  $109 \pm 3.0$  m, respectively (Figure 8).

Based on the uranium series age of  $70 \pm 2$  ka for the first emergent marine terrace at SBCC, a total surface uplift of approximately  $88.5 \pm 13.5$  m and a rate of local surface uplift of approximately  $1.3 \pm 0.20$  m/ky is estimated (Figure 6).

Assuming a constant rate of uplift and using the method by Bull (1985), the  $30 \pm 1.5$  m and the  $75 \pm 2.0$  m terrace shorelines correlate to substage 5a and to substage 5c sea level highstands. The paleo-shorelines positioned at elevations of  $44 \pm 1.5$  m and  $54 \pm 2.0$  m do not correlate to any paleo-sea level highstands hypothetically formed as the result of coseismic surface uplift.

South of SBCC at Santa Barbara Point, a series of five flights of terraces with associated shorelines are preserved at approximate elevations of 15 +/- 1.0 m, 28 +/- 1.5 m, 47 +/- 2.0 m, 57 +/- 2.0 m, and 76 +/- 2.5 m (Figure 8). A higher marine abrasion platform with the strandline absent is preserved at an elevation of approximately 127 +/- 3.0 m.

The paleo-shoreline of the first emergent marine terrace at Santa Barbara Point is discontinuous. To the west the paleo-shoreline trends offshore and to the east is buried by alluvial fan-delta deposits, several terrace shoreline angles are mappable at SBCC. The 70 ka terrace shoreline is apparently present as the second emergent terrace at Santa Barbara Point (Figure 8).

OSL measurements of quartz grains sampled from terrace sands at Santa Barbara Point determine an age of 58 +/- 11 ka for the first emergent terrace (Figure 6; Table 4). Given the error range assigned to the 58 +/- 11 age, the terrace may have formed as a result of paleo-sea level highstands associated with oxygen isotope substages 3a (45 ka) or 3c (58 ka). Oxygen isotope data from fossil mollusks from Santa Barbara Point indicate a cool paleo-ocean temperature (Trecker et al., 1998).

Based on the OSL age of terrace sands, the isotopic signatures of fossil mollusks, and the position of the second emergent terrace at Santa Barbara Point (hypothetically 70 ka), the first emergent terrace is correlated to oxygen isotope substages 3c and a local vertical rate of surface uplift of **1.2 +/- 0.1 m/ky** is estimated (Figure 6; Table 4). This is in agreement with the calculated local vertical surface uplift rate of **1.3 +/- 0.2 m/ky** at SBCC.

Assuming a constant rate of terrace uplift and the method by Bull (1985), the flight of terraces correlate to oxygen isotope substages 3c (58 ka), 5a (72 and 80 ka), 5c (105 ka) and 5e (125 ka), respectively (Figures 6 and 8).

West of Santa Barbara Point at Meigs Road, laterally continuous terrace strandlines are geomorphically well-expressed (Figure 8). The elevations of the terrace strandlines are approximately 34 +/- 1.5 m, 48 +/- 1.5 m, 61 +/- 2.0 m, 75 +/- 2.0 m, and 114 +/- 3.0 m. A mostly stripped marine abrasion platform also occurs at an elevation of approximately 128 +/- 3.0 m.

Based on geomorphic mapping, the 70 ka strandline corresponds to the first emergent shoreline angle (33 m) which yields total surface uplift of 91.5 +/- 13.5 m above paleo-sealevel at time of platform erosion (Figure 8). A local vertical surface uplift rate of 1.3 +/- 0.2 m/ky. is estimated (Figure 6). Based on an assumed rate of constant uplift, the terraces correlate to the substages 5a (72 and 80 ka) and 5c (105 ka) ( Figure 8 ). The second and third terrace levels do not correlate to a paleo-sea level highstand and may be the result of coseismic surface uplift.

The terrace shorelines are mappable to the west at Mesa Lane, where drainage truncates the first and second flights of terrace strandlines (Figure 8). West of the water gap, we identify terrace shoreline angles at approximate elevations of 35 m, 48 m, 61m, 75 m, and 114 m. A marine abrasion platform positioned at approximately 128 m elevation is present but the shoreline angle is removed by erosion.

## ***6.45 Montecito Terraces***

Two, possibly three flights of marine terraces are uplifted and preserved east of Santa Barbara. The first emergent terrace is a 1 to 2 km long surface in the Montecito area, is truncated by surficial drainage and is deformed across the Santa Barbara Cemetery anticlinal fold (Figure 9).

A steep, south-facing paleo-sea cliff is preserved north of the fold at an elevation of approximately 31 +/- 2.0 m. The second emergent terrace is apparently preserved on the south limb of the Mission Ridge anticline where the back edge of the platform coincides with the Montecito fault. The shoreline angle of this marine platform is buried or eroded due to faulting, so the maximum platform elevation of approximately 94 m is measured.

Marine sands were sampled from the first emergent terrace along the modern sea cliff near Butterfly Beach in order to measure OSL of terrace sands (K-feldspar grains). The OSL analysis indicates an age of 79 +/- 10 ka for the terrace sand (Table 4). The maximum elevation of the first emergent terrace is approximately 25 m and a total surface uplift of 56 m is calculated. A local rate of surface uplift of 0.7 +/- 0.1 **m/ky** for the Santa Barbara Cemetery terrace is calculated (Figure 6). The first emergent Montecito terrace is synclinally folded below sea level eastward toward the Romero Creek water gap.

## ***6.46 Summerland Marine Terraces***

East of the Romero Creek water gap, three emergent terraces are uplifted and preserved on the hanging wall of the Arroyo Parida

segment of the MRFS (Figure 9). The shoreline angle of the first emergent terrace extends 2 km from the Ortega Hill anticline eastward to where it trends offshore. The shoreline angle trends offshore west of the (second emergent) Loon Point terrace (Figure 9).

The shoreline angle of the first terrace increases in elevation westward from approximately  $19 +/ - 1.5$  m to  $23 +/ - 1.0$  m. The marine platform and associated shoreline angle is exposed in a railroad-cut exposure on the south flank of the Ortega Hill anticline (Figure 9). The wave-cut abrasion platform is inclined about  $2^{\circ}$  to the southeast and is denoted by a boulder line 0.2 to 1 m thick. The boulder line contains cobble clasts with occasional pholad borings indicating a near-shore beach, depositional environment. The cobble conglomerate is overlain by a thin, discontinuous 0.5 m thick bed composed of well-sorted, medium to fine (beach) sand. The boulder line is terminated against steeply south-dipping, non-marine Casitas strata (paleo-sea cliff) forming a wave-cut notch at an elevation of approximately  $23 +/ - 1.0$  m. The age of this marine platform and terrace is unknown.

The first emergent terrace at Loon Point, which is the second emergent terrace of the Summerland sequence, is exposed along the modern beach sea cliffs at Loon Point. The elevation of the shoreline angle is approximately  $50 +/ - 3.0$  m, however the terrace is synclinally folded below sea level into the Carpinteria syncline to the east. Terrace sands were sampled from the first terrace flight near Loon Point in order to obtain an age-date by optically stimulated luminescence analysis. OSL analysis yielded age

estimations of 105 +/- 15 ka for and 167 +/- 15 ka for quartz and potassium feldspar grains, respectively (Table 4). The oldest first emergent marine terraces preserved in the SBFB are no older than 125 ka, therefore the age of the Loon Point terrace is assumed to be **105 +/- 15 ka**. The estimated amount of surface uplift is approximately 73.5 +/- 3.0 **m** and the estimated surface uplift rate is approximately 0.7 +/- 0.1 **m/ky** (Figure 6; Table 4).

## **7.0 TECTONIC GEOMORPHOLOGY AND PALEOSEISMICITY OF FOLDS AND FAULTS**

The SBFB exhibits numerous geomorphic features related to active, shallow subsurface folding (Gurrola and Keller, 1997a). The belt contains numerous active folds developing on the hanging-walls of blind reverse and thrust faults. These active folds form well-expressed, *en echelon* anticlinal ridges and synclinal basins on the coastal piedmont (Figure 2).

Geomorphic expression of active folds in the SBFB includes forelimb fold scarps, transverse wind (air) and water gaps, deflected and defeated stream courses, and uplifted marine terraces. Anticlinal and monoclinal folds form topographically well-expressed anticlinal ridges or fold scarps, whereas synclinal folds form subsiding basins. We will discuss in greater detail several faults and associated folds including the Mission Ridge Fault System (MRFS) and Loon Point fault. Paleoseismic data, collected for two sites: Ellwood Mesa (More Ranch segment of the MRFS) and Loon Point will be presented.

## **7.1 FAULT SEGMENTATION**

Geometric, geomorphic and structural segments of the MRFS including the More Ranch, Mission Ridge, and Arroyo Parida segments, are defined by changes in structural style, geometry, termination of folds, and geomorphology. Segment boundaries also coincide with faults that strike at a high-angle to the MRFS, termed cross faults (tear faults) (Figure 1; Gurrola and Kamerling, 1996). Mapping of the tectonic geomorphology of reverse faults and related folds identified left-lateral displacement of folds at the More Ranch-Mission Ridge segment boundary, truncation of folds and subsidiary faults at the Mission Ridge-Arroyo Parida segment boundary, and differential faulting, uplift and related folding at the west-east Arroyo Parida segment boundary. These segment boundaries correlate with northeast-striking cross faults including, from west to east: the Goleta Point, the Fernald Point, and Rincon Point faults (Gurrola and Kamerling, 1996). These NE-striking faults are subparallel to the present axis of compression and are favorably oriented to behave as tear faults during coseismic deformation.

Some recent Santa Barbara area earthquakes show rupture zones limited by boundaries demonstrated to be steeply-dipping cross faults behaving as tears. Tear faults segment larger reverse (and thrust) faults transferring slip to adjacent thrust ramps. Tear fault segment boundaries in the western Transverse Ranges and Los Angeles may limit the size of rupture zones during an earthquake and therefore the potential magnitudes of expected earthquakes. These cross faults or segmentation boundaries are difficult to observe and map, and are often discovered only after a large

earthquake on the basis of aftershock hypocenters and focal mechanism defining near-vertical strike-slip tear faults at the edges of the main shock rupture (Hauksson and Jones, 1989).

Tear faults may control the nucleation or termination of moderate to large earthquakes in the Los Angeles basin and the western Transverse Ranges. The 1994 Northridge earthquake nucleated at the intersection of a thrust ramp and tear fault rupturing up the ramp. Corbett and Johnson (1984) map the seismicity associated with the 1978 Santa Barbara earthquake which reveals an abrupt termination of earthquakes on the eastern boundary that coincides with the NE-striking Goleta Point fault (Gurrola and Kamerling, 1996).

If we assume that the MRFS is capable of producing earthquakes similar in magnitude to the 1994 Northridge and 1971 San Fernando earthquakes, then we can assume similar rupture lengths, area, and depth. Therefore, we might expect the MRFS to rupture along two or possibly more geomorphic/structural segments and the rupture may nucleate or terminate near a tear fault such as the Goleta Point, Fernald Point, or Rincon Point faults.

## **7.2 MISSION RIDGE FAULT SYSTEM (MRFS)**

The 70 km long, south-dipping, reverse MRFS is the principal seismic source on the coastal piedmont of Santa Barbara. To the west at Ellwood, the MRFS continues offshore and is expressed as a bathymetric high on the sea floor. To the east at Ojai Valley, the MRFS is truncated by the north-dipping San Cayetano fault.

The MRFS forms prominent, topographically expressed folds whereas other secondary blind reverse faults on the coastal piedmont form shorter, discontinuous landforms (Figure 2). Along strike, the MRFS is characterized by fault-propagation folds associated with active folding. These folds and associated landforms include hanging wall anticlines producing anticlinal ridges and footwall synclines producing synclinal basins.

The MRFS is subdivided into geometric, geomorphic, and structural segments including, from west to east, the More Ranch, the Mission Ridge, and the Arroyo Parida segments (Figures 1 and 2). These left-stepping, en echelon segments exhibit fault geometric, geomorphic, and structural homogeneity along strike. However, abrupt changes in these characteristics occur across what we interpret to be segment boundaries.

The 15 km long More Ranch segment strikes through the Goleta basin and uplifts the More Mesa, the UCSB-Isla Vista, and the Ellwood marine terraces. The 17 km long Mission Ridge segment strikes through the community of Santa Barbara and dips south beneath the urban corridor on the coastal piedmont. The Arroyo Parida segment strikes north of Carpinteria and can be subdivided into west (17 km long) and east (15 m long) subsegments as well as the 5 km long Santa Ana fault that strikes through northern Ojai Valley terminating at the San Cayetano fault.

MRFS folds, from west to east, include: the Ellwood Mesa anticline; the UCSB and More Mesa-Hope Ranch anticlines on the More Ranch segment; the Mission Ridge anticline on Mission Ridge segment; and the Arroyo Parida uplift on the Arroyo Parida segment.

Near the city of Santa Barbara, Mission Ridge (the Riviera) anticline forms the most prominent topographic high on the Santa Barbara coastal plain. The ridge extends for most of the length of the Mission Ridge fault segment.

Emergent flights of late Pleistocene marine terraces are preserved on the flanks of hanging wall anticlines of the MRFS and late Pleistocene terrace chronology of the terraces allows for rates of surface uplift and faulting to be estimated.

### **7.21 More Ranch Segment**

The roughly east to west striking, 17 km long, More Ranch segment is mostly blind along strike and can be subdivided into western and eastern subsegments (Figures 2 and 5). The western subsegment uplifts the Ellwood and UCSB terraces and bounds the south margin of Goleta basin. The Goleta Slough syncline (water gap) is located at the boundary between the segments.. The eastern subsegment uplifts the More Mesa and Hope Ranch anticlines and separates the onshore Goleta and the Santa Barbara basins (Figure 5). The More Ranch segment terminates eastward at a complex segment boundary where it truncates the Mission Ridge segment and the northwest-striking San Jose and Mesa faults (Figure 2).

Tectonic landforms along the western and eastern More Ranch subsegments include flights of late Pleistocene wave-cut platforms on the crests and flanks of anticlinal folds. West to northwest-trending, anticlines are north-verging hanging wall folds with *en echelon*, fore- and/or back limb fold scarps.

Pre-Quaternary strata is exposed in the core of folds and form the bedrock on which the late Pleistocene wave-cut platforms are eroded. The blind More Ranch segment also folds and warps several flights of marine terraces including isotope substage 3a (45 ka) (Figures 5 and 6).

**7.211 Ellwood Fold:** The westernmost extent of the More Ranch fault is exposed in a sea cliff exposure forming a north-verging, monoclinal fold at Ellwood Beach. However, for most of the length of the fold along strike, the main fault is blind forming a north-verging, hanging wall anticline with associated bending moment faults. The en echelon, west-trending anticlinal folds form a geomorphically well-expressed convex fold scarp on the first emergent 45 ka marine terrace. From Devereaux Creek eastward to the sea cliff exposure of the fault the zone of deformation decreases from approximately 150 m to several meters wide.

The westernmost More Ranch fault is exposed in the modern sea cliff; the fault deforms the first emergent marine terrace and is expressed on the surface as a north-facing fold scarp approximately 5 m high. Aerial photographs from 1929 reveal a several hundred meter long, linear fold scarp with greater relief than what is presently preserved suggesting that the scarp has been denuded due to grading.

The sea cliff exposure reveals a south-dipping, reverse fault that offsets the Miocene Monterey Formation and wave-cut platform (Figure 10). The overlying late Pleistocene marine terrace and fluvial units are folded into a monoclinal drape anticline. The vertical

throw on the 45 ka, wave-cut platform is approximately 7 m. A paleosol has formed and is preserved in the lower section of folded, fluvial strata. However the steep terrain of the sea cliff prevents detailed study of the fault exposure.

A channel fill exposed in the sea cliff face is abutted up against the fold scarp on the footwall. The channel is an upstream reach of Devereaux Creek truncated by coastal erosion.

At Devereaux Creek, the More Ranch fault forms a broad, asymmetric, north-facing fold scarp on the Ellwood Mesa. Along the fold scarp, Devereaux Creek flows against the scarp eastward to Devereaux Slough. A left-stepping fold scarp bounds the landward edge of Ellwood terrace and the gently south-sloping terrace surface north of Devereaux Creek. The zone of deformation across the north (fore-) limb of the fold is approximately 150 m wide. The fold exhibits a broad, planar crest with vertical relief of approximately 14 m on the 45 ka Ellwood terrace .

Several trench pits were excavated at various locations on the Ellwood fold at Devereaux Creek as part of a geotechnical investigation by Hoover and Associates (1985) and Santa Barbara County soil remediation projects. Hoover and Associates (1985) identified several parallel, west-striking faults, one of which is equivalent to Dibblee's (1986) mapped trace of the More Ranch fault along the channel of Devereaux Creek.

A trench was excavated for soil remediation to depths up to 10 m and 600 m long in the Devereaux Creek channel. The trench did not reveal offset terrace strata but did expose the geometry of the marine platform and overlying terrace sediments. The main strand

of the More Ranch is blind at this site and is expressed as an anticlinal fold.

Paleoseismic investigations involved determining the nature of the deformation of the subsurface wave-cut platform across the fold scarp. This included seismic refraction to determine depth and geometry of the contact between the marine terrace strata and the underlying wave-cut platform eroded on the Sisquoc Formation. Two north-south seismic refraction lines revealed that wave-cut platform terrace sediments are uniform and mantle the deformation on the wave-cut platform. The surface expression of the fold mirrors the geometry of the subsurface wave-cut platform unconformity except where two near vertical offsets were identified on the north-facing fold scarp. These offsets of the marine unconformity were in the approximate location of the faults identified by Hoover and Associates (1985).

Direct sampling of the terrace sediments to shallow depths through continuous drill core-sampling was conducted to verify vertical offsets as faults and determine potential fault-trench locations. A total of eight small diameter (4.5 cm) cores were drilled in a north-south profile from north of Devereaux Creek to the crest of the anticline and were continuously sampled from depths of -1 m to maximum depths of -10 m (Figure 11). The shallow drill core-sampling data corroborated the seismic refraction results of the terrace strata thickness and two faults that vertically offset the wave-cut platform by approximately 1.5 m each.

A fault-trench was excavated on the fold scarp across the southern fault splay to evaluate and characterize earthquake history

of the More Ranch fault. The continuous drill-core data revealed greater stratigraphic resolution across the southern fault splay than the northern fault splay on the fold scarp. The location of the 25 m long, 6.5 m deep trench is shown on Figure 12. The southern part of the trench was excavated as a narrow 0.60 m wide slot trench, whereas the northern part of the trench was benched at - 2.0 m to allow easier access to details of faulting at shallow depths. The east trench wall was scraped clean and a 0.5 to 2.0 m grid was constructed for detailed, mapping of terrace and fault contacts.

The fault trench revealed a 3 to 4 m thick, marine terrace sequence and several west-striking, south-dipping, thrust faults that vertically offset and warp the basal marine abrasion unconformity approximately 1.5 m (Figure 13). Generally, the zone of faulting was approximately 0.6 m wide, defined by five fault strands that terminated at different stratigraphic horizons. Dip on the fault strands increased with depth from approximately  $25^{\circ}$  to  $45^{\circ}$ .

On both sides of the fault, the trench wall exposed a stratigraphic sequence of, denoted unit I to unit A from bottom to top, Miocene Monterey Formation (unit I), a late Pleistocene wave-cut unconformity, marine terrace sediments (units H-D), and alluvial cover (units C-B) (Figure 13). Unit A is the anthropogenic zone in which a modern A soil horizon is presently forming.

The terrace sequence includes basal silts (units H and F) that include poorly re-worked angular clasts of the Monterey Formation indicating an offshore marine environment. Units E and D were bimodal, well-sorted, medium to fine-grained sands with locally preserved cross-bedding structure. These units (E and D) are aeolian

beach dune deposits indicating subaerial emergence of the marine platform. Alluvial units B and C are massive clays with no structure and are probably the result of alluvial floodplain deposition following regression of the beach environment.

The reverse fault strands juxtaposed dissimilar geologic units including the basal Miocene Monterey Formation (unit I) and lowermost terrace units (H and G). The overlying terrace and alluvial units (F-B) were deformed but were similar on both sides of the fault strands. Unit A was not deformed but is deposited across and mantles the underlying scarp. The footwall terrace section was not only thicker but preserved additional units not exposed in the hangingwall section.

The semi-parallel fault strands offset different sequences of terrace strata up to three different stratigraphic levels or horizons. The stratigraphic horizons were overlain by undeformed strata which are termed seismic or paleo-earthquake horizons. These paleo-earthquake horizons indicate within the trench stratigraphy when slip associated with a paleo-earthquake occurred on the specific fault strand. These seismic horizons or paleo-earthquakes are denoted, from lowest to highest in section, EQ3, EQ2, and EQ1, respectively (Figure 13).

The three seismic horizons, EQ3, EQ2, and EQ1, are positioned between terrace units G and F, units E and C, and units B and A, respectively (Figure 13). The northernmost fault strand corresponded to the lowest seismic horizon (EQ3). The central three fault strands terminate at the middle seismic horizon (EQ2)

and the southernmost fault strand terminate at the highest seismic horizon (EQ1).

In stratigraphic order, the orientation of the northernmost fault strand is strike  $098^{\circ}$  with  $39^{\circ}$  dip to south and offsets units I, the marine abrasion unconformity, unit H, and unit G with reverse-slip. However, the fault was abruptly terminated by unit F. This fault strand juxtaposes different facies of the Miocene Monterey Formation and unit G. Unit G contains two additional units ( $G_2$  and  $G_3$ ) in the footwall section not preserved in the hangingwall section. The youngest of unit G (denoted  $G_1$ ) was mappable across the fault but was texturally very different. The abrasion unconformity and the base of unit  $G_1$  were vertically offset approximately 40 cm. Detrital charcoal were sampled from units H and  $G_3$  on the footwall section and submitted for accelerated mass spectrometry (AMS) analyses. The measured radiocarbon age of units H and  $G_3$ , are about 47 ka. These age-dates of the basal terrace units are stratigraphically consistent and in agreement with the UCSB terrace age to the east. Unfortunately, organic material was not found in units  $G_1$  and F. The closest overlying unit radiocarbon age-dated was unit D at 37 ka (Table 4). Therefore, vertical slip on the northernmost fault strand is approximately 0.40 m and dip slip along the fault plane is approximately 0.52 m for the earliest paleo-earthquake (EQ3). This paleo-earthquake occurred sometime between about 47 and 37 ka.

The central three fault strands were generally oriented at strike of  $099^{\circ}$  with dip  $30^{\circ}$  south and vertically offset units I-E with reverse slip. The thrust fault strands are abruptly terminated at the

base of alluvial unit C (Figure 13). The wave-cut platform has a cumulative vertical offset across all three strands of approximately 0.50 m. The uppermost faulted terrace unit (E) was a beach indicating subaerial emergence of the marine platform prior to EQ2. Also, a sand blow injection pipe is preserved within unit D and is truncated by the base of the overlying unit C. Unit E was the source ejecta for the sand blow structure that intrudes unit D and suggests intense shaking was associated with EQ2 and shallow groundwater conditions at the trench site.

The uppermost terrace unit deposited at the trench site prior to EQ2 was unit E and through association unit D (Figure 13). Radiocarbon analyses based on sampled organic detritus from units D and C yield approximate ages of about 37 ka and 36 ka (Table 4). Therefore, EQ2 occurred about 37 ka following emergence of the marine platform.

The southernmost fault strand has a strike of 085° and dip of 44° south and vertically offsets units I-B with reverse displacement. The wave-cut platform has a vertical offset of approximately 0.17 m, however the terrace is warped on the hangingwall section which yields a vertical separation of 0.3 m. This reverse fault reaches the highest stratigraphic level in the trench where it is truncated by alluvial unit A.

The fault strand offsets unit C but deforms unit B through monoclinal folding. There are several pervasive synthetic and antithetic shears within unit B with slickensides that indicate backthrusts. However, the fault is well-expressed with discrete, reverse separation of strata on the west trench wall. The uppermost

area on the east trench wall was correlated to the exact same area on the west trench wall for evaluation of EQ1.

On both east and west trench walls, the uppermost faulted alluvial clay unit B can be subdivided into lower ( $B_2$ ) and upper ( $B_1$ ) units based on the presence and absence of brecciated Monterey clast respectively (Figure 13). However, on the west trench wall, the fault strand vertically offsets the base of unit  $B_2$  approximately 0.1 m with a dip separation of approximately 0.3 m.

The most recent earthquake faulted and/or folded strata approximately 0.4 m (vertical slip) and occurred post 36 ka. The penultimate earthquake occurred between about 37 ka and the oldest earthquake occurred between 47 ka and 37 ka. Based on radiocarbon age-dating of the basal marine terrace unit we calculate a vertical rate of uplift of about 2 m/ky for the Ellwood Mesa (Figure 6). A vertical rate of folding of  $0.22 +/- 0.03$  m/ky and a dip slip rate of 0.3 m/ky are calculated at this location.

**7.212 UC Santa Barbara-Isla Vista:** Detailed studies of the More Ranch segment include: trenching; subsurface mapping; and u-series, OSL and isotope analysis. U-series analysis of a marine terrace fossil coral yielded an age of  $47 +/- 0.5$  ka for the UCSB-Isla Vista terrace (Table 4) and is a minimum age for the platform. Based on isotopic studies of Greenland GSIP ice cores, Dansgaard-Oeschger event 14 is the most likely candidate for the formation of the UCSB-Isla Vista platform. Chappell et al. (1996) estimate that the paleosea level elevation for oxygen isotope substage 3a at 51 ky is approximately -85 m. The shoreline angle elevation is approximately

25 m for the first emergent (Ellwood) terrace, which correlates to the UCSB-IV terrace and is also collaborated with radiocarbon data. The amount of total vertical uplift in the last 47 to 51 ky is about 110 m yielding an estimated local vertical surface uplift rate of about 2 m/ky. The local vertical uplift rate of the More Mesa terrace is approximately 1.8 m/ky.

Along the western subsegment, geomorphic and subsurface mapping of the first emergent marine terraces at UC Santa Barbara and Isla Vista (UCSB-IV) establish the continuity of the associated wave-cut platforms (Figure 5). The UCSB-Isla Vista platform is broadly folded into an open, north-verging, anticline. A 2 m high, north-facing scarp is present in the subsurface on the marine platform at UC Santa Barbara. However, review of geotechnical trenching data indicate this feature formed as the result of faulting on the north-dipping Campus fault (Figure 14).

The UCSB-IV marine platform is downwarped to the west into a syncline at Devereaux Slough and re-emerges as the first emergent terrace at Ellwood. The Ellwood terrace is folded along strike of the More Ranch fault into a hanging wall anticline or monocline. On the hanging wall, the elevation of the marine platform is approximately 26m, whereas on the footwall, the elevation of the marine platform is approximately 13 m. Therefore, the More Ranch segment offsets the radiocarbon age-dated 47 ka and correlated 125 ka terraces 13 m and 43 m respectively, yielding a vertical rate of faulting (rock uplift) of about 0.3 m/ky, a rate similar to that at Ellwood and 70 km east near Ventura (Figure 15).

**7.213 More Mesa-Hope Ranch anticlines:** The first emergent terraces at More Mesa, UCSB, and Ellwood are discontinuous as the result of erosion to the inlet of the Goleta and Devereaux Sloughs. The Goleta Slough is the product of local down warping as a result of left-stepping geometry, complex cross-faulting, and oblique slip (Figures 16 and 17). Along the eastern subsegment, the More Ranch fault forms hanging wall anticlines at More Mesa and Hope Ranch. Flights of marine terraces are preserved on the crests and limbs of these folds and can be correlated to the La Mesa marine terraces (Figures 7 and 8). The first emergent marine terrace at More Mesa extends across a series of northwest-trending folds for a distance of about 1.5 km. The elevation of the associated paleoshoreline is poorly preserved at about 36m.

## 7.22 Mission Ridge Segment

**7.221 Mission Ridge:** The south-dipping, blind Mission Ridge segment (MsR) of the MRFS, located just north of the city of Santa Barbara, forms the most prominent tectonic landform on the coastal piedmont (Figure 2). The MsR is not exposed in natural outcrop, but forms a topographically, well-expressed hanging-wall anticlinal fold (Mission Ridge). The fold extends 15 km westward from Montecito to Santa Barbara and varies in height from 25 m to 175 m.

The anticline uplifts and folds late Pleistocene fanglomerates and pre-Quaternary strata. Mission Ridge is the result of hanging-wall folding and the core of the anticline consists of Tertiary Rincon and Monterey Formations unconformably overlain by Quaternary

fanglomerate. Near Las Alturas Road a fault investigation exposed the Monterey-fanglomerate unconformity which is dipping nearly 50° to the south. A river bank exposure in Rocky Nook Park near the Mission exposes south-dipping backlimb fanglomerate deposits at approximately 20°. A road cut outcrop on Mountain Drive exposes alluvial forelimb strata dipping approximately 65° to the north. These deposits are part of a steep north limb (forelimb), suggesting that Mission Ridge is a hanging-wall anticlinal fold.

**7.222 Montecito anticline:** The Montecito anticline is a 2 km long hanging-wall fold formed on the Mission Ridge fault segment. The fold deforms Quaternary fanglomerate and produces a surficial fold scarp. Geotechnical studies document that the fold is cored by Tertiary Rincon Fm in the shallow subsurface (Slayman, pers. comm., 1997). Though there are no exposed limbs of the fold, the alluvial terrace is warped and exhibits a fold morphology. Buckled street curbs, road and sidewalk cracking, and a sloping tennis court suggest this fold may be active and deforming aseismically.

### **7.3 NORTHWEST-STRIKING FAULTS**

A number of faults and associated folds in the SBFB strike roughly northwest. These folds include: Goleta Valley anticline; La Mesa anticline; and the cemetery anticline; Ortega Hill anticline; and Loon Point anticline (Figure 2). These more northwest-striking features are often truncated by the MRFS (see Figures 2 and 5). We hypothesize that those faults and folds truncated by the MRFS are older and have been rotated clockwise with the Transverse Ranges

(Luyendyk, 1991), and may be evidence for continued Quaternary rotation.

### **7.31 Goleta Valley Anticline**

In the Goleta basin, the Goleta Valley anticline forms a well-expressed linear anticlinal hill that is located immediately north of HWY 101. The anticline is a 2 km long, northwest-trending, north-verging fold formed on the hanging wall of the south-dipping, reverse San Jose fault (Figure 5). The fold plunges westward and deforms Tertiary Rincon Fm, Quaternary Santa Barbara Fm and fanglomerate as well as overlying marine terrace deposits. On the south limb, dips in the Santa Barbara Fm range from 20° to 35° whereas on the north limb the fanglomerate dips about 40°. On the forelimb of the anticline, the San Jose fault scarp is well-expressed immediately south of Cathedral Oaks Road.

Well-developed drainages with moderately-incised valleys and associated wind (air) gaps are preserved on the anticline. At the western end of the anticline, San Antonio Creek is diverted to the west by the anticline and together with the presence of wind (air) gaps and apparent older more eroded topography may indicate westward propagation of the Goleta Valley anticline (Figure 18).

### **7.32 La Mesa Anticlines**

The northwest-trending La Mesa hills are the expression of a hanging-wall anticline on the south-dipping, reverse Mesa fault. The folds plunge offshore to the east at Santa Barbara Point are truncated to the northwest by the Mission Ridge segment of the

MRFS. Along the north facing fold scarp, the forelimb of the anticline is mostly absent due to erosion by Mission Creek where two prominent meander scars north of Santa Barbara City College are present. A remnant of the north-dipping limb is reported by Dibblee (1986) and the south-dipping limb is poorly exposed in a road cut on Meigs Road.

The Mesa anticline folds wave-cut platforms of stage 3 and stage 5 near Santa Barbara Point. The rate of surface uplift of about 1 m/ky for the Mesa (Figures 6 and 19) probably represents combined deformation on several (blind) structures, one of which is the Mesa fault.

### **7.33 Santa Barbara Cemetery (Zoo) Anticline**

The Santa Barbara Cemetery (Zoo) anticline is a 2 km long, northwest-trending fold that is exposed in the seacliff just east of East Beach (Figures 2 and 9). The anticline folds Quaternary Casitas Formation and the first emergent terrace into a steepened north-facing fold scarp and anticlinal hill. Strata of the Casitas Formation dip approximately  $25^{\circ}$  to the north at the base of the sea cliff and decreases up section. East along the exposure of the sea cliff the strata of the south-dipping limb are exposed. Some units thin and onlap against the fold crests suggesting that syntectonic Casitas deposition occurred during fold growth and uplift. The wave-cut platform is warped across the fold crests, and the sea cliff is nearly parallel to the fold axis providing apparent dips. A synclinal basin is formed to the north and expressed as part of the now mostly filled Santa Barbara coastal lagoon (historic El Estero). These folds are most likely related to a blind reverse fault.

### **7.34 Ortega Hill Anticline**

At the left-stepping segment boundary of the MRFS, the strike-slip (?) Fernald Point fault strikes at a high angle to the MRFS and truncates northwest-striking, hanging-wall folds such as the Ortega Hill anticline. The fold is the prominent topographic landform immediately to the west (Figure 9). Ortega Hill is the expression of an anticlinal fold deforming Quaternary Casitas Formation and overlying late Pleistocene terraces sediments. Strata of the Casitas Formation dip approximately  $50^{\circ}$  to the south whereas strata on the

north limb dip  $30^{\circ}$  to the north. The trend of the anticline is northwest and plunges to the southeast. The fold is open with interlimb angle of approximately  $100^{\circ} +/- 5^{\circ}$ . Structural studies suggest that the Ortega Hill anticline is contemporaneous with and forms part of the north limb of the Carpinteria basin (Jackson, 1981; Jackson and Yeats, 1982).

### **7.35 Loon Point Fault and Propagation Fold**

At Loon Point (Figure 9), Casitas Formation and a late Pleistocene (oxygen isotope SC at 105 ka, Table 4) marine terrace are folded and faulted by a low-angle reverse fault (Figure 20). The nearly vertical 30 m high sea cliff prevents detailed stratigraphic analysis, however, photographic mosaic mapping and subsequent trenching of the fault have provided additional information.

The Loon Point fault strikes approximately  $085^{\circ} +/- 5^{\circ}$  with a dip of  $30^{\circ} +/- 4^{\circ}$  to the south. The fault juxtaposes steeply-inclined strata on the hanging wall against gently-dipping strata on the foot wall. The forelimb strata, although clearly defined, are inaccessible due to steep slopes. The forelimb of the fold is overturned dipping about  $80^{\circ}$  to the southeast and terminates against the fault. A colluvial growth wedge exhibiting tapering beds is preserved on the forelimb.

The position of the wave-cut platform is preserved on the forelimb overlying the growth wedge and identified by a thin cobble conglomerate (boulder line) with pholad boreholes. The age of the marine terrace is most likely either 45 ka or 81 ka, the age of the first emergent marine terraces in the SBFB. Across the axial surface,

the boulder line is eroded out of the sea cliff section and projects into space (Figure 20). To the east, the boulder line is preserved on the back limb and can be followed to the east until it disappears below sealevel.

The backlimb strata on average strike  $080^{\circ}$  and dip  $27^{\circ}$  to the southeast and consist of Casitas Formation, marine terrace, and alluvial sediments. Strata of the Casitas Formation beds at Loon Point consists of fluvial and massive debris flow deposits that taper and thicken, indicating syntectonic deposition during fold growth. The interlimb angle is approximately  $57^{\circ}$  and is a tight fold. The axial surface is moderately inclined and the fold thickens in the hinge area and forelimb. Displacement is south-side up with associated north-directed fold vergence. Strata on the foot wall strike  $075^{\circ}$  and dip  $16^{\circ}$  to the southeast.

The faulted, asymmetric Loon Point anticline is a fault-propagation fold in which the fold formed as the thrust fault propagated to the surface. Suppe (1985) and Suppe and Medwedeff (1990) describe asymmetric folds with one steep or possibly an overturned limb adjacent to a thrust fault as a fault-propagation fold. They describe these folds as a result of the process of fault propagation and suggest that the fold records deformation that occurs in front of the propagating fault surface which ramps from a detachment at depth. With time, the fault juxtaposes a foot wall syncline against a hanging-wall anticline across the fault (Suppe, 1985). As the fault propagates upward, the fault ramp lengthens and commonly, the fault-propagation fold becomes locked and the fault may rupture through the anticlinal or synclinal axial surface, or

somewhere in between (Suppe, 1985; Suppe and Medwedeff, 1984 and 1990).

The reverse fault and asymmetric, hanging-wall folds documented in this study are similar to the fault-propagation fold geometry described by Suppe (1985) and Suppe and Medwedeff (1984 and 1990). Absent from the foot wall block of the Loon Point fault is an associated syncline (Figure 20). Therefore, the fault ruptured through the syncline and is classified as a synclinal fault breakthrough (Suppe and Medwedeff, 1990).

Suppe and Medwedeff (1990) propose two models by which folding occurs in brittle conditions. Both models describe fold-propagation by reverse-faulting. The constant thickness fault-propagation folding model is based on conservation of bedding thickness and bed length. The fixed front anticlinal axial surface model allows for bed thickening or thinning in the steep fore-limbs of the fold. Beds of the Loon Point fold thicken in the steep fore-limb of the anticlinal fold and indicates that this fault-propagation fold can be best described with the fixed front anticlinal axial surface model.

**7.351 Paleoseismic Evaluation:** Excavation of a fault trench across the fold scarp of the Loon Point fault-propagation fold revealed a shallow-dipping reverse fault (Figure 21). The fault juxtaposed marine terrace sands against Quaternary alluvium. The marine sands were absent from the foot wall block and were exposed in a secondary trench and surveyed into the fault to measure a vertical displacement of 5 m (Gurrola et al., 1998). In the

seacliff exposure, the marine abrasion platform is folded and vertically offset several m. Several buried (A-horizon) soils are preserved and the lowermost A-horizons appear to be folded. Detrital charcoal sampled from a faulted alluvial unit with 2 m of offset yielded a  $^{14}\text{C}$  date of about 4 ka (Table 4). The age is too young to calculate a reasonable slip rate. The Loon Point fault is classified as an active fault and seismic source in the SBFB.

## **8.0 STYLE OF QUATERNARY FOLDING**

Folding and reverse faulting accommodate crustal shortening of the western Transverse Ranges Province. In the SBFB, the amplitude of synclinal basins are an order of magnitude greater than anticlinal folds resulting in relatively deep basins (0.5-1 km) in contrast to anticlines with moderate (0.05 - 0.25 km) topographic relief.

Topographically, well-expressed folds in the SBFB along with natural and trench exposures allow for 3D mapping and analysis of surface and shallow fold deformation. Subsurface data integrated from Jackson and Yeats (1982) and Olson (1982) provide deeper subsurface data important to understanding the style of folding. The principal style of fold deformation documented is fault-propagation folding and monoclinal folding associated with basement compressive deformation.

Fault-propagation folds initially develop as a geomorphically expressed, asymmetric anticline-syncline pair formed as the result of displacement on an initially buried reverse fault that propagates to the surface (Suppe, 1985; Suppe and Medwedeff, 1984 and

1990). Subsequent shortening locks up the fold and the propagating reverse fault typically ruptures through the synclinal axis resulting in a faulted hanging-wall anticline and foot wall syncline. With subsequent slip, either the syncline or anticline may provide critical data concerning direction and rate of lateral propagation (Keller et al., 1999).

## **9.0 LATERAL PROPAGATION OF FOLDS: GEOMORPHIC ANALYSIS**

The SBFB contains numerous folds developing on the hanging-walls of buried reverse faults. The lateral propagation or growth of folds is an important active tectonic process with important ramifications concerning modeling deformation and mechanics of folding and reverse fault (Keller et al., 1999). Fold deformation is intimately related to reverse faulting (Davis, 1983; Jackson et al., 1996) and surface folding produced by a buried propagating fault provides critical data concerning direction and rate of lateral propagation.

Lateral propagation of folds at rates of several cm/yr (approximately ten times the vertical rate of displacement on the fault producing the fold) is perhaps the most rapid tectonic process not yet well understood (Keller et al., 1999).

Geomorphic relationships are a primary way to demonstrate lateral propagation of folds (Jackson et al., 1996; Keller et al., 1999). Geomorphic indicators of lateral fold propagation resulting from buried reverse faulting include (in direction of propagation):  
(1) decrease in drainage density and degree of dissection;

(2) decrease in elevation of wind gaps; (3) decrease in relief of the topographic profile along the crest of the fold (i.e., a fold plunges in the direction of propagation); (4) development of characteristic drainage patterns; (5) deformation of progressively younger materials, and (6) decrease in rotation and inclination of the forelimb. As a result of style of folding and variable geomorphic response, all of the criteria may not be evident at a particular fold.

The six geomorphic criteria are consistent with but not proof of lateral propagation, because the criteria are consistent (given specific scenarios) with both fold propagation and fold rotation models of fold growth. Criteria 4 and 5 are strong evidence of lateral propagation, and if there are at least two wind or wind and water gaps (from the same stream), then this is very strong evidence of lateral propagation.

Assuming that the stream can only be in one place at a time, the model of rotation is unlikely to produce two wind gaps or a wind and water gap at lower elevations in the direction of fold growth. There could be only one wind gap and one diversion. Once a stream is defeated by uplift in the rotation model it would be deflected to the nose of the fold (which is fixed, in that model) and would not form another gap.

Topographic profiles along the crest, profiles normal to the fold, and digital elevation models can help identify geomorphic parameters of folds. The elevations of wind gaps along an anticline are measured directly, and we postulate, as did Jackson et al. (1996), that these elevations are usually lower in the direction of propagation. The topographic profile along the crest of the fold, may reveal the direction of fold plunge. These relationships are shown for the apparent westward propagation of Mission Ridge at Santa Barbara, California

(Figures 22 and 23). Jackson et al. (1996) argue that drainage parallel to a fold will likely be diverted in the direction of propagation. As the diversion develops, streams are captured and the drainage basin area increases until there is sufficient stream power to temporarily maintain a channel at the nose of a fold where propagation has not yet occurred. As fold propagation continues this area becomes a water gap, and eventually may become a new wind (air) gap if the channel is defeated by uplift or stream capture. If this occurs, then the channel is diverted again in the direction of propagation and may make several passes around the fold as the drainage develops. In some folds there may be several wind (air) gaps produced in this manner and the major drainage will be repeatedly diverted around the nose of the fold. In this sense, the streams are antecedent where they cross an active fold as their position is established at the nose of the fold before folding and uplift propagates through the area. These relationships are clearly shown for Mission Ridge (Figure 23). Streams are diverted in the direction of propagation, and for Mission Ridge where there are two wind (air) gaps and the elevation of the gaps decreases in the direction of propagation. This is strong evidence that the ridge is propagating westward. Finally, dissection of the fold decreases to the west as does limb rotation (Figure 23).

## **10.0 HYPOTHESIS OF TECTONIC EXTRUSION**

Shortening across the western Transverse Ranges is the result of right-slip and contraction in the vicinity of the “Big Bend” of the San Andreas Fault System (SAF). Right-slip along the “Big Bend” produces (north and south of the SAF) parallel to sub-parallel faults

with predominantly left-slip strike slip faults and reverse faults with a left-slip component (if they have a component of strike-slip).

Major folds and (buried) faults tend to propagate laterally to the west, south of the San Andreas fault, and to the east, north of the SAF. We hypothesize that the lateral propagation of fault rupture during earthquakes will tend to be to the west, south of the SAF; and to the east, north of the SAF (Figure 24) (Keller et al., 1997). North and south of the extrusion zone, plate bounding deformation terminates and this may coincide with the left-lateral, Santa Cruz Island and White Wolf faults, respectively.

The concept of tectonic extrusion has been used in a variety of tectonic settings including the Mediterranean region (McKenzie, 1972); Asia (Tapponnier et al., 1982); and the Los Angeles Region (Walls et al., 1998). The driving mechanisms for each of these locations is somewhat different, depending upon specifics of the regional tectonic framework. In the case of the "Big Bend" of the San Andreas Fault, the extrusion is evidently driven by the contraction produced by the bend in conjunction with the orientation of left-lateral strike-slip faults such as the White Wolf, Santa Ynez and Santa Cruz Island faults. An analogy that has sometimes been drawn is the squeezing of a watermelon seed between the thumb and index finger until it pops laterally. In the case of the "Big Bend" we might envision two watermelons seeds being squeezed with one extruding to the east north of the fault and the second to the west south of the fault.

In order for a fault to propagate laterally it must rupture and displace new ground in the direction of propagation. Thus, earthquake ruptures would hypothetically tend to propagate in the same direction

as the growth of the fault and associated folds. It has been argued that as total fault displacement for repeated earthquakes increases so does total fault length (Cowie and Scholz, 1992; and Jackson et al., 1996). The hypothesis that direction of rupture during earthquakes would tend to be the same as the direction of propagation of the fault that produced the earthquake is highly speculative. This leads to the question: Can we predict lateral direction of rupture during earthquakes? The answer to this question is possibly "yes" in specific instances for buried reverse faults that have produced an anticline with surficial expression for which a single direction of lateral propagation may be determined. In other cases, a fold may propagate laterally in two directions, and some earthquakes may rupture laterally in a direction opposite to the direction of the propagation of the fold. Nevertheless, we hypothesize that the dominant direction of lateral propagation of rupture during moderate to large earthquakes will be in the direction of the fold propagation.

Although there is a very limited data set for which to test the hypotheses of lateral propagation of faulting and folding as well as rupture during earthquake, Table 5 provides some examples from southern California earthquakes. The table lists earthquakes and location relative to the San Andreas Fault, direction of lateral propagation of rupture and lateral component of displacement. Also indicated are whether or not a particular event supports the hypothesis of westward propagation of structure and rupture during earthquake, and predicted left-oblique component of displacement.

The majority of earthquakes for which data is available concerning direction of propagation of rupture and sense of lateral

displacement tend to support the hypothesis that fault rupture during moderate to large earthquakes tends to have a westward component of propagation south of the SAF and an eastward component, north of the SAF. The evidence is particularly good for the 1952 **M<sub>w</sub>** 7.5 Kern County earthquake which is north of the San Andreas fault, has left-oblique displacement during the event, and the rupture propagated to the northeast as indicated by the pattern of aftershocks. The 1975 San Fernando **M<sub>w</sub>** 6.6 earthquake had a left-lateral component of slip which apparently increased from east to west (Palmer and Henyey, 1971), but the direction of propagation of the rupture was up and to the southeast. However, the fault is reasonably far removed from the influence of the "Big Bend" and more likely to be within the tectonic framework of the Los Angeles Basin. The 1978 Santa Barbara earthquake was characterized by left-oblique displacement and there is evidence from the aftershock locations that the direction of propagation of the rupture was to the northwest (Corbett and Johnson, 1982; Yeats and Olson, 1984). Finally the 1994 Northridge **M<sub>w</sub>** 6.7 demonstrated a component of northwest direction of lateral propagation of rupture, based upon aftershock locations (USGS, 1996). Thus the earthquakes of 1952, 1978, and 1994 for which data exists concerning the direction of propagation of rupture, support the hypothesis that there is a tendency for rupture propagation to have an eastward component north of the San Andreas fault and a westward component south of the fault.

This hypothesis has important ramifications for earthquake hazards because earthquake damage is often most severe in the direction of a propagating rupture (Benioff, 1955; USGS, 1996)

(Figure 25). Anticipating potential direction of rupture during earthquakes will allow for better modeling of potential damages to human structures as a result of seismic shaking.

## **11.0 EARTHQUAKE MAGNITUDES**

Estimated moment magnitudes of future earthquakes of seismic sources in the onshore and offshore SBFB are listed on Table 1. Segments of the MRFS vary from 15 to 17 km in length. Assuming these represent earthquake segments then, using the method of Wells and Coppersmith (1994) we estimate a maximum  $M_w$  6.5 earthquake on these segments. If multiple segments were to rupture, then a  $M_w$  6.8 to 7.0 (moment magnitude) earthquake is possible. Assuming a vertical displacement of about 1.0 m per event on a segment of the MRFS, the average return period is approximately 3 ky.

Several seismic sources such as the North Channel Slope, Oak Ridge and Santa Cruz Island faults are capable of producing a  $M_w$  7.1-7.5 event as is the Santa Yñez fault, located about 10 km north of Santa Barbara. We believe that the Oak Ridge fault system and associated fold presents a potentially serious hazard.

Estimated earthquakes are consistent with historic seismicity in the SBFB. In this century two events of M 5.9 (1941 and 1978) occurred offshore of Carpinteria and Goleta, respectively. The 1925  $M_w$  6.8 Santa Barbara earthquake is the 7<sup>th</sup> largest out of 40 earthquakes in southern California with  $M_w$  greater than 6.0 in the 20<sup>th</sup> century (Stein and Hanks, 1998). If this estimated magnitude is correct, then it released about 1.5 times the energy of the 1994  $M_w$

6.7 Northridge earthquake and 2 times as much energy as the 1971 **M<sub>W</sub>** 6.6 San Fernando earthquake. However, Olsen and Sylvester (1975) report the earthquake to be a M 6.3 based on similar seismic records. The 1994 **M<sub>W</sub>** 6.7 Northridge earthquake is a recent example of the most likely earthquake we expect in the future for the SBFB. Unusually large onshore and/or offshore seeps of oil accompanied by small foreshocks may precede some large earthquakes by several hours in the SBFB. Seeps were reported about 3 hours prior to the 1925 earthquake (Hamilton, 1969). Smaller **M<sub>W</sub>** 5-6 earthquakes evidently do not have such precursors or they are too small to be observed

In summary, the Santa Barbara urban corridor is in an area of known seismicity with an earthquake hazard similar to the cities of Ventura and Los Angeles. The city of Santa Barbara is located on the hanging wall of the blind Mission Ridge segment of the MRFS and is subject to amplified shaking during an earthquake as the result of free surface effects of the hanging wall and possible directivity of seismic waves. Parts of the downtown area are susceptible to liquefaction where the historic el estero (salt marsh) has been filled (in part from debris from the 1925 earthquake (Simmons, pers. comm., 1999)) and is susceptible to a tsunami from an earthquake generated in the Santa Barbara Channel. An earthquake on the MRFS or a fault offshore with a maximum **M<sub>W</sub>** 6.5 to **M<sub>W</sub>** 7.5 respectively will cause extensive damage to the Santa Barbara urban area inflicting several hundred million to a billion or more dollars of property damage, with several to several tens of deaths (depending on the time and day of the earthquake) and thousands of injuries.

## **12.0 CONCLUSIONS**

Based upon development of Quaternary stratigraphy and rates of uplift for wave-cut platforms in the Santa Barbara Fold Belt (SBFB) and investigation of active folding and faulting we conclude:

- First emergent marine terraces in the Santa Barbara Fold Belt range in age from 45 ky to 125 ky. That is, oxygen isotope stage 3 or 5.
- Rates of surface uplift for marine terraces in the SBFB is approximately 1 to 2 m/ky. This is approximately an order of magnitude higher than was believed prior to our study.
- Tectonic geomorphology of the SBFB suggests that those areas that are topographically high are for the most part elongated hills which are active anticlines which conceal buried reverse faults. Topographically lower areas within the fold belt such as the alluvial fan and el estero areas of the city of Santa Barbara as well as the Goleta Valley and Carpinteria slough are areas of active subsidence associated with faulted synclines.
- Active folds and reverse faults in the SBFB predominately are propagating to the west, consistent with the hypothesis of tectonic extrusion.
- The most serious earthquake hazard to the Santa Barbara urban area is active faults and folds within the offshore portion of the Santa Barbara Fold Belt in the Santa Barbara Channel. Several sources including the North Channel Slope, Oak Ridge, and Santa Cruz Island faults are capable of producing an **M<sub>w</sub>** 7.1 to 7.5

event, as is the Santa Ynez fault located about 10 km north of Santa Barbara.

- Faults in the onshore SBFB are capable of producing earthquakes of  $M_w$  6.0 to 6.5. If several segments of the Mission Ridge Fault System were to rupture simultaneously an earthquake with magnitude of approximately  $M_w$  7 is possible.
- The most likely scenario for a damaging earthquake to the Santa Barbara urban corridor would be a "Northridge-like event" with  $M_w$  approximately 6.5. The  $M_w$  6.8 Santa Barbara earthquake in 1925 is the seventh largest out of 40 earthquakes in southern California with  $M_w$  greater than 6.0 in the 20th century and a repeat of that event would inflict several hundred million to a billion or more dollars of property damage with several to several tens of deaths (depending upon time of day the earthquake occurs).

### **13.0 ACKNOWLEDGMENTS**

Research on the Santa Barbara Fold Belt is funded by the Southern California Earthquake Center award no. USC 572726 and the U.S.G.S National Earthquake Hazards Reduction Program awards nos. 143HQ97GA-02978 and 99HQGR0081. We thank Brian Baca and Bill Tracy (Santa Barbara County), Roger Slayman (CFS Inc.), Mike Hoover, Dean May (La Cumbre Mutual Water Co.), and Bill Hanna (UCSB) for providing and sharing geotechnical data. Jim Chen conducted u-series analyses of sampled terrace corals. Mike Fuller, Bob Dunn, and Chuck Anderson provided assistance and technical support in sedimentary sampling, preparation and paleomagnetic

analyses. Oxygen isotope analyses were conducted in James Kennett's lab with Karen Thompson's lab assistance. X-ray diffraction analyses of the u-series dated fossil corals was conducted by Sam Iyengar, and XRD of the *Olivella* shells was conducted by Dave Pierce (UCSB). OSL analysis was conducted by J. Spencer and L. Owen from UC Riverside. David Valentine produced DEM graphics, David Crouch and Steve Brown drafted several illustrations, and Yann Ricard provided computer support. We benefited from fruitful discussions in the field with Barry Keller, Butch Brown, and Ray Coudray. The Santa Barbara Parks Department permitted fossil sampling by seacliff repelling at Santa Barbara Point. Reading of the manuscript by A. Selting and T. Tierney is appreciated.

#### **14.0 BIBLIOGRAPHY**

Publications resulting from this project:

Gurrola, L. D. and Kamerling, M. 1996a, Role of cross faults as tears in thrust ramps in the Ventura and Santa Barbara Fold Belts,

California, 1996: Abstracts for the Southern California Earthquake Center Annual Meeting, p. 49.

Gurrola, L. D. and Kamerling, M. 1996b, Segmentation of principal east-west trending reverse/thrust fault and earthquake nucleation sites in the western Transverse Ranges, California: EOS, Transactions, AGU, v. 77, no. 46, p. 512.

Gurrola, L. D. and Keller, E. A. 1998, Active folding of emergent marine terraces: Summerland to Carpinteria, Santa Barbara

- fold belt: California, Geol. Soc. Amer. Abs. with Prog., v. 30, no. 5, p. 17.
- Gurrola, L. D. and Keller, E. A., 1997, Seismic hazards of the Santa Barbara fold belt, California, Geol. Soc. Amer. Abs. with Prog., v. 31, no. 7, p. 474.
- Gurrola, L. D., Keller, E. A., Trecker, M. A., Hartleb, R., and Dibblee Jr., T. W., 1998, Active folding and buried reverse faulting of the Santa Barbara Fold Belt, California: Geol. Soc. Amer. Field Trip Guide Book Number 11, 43 p.
- Gurrola, L. D., Keller, E. A., Dibblee Jr., T. W., Trecker, M., and Hartleb, R. 1999, Active folding and blind reverse faulting of the Santa Barbara Fold Belt, California: Coasts Geological Society Field Trip Guide Book, 86 p.
- Hartleb, R., Keller, E. A., and Gurrola, L.D., 1998, Santa Barbara, CA Flood Hazard: A Story of Paleochannels and Earthquakes: Geol. Soc. Amer. Abs. with Prog., v. 30, no. 5, p. 18.
- Keller, E. A. and Gurrola, L. D. 1997a, Can we predict lateral propagation of rupture during earthquakes? Geomorphic indicators of propagation of reverse faults, Santa Barbara Fold Belt, California: Southern California Earthquake Center Annual Meeting, October 1997 p. 69.
- Keller, E. A., Gurrola, L. D., and Tierney, T., 1999, Geomorphic criteria to determine direction of lateral propagation of reverse faulting and folding: Geology, v. 27, no. 6, p. 515-518.
- Keller, E. A., Gurrola, L. D., and Trecker, M. A. 1998, Geomorphic Criteria to Determine Direction and Rate of Lateral

- Propagation of Reverse Faulting and Folding, Geol. Soc. Amer. Abs. with Prog., v. 30, no. 5, p. 22.
- Keller, E. A., Mueller, K., and Gurrola, L D.1997b, 'Big Bend' of the San Andreas fault: Hypothesis of tectonic extrusion: Geol. Soc. Amer. Abs. with Prog., v. 29, no. 6, p. A-235.
- Ronald, E. C., Keller, E. A., Gurrola, L. D., and Trecker, M. A. 1998, Shoreline Features of the Santa Barbara Fold Belt: A Case of Forensic Seismology: Geol. Soc. Amer. Abs. with Prog., v. 30, no. 5, p. 62.
- Trecker, M. A., Gurrola, L. D., and Keller, E. A., 1998, Oxygen-Isotope correlation of marine terraces and uplift of the Mesa Hills, Santa Barbara, California, USA: In: Stewart, I. S. and Vita Finzi, C. (eds.) Coastal Tectonics: Geological Society of London, Special Publication 146, p. 57-69.

## 15.0 REFERENCES CITED

- Benioff, H., 1955, Mechanism and strain characteristics of the White Wolf fault as indicated by the aftershock sequence. In G. B. Okeshott (ed.) Earthquakes in Kern County, California during 1952. California Division of Mines Bulletin 171, p. 199-202.
- Bloom, A. L., Broecker, W. S., Chappell, J., Matthews, R. K., and Mesolella, K. J. 1974, Quaternary sea level fluctuations on a tectonic coasts; new  $^{230}\text{Th}/^{234}\text{U}$  dates from the Huon Peninsula, New Guinea, Quat. Res. 4, p. 185-205.
- Bull, W. B., 1985, Correlation of flights of global marine terraces, IN: Morisawa, M., and Hack, J., eds., Tectonic Geomorphology.

- Proceedings, Binghamton Geomorphology Symposium, 15th, p. 129-152.
- Chappell, J. 1983, A revised sea-level record for the last 300,000 years from Papua, New Guinea: Search, vol. 14, no. 3-4, p. 99-101.
- Chappell, J. and Shackleton, N. J. 1986, Oxygen isotopes and sea level: Nature, vol. 324, p. 137-140.
- Chappell, J., Omura, A., Esat, E., McCulloch, M., Pandolfi, J., and Pillans, B., 1996, Reconciliation of late Quaternary sea levels derived from coral terraces at Huon Peninsula with deep sea oxygen isotope records, Earth and Planetary Science Letters 141, p. 227-236.
- Chen, J. H., Edwards, R. L., and Wasserburg, G. J., 1986,  $^{238}\text{U}$ ,  $^{234}\text{U}$ , and  $^{233}\text{Th}$  in sea water, Earth and Planetary Science Letters, vol. 80, p. 241-251.
- Corbett, E. J., and Johnson, 1982, The Santa Barbara, California earthquake of 13 August 1978, Bull. Seism. Soc. Amer. 72, p. 2201-2226.
- Cowie, P. A., and Scholz, C. H., 1992, Growth of faults by accumulation of seismic slip, Journal of Geophysical Research 97(B7), p. 11,085-11,095.
- Davis, T. L., 1983, Late Cenozoic structure and tectonic history of the western "Big Bend" of the San Andreas fault and adjacent San Emigdio Mountains [Ph.D. thesis], Santa Barbara, University of California, 508 p.
- Dibblee, T.W., Jr. 1986, Geologic map of the Santa Barbara quadrangle, (Ehrenspeck, ed.), Dibblee Geological Foundation.

- Dibblee, T. W., Jr., 1988, Geology of the Ventura Basin area, in Ventura Basin: Geologic Introduction and Field Trip Guidebook (M. H. Link, ed.), Pac. Sec. Amer. Assoc. Petroleum Geologists and Los Angeles Basin Geological Society, p. 7-18.
- Gurrola, L. D. 1993, Structural analysis of a fault-propagation fold and tectonic geomorphology of the Summerland coastal region, Summerland, California, unpub. research report, University of California, Santa Barbara, 21 p.
- Gurrola, L. D. and Kamerling, M. 1996, Role of cross faults as tears in thrust ramps in the Ventura and Santa Barbara Fold Belts, California, 1996: Abstracts for the Southern California Earthquake Center Annual Meeting, p. 49.
- Gurrola, L. D. and Keller, E. A. 1997b, Tectonic geomorphology of the Santa Barbara fold belt, western Transverse Ranges, California: GSA abstracts with programs, vol. 29, no. 6, p. 344-345.
- Gurrola, L. D. and Keller, E. A. 1997c, Style of Quaternary Deformation of an Active Fold Belt: The Santa Barbara Fold Belt, Western Transverse Ranges, California: EOS, Transactions, AGU, vol. 78, no. 46, p. F632.
- Gurrola, L. D., Chen, J. H., and Keller, E. A., 1997a, Uranium-series age and rate of uplift of the Mesa marine terraces, Santa Barbara Fold Belt, California: Southern California Earthquake Center Annual Meeting, October 1997 p. 64.
- Gurrola, L. D., Chen, J. H., Keller, E. A., and Metcalf, J. G. 1996, Dating of emergent marine terraces and rate of uplift for the

- western Santa Barbara Fold Belt, California: GSA Abstracts with Programs, vol. 28, no. 7, p. A-301.
- Gurrola L. D., Keller, E. A., Dibblee Jr., T. W., Dolan, J., Campbell, S., and Hoover, M. 1998 Active Folding of Emergent Marine Terraces; Summerland to Carpinteria, Santa Barbara Fold Belt, California. The Geological Society of America, Abstracts with Programs, Cordilleran Section, 30(5):8107.
- Hamilton, R. M., 1969, Geology, petroleum development, and seismicity of the Santa Barbara channel region, California, U.S. Geological Survey Professional Paper 1044-9612, p. 47-68.
- Hauksson, E., and Jones, L. M., 1989, The 1987 Whittier Narrows earthquake sequence in Los Angeles, southern California: Seismological and tectonic analysis, Jour. Geophys. Res. 94(7), p. 9569-9589.
- Hoover and Associates, 1985, Unpublished report.
- Izett, G. A., Naeser, C. W., Obradovich, J. D., 1974, Fission track age of zircons from an ash bed in the Pico Fm (Pliocene and Pleistocene) near Ventura, California, in GSA Abstracts with Programs 6(3), p. 197.
- Jackson, P.A., 1981, Structural evolution of Carpinteria basin, western Transverse Ranges, California, unpub. M.S. thesis, Oregon State University, 107 p.
- Jackson, P. A. and Yeats, R. S. 1982, Structural evolution of the Carpinteria basin, western Transverse Ranges, California: The American Association of Petroleum Geologist Bulletin, vol. 66, no. 7, p. 805-829.

- Jackson, J., Norris, R., and Youngson, J 1996, The structural evolution of active fault and fold systems in central Otago, New Zealand; evidence revealed by drainage patterns: *Jour. Struct. Geol.*, vol. 18, no. 2-3, p. 217-234.
- Keller, E. A., Gurrola, L. D., and Tierney, T., 1999, Geomorphic criteria to determine direction of lateral propagation of reverse faulting and folding: *Geology*, v. 27, no. 6, p. 515-518.
- Keller, E. A., Mueller, K., and Gurrola, L D.1997, 'Big Bend' of the San Andreas fault: Hypothesis of tectonic extrusion: GSA abstracts with programs, vol. 29 no. 6, p. A-235.
- Kern, J. P. 1977, Origin and history of upper Pleistocene marine terraces, San Diego, California: *Geol. Soc. Amer. Bull.*, vol. 88, p. 1553-1566.
- Lajoie, K. R., Sarna-Wojcicki, A. M., and Yerkes, R. F. 1982, Quaternary chronology and rates of crustal deformation in the Ventura area, California, In: Cooper, J. D., ed., *Neotectonics in southern California, Guidebook for fieldtrips*, Anaheim, CA, p. 43-51.
- Lajoie, K. R., Kern, J. P., Wehmiller, J. F, Kennedy, G. L, Mathieson, S. A., Sarna-Wojcicki, A. M., Yerkes, R. F. and McCrory, P. F. 1979, Quaternary marine shorelines and crustal deformation, San Diego to Santa Barbara, California, In: Abbot, P. L., ed., *Geological excursions in the southern California area: Guidebook for field trips*, GSA Annual Meeting, Nov. 1979, Department of Geological Sciences, San Diego State University, San Diego, CA., p. 3-16.

- Luyendyk, B. P., 1991, A model for Neogene crustal rotations, transtension, and transpression in southern California, Geological Society of America Bulletin 103(11), p. 1528-1536.
- MacKenzie, D. 1972, Active tectonics of the Mediterranean region: R. Astron. Soc. Geophys., vol. 30, no. 2, p. 109-185.
- Matthews, R. K. 1973, Relative elevation of Late Pleistocene high sea level stands: Barbados uplift rates and their implications, IN: CLIMAP program, Quat. Res., vol. 3, no. 1, p. 147-153.
- Muhs, D. R., Rockwell, T. K., and Kennedy, G. L. 1992, Late Quaternary uplift rates of marine terraces on the Pacific Coasts of North America, southern Oregon to Baja California Sur, IN: Impacts of tectonics on Quaternary coastal evolution, Quat. Inter., vol. 15-16, p. 121-133.
- Muhs, D. R., Rockwell, T. K., and Kennedy, G. L. 1994a, Uranium-series ages of marine terrace corals from the Pacific Coast of North America and implications for last-interglacial sea level history, Quaternary Research, vol. 42, p. 72-87.
- Muhs, D. R., Miller, G. H., Whelan, J. F., and Kennedy, G. L. 1994b; Aminostratigraphy and oxygen isotope stratigraphy of marineterrace deposits, Palos Verdes Hills and San Pedro areas, Los Angeles County, California, In: Quaternary Coasts of the United States: Marine and Lacustrine Systems, SEPM Special Publication no. 48, p. 363-376.
- Namson, J. and Davis, T. 1992, Late Cenozoic thrust ramps of Southern California: Final report of 1991 to the Southern California Earthquake Center.

- Okeshott, G. B. (ed.), 1955, Earthquakes in Kern County, California during 1952. California Division of Mines Bulletin 171, 277 p.
- Olson, D. J., 1982, Surface and subsurface geology of the Santa Barbara-Goleta metropolitan area, Santa Barbara County, California: Unpub. M .S. thesis, Oregon State University, 71 p.
- Olsen, P. G., and Sylvester, A. G., 1975, The Santa Barbara earthquake, 29 June 1925: California Geology, vol. 28, no. 6, p. 123-131.
- Palmer, D. F., and Henyey, T. L., 1971, San Fernando earthquake of 9 February 1971, Pattern of faulting, Science, v. 172, p. 712-715.
- Southern California Earthquake Center, 1995, Seismic Hazards in Southern California: Probable Earthquakes, Working Group on California Earthquake Probabilities, Bull. Seis. Soc. Amer., vol. 85, no. 2, p. 379-439.
- Spencer J. and Owen, L., 1999, Luminescence Dating of Santa Barbara Terraces/Raised Beaches: Preliminary Results, unpub. report, 22 p.
- Stein, R. S., and Hanks, T. C., 1998, M>6 earthquakes in southern California during the twentieth century: No evidence for seismicity or moment deficit, Bull. Seis. Soc. Amer. 88(3), p. 635-652.
- Suppe, J., 1985, Principles of Structural Geology: Prentice-Hall, Englewood Cliffs, New Jersey, 537 p.
- Suppe, J., 1997, Mapping and kinematic analysis of compressive growth structure to define slip rates, Princeton University, 154 p.

- Suppe, J., and Medwedeff, D. A., 1984, Fault-propagation folding: Geol. Soc. Amer. Abst. Prog. vol. 16, p. 670.
- Suppe, J., and Medwedeff, D. A., 1990, Geometry and kinematics of fault-propagation folding: Eclogae geol. Helv. vol. 83, no. 3, p. 409-454.
- Sylvester, A. G. and Mendes, S. H. 1981, Case Studies of Earthquake Damage and Repair: Earthquake History of Santa Barbara, contributions by Hart, G. C. and Huang, S., Guidebook for the Field Seminar; Annual Meeting of the Earthquake Engineering Research Institute, 56 pp.
- Tapponnier, P., Peltzer G., Ledan, A.Y. 1982, Propagating extrusion tectonics in eastern Asia: EOS, vol. 63, no. 45. p. 1097.
- Trecker, M.A., 1999, Oxygen isotope stratigraphy as a means of correlating deformed marine terraces, unpub. M. S. thesis, Univ. Calif., Santa Barbara, 74 pp.
- Trecker, M. A., Gurrola, L. D., and Keller, E. A. 1998, Oxygen Isotope Correlation of Marine Terraces and Uplift of the Mesa Hills, Santa Barbara, California: U.S.A, IN: Stewart, I.S and Vita-Finzi, C. (eds), Coastal Tectonics, Geol. Soc. London, vol. 146, p. 57-69.
- United States Geological Survey, 1996, USGS response to an urban earthquake Northridge '94, U.S.G.S. Geol. Surv. Open File Report 96-263, 78 pp.
- Voelker, A., Sarnthein, M., Grootes, P., Erlenkeuser, H., Laj, C., Mazaud, A., Nadeau, M., and Schleicher, M., 1998, Correlation of Marine  $^{14}\text{C}$  Ages from the Nordic Seas with the GISP2 Isotope Record: Implications for  $^{14}\text{C}$  Calibration Beyond 25 ka BP, Radiocarbon, vol. 40, no. 1, p. 517-534.

- Wallace, R (ed.) 1990, The San Andreas Fault System, California: U. S. Geol. Surv. Prof. Paper 1515, 283 p.
- Walls, C., Rockwell, T., Mueller, K., Bock, Y., Williams, S., Pfanner, J., Dolan, J., and Fang, P., 1998, Escape tectonics in the Los Angeles metropolitan region and implications for seismic risk, *Nature*, vol. 394, p. 356-360.
- Wells, D. L., and Coppersmith, K. J., 1994, New empirical relationships among magnitude, rupture length, rupture width, rupture area, and surface displacement, *Bull. Seis. Soc. Amer.* 84(4), p. 974-1002.
- Willis, B., 1925, A study of the Santa-Barbara earthquake of June 29, 1925: *Seis. Soc. Amer. Bull.*, vol. 15, no. 4, p. 255-278.
- Yeats, R. S. and Olson, D. J., 1984, Alternate fault model for the Santa Barbara, California earthquake of 13 August 1978: *Seis. Soc. Amer. Bull.*, vol. 74, no. 5, p. 1545-1553.

Table 1. Seismic sources of the onshore and offshore Santa Barbara Fold Belt with fault/fold dimensions, activity, and maximum expected earthquake ( $M_w$ ) are determined using the methodology of Wells and Coppersmith (1994). Names of seismic source abbreviations for Figure 1 are in parenthesis.

Fault	Folds(s)	Length (km) <sup>a</sup>	Slip	Vertical rate of faulting (m/ky)	Activity <sup>b</sup>	Max. $M_w$
<i>Mission Ridge System</i>						
More Ranch segment (MrR)	Ellwood, UCSB, More Mesa anticlines	15	Oblique: reverse-left	0.3	Apparently active	6.4
Mission Ridge segment (MsR)	Mission Ridge, Montecito, Eucalyptus Hill, and Barker Pass anticlines	17	Reverse-(left?)	0.3 – 0.4	Apparently active	6.5
west and east Arroyo Parida segments (AP)		17 15	Oblique: reverse-left	0.4 (Ojai, CA)	Potentially active	6.5 6.4
<i>Northwest striking sources</i>						
Mesa (MF)	Mesa anticline Honda Valley syncline	12	Reverse	Unknown	Potentially active	6.3
Lavigia (LF)	Hope Ranch anticline	15	Reverse	0.1	Potentially active	6.4
San Jose (SJ)	Goleta Valley anticline	7	Reverse-(oblique?)	Unknown	Potentially active	6.1
San Pedro (SP)	unnamed anticlines	8	Oblique: Reverse-left	Unknown	Potentially active	6.1
Loon Point(LP)	Loon Point anticline	1	Reverse	Unknown	Active	5.1
Ortega Hill (OH)	Ortega Hill anticline	1	Reverse-(oblique?)	Unknown	Potentially active	5.1
Santa Barbara Cemetery(SBC)	Santa Barbara Cemetery anticline	1	Reverse	0.1	Apparently active	5.1
Los Carneros (C)		7	Left	Unknown	Potentially active	6.1
Dos Pueblos (DP)		6	Left	Unknown	Potentially active	6.0
<i>Offshore sources</i>						
Oak Ridge(OR)	Oak Ridge trend	90	Reverse	3.5 to 6.0	Active	7.5 <sup>c</sup>
Pitas Point (PP)	Pitas Point trend	22	Left-reverse	Unknown	Potentially active	6.6 <sup>c</sup>
Red Mountain (RM)		39	Reverse	0.4 to 1.5	Apparently active	6.8 <sup>d</sup>
Rincon Creek (RC)	Rincon Creek anticline	20	Reverse	0.3	Apparently active	6.6
North Channel Slope(NCS)		60	Reverse	2.0	Apparently active	7.1 <sup>d</sup>
Mid Channel (MC)		20	Reverse	Unknown	Active	6.6
Coal Oil Point (COP)	Coal Oil Point anticline	4	Reverse	Unknown	Apparently active	5.8
<i>Other sources</i>						
Santa Yñez		130	Left-reverse	0.1 to 0.7	Active	7.5 <sup>c</sup>

- a. We assume fault length is the surface rupture length and may be slightly different than map lengths of seismic sources shown on Figure 1.
- b. Active = demonstrated Holocene (last 10,000 yr.) activity;  
Apparently Active = very young (probably Holocene) topographic expression of activity;  
Potentially Active = active in Pleistocene (last 1.65 million years)
- c. Data from Southern California Earthquake Center (SCEC, 1999)
- d. Data from California Division of Mines and Geology (1999)

Table 2. Table of regional historic seismicity of the Santa Barbara Fold Belt  
(Nicholson, pers. comm., 1999).

Date	Magnitude	Location	Modified Mercalli Scale (MM)	Damage	Measured or Inferred Peak Accel. (g)	Estimated Peak Accel. at Santa Barbara	Distance to Santa Barbara (km)
24 Mar., 1806	?	?	?	Damage to Mission Santa Barbara and Royal Presidio	?	0.05-0.10	?
21 Dec., 1812	7.1+	Santa Barbara Channel	X-XI	Destroyed La Purisma Mission (near Lompoc) and Santa Barbara Mission; tsunami?	0.60+	0.20-0.40	< 50
9 Jan., 1857	8.2 +	San Andreas fault	X+	Ruptured 300 km of the San Andreas fault; intensity VI-VII at Santa Barbara; > 90 sec. of shaking	0.80+	0.10+	60-190
27 July to 12 Dec., 1902	6.0?	near Los Alamos	VIII-IX	Several EQ's totally destroy Los Alamos	0.40-0.50	0.05	60
29 June, 1925	6.3 or 6.8	Santa Barbara	VIII-IX	Extensive damage to downtown Santa Barbara and city	0.50-0.60	0.40-0.60	< 5
29 June, 1926	5.5?	Santa Barbara	VIII	Moderate damage to Santa Barbara; aftershock of 1925 EQ	0.30	0.20	< 5
4 Nov., 1927	7.3	off Pt. Arguello	VIII+	Tsunami (2m) generated along coast; slight damage to Santa Barbara	0.60++	0.10	100
30 June, 1941	5.9	offshore Carpinteri	VII	Slight damage to Santa Barbara	0.40-0.50	0.10	10
21 July, 1952	7.7	Kern County	XI	Moderate damage to Santa Barbara; liquefaction along Laguna Street paleochannel	0.80+	0.15	85
5 July, 1968	5.2	Santa Barbara Channel	VI	EQ swarm with largest event causing slight damage to Santa Barbara	0.20	0.07-0.10	15
13 Aug., 1978	5.9	off Goleta Pt.	VII-VIII	Moderate damage mainly to UCSB campus	0.44	0.28	< 5

Table 3. Generalized stratigraphic section of the Santa Barbara Fold Belt, California (modified after Dibblee, 1966; Olson, 1982).

SERIES	FORMATION	DESCRIPTION	ESTIMATED THICKNESS
Plio-Pleistocene	Holocene alluvium older alluvium and gravels, fanglomerate Qa, Qoa, Qog, Qf	Gravel, sand, silt; non-marine Older alluvium: gravel, sand, silt; marine terrace deposits capping coastal mesas Fanglomerate: boulders, gravel, sand; non-marine	0 - 75 m (0 - 250')
	Casitas Qca	Buff to brownish-gray pebbly sandstone and cobble gravel; non-marine	?
	Santa Barbara Qsb not in contact	Yellow, fossiliferous, fine sand, local consolidated sandstone, and minor siltstone and claystone; marine (<790 ka in Santa Barbara Fold Belt)	0 - 900 m (0 - 3000')
	"Pico"	Blue-gray siltstone, fine-grained sandstone with a fossiliferous basal conglomerate; marine	
	Sisquoc Tsq	Diatomaceous clay-shale and siltstone; marine	0 - 245 m (0 - 800')
Miocene	Monterey Tm, Tml	Dark brown, laminated siliceous shale, mudstone, and siltstone; bentonite at base; marine	425 - 670 m (1400 - 2200')
	Rincon Tr	Gray to dark brown mudstone and siltstone with occasional bentonite beds and carbonate lenticules; marine	425 - 520 m (1400 - 1700')
Oligocene	Vaqueros Tvq	Gray, thick-bedded sandstone; marine	100 m (325')
	Sespe Tsp, Tspss	Predominantly red sandstone, shale, and conglomerate interbedded with gray to green siltstone; non-marine	760 - 900 m (2500 - 3000')
Eocene	Coldwater Tcw, Tcwsh	Gray, arkosic sandstone, minor siltstone; marine	1000 m (3300')

Table 4. Uranium-series, radiocarbon, and optically stimulated luminescence age results from terraces in the SBFB.

Sample Location – Terrace Site	Sample Number	Uranium Series Age (ka) <sup>a</sup>	Measured C14 Age (RCYBP) <sup>b</sup>	Measured Luminescence Age <sup>c</sup> (ka)	
				Quartz	K-feldspar
UC Santa Barbara- Isla Vista terrace	IV-1-96 IV-2-98	47 +/- 0.5	43,790 +/- 770		40 +/- 3
Ellwood terrace	C-5		35,860 +/- 570		
Ellwood terrace	C-12		37,000 +/- 570		
Ellwood terrace	C-14		47,020 +/- 1,500		
More Mesa terrace	MM-1-96 MM-2-98		36,830 +/- 330		53 +/- 7
Santa Barbara City College terrace	SBCC-1-98 SBCC-2-98	70 +/- 2.0		109 +/- 23	
Santa Barbara Point	SBP-1-98			336 +/- 64 <sup>d</sup>	58 +/- 11
Santa Barbara Cemetery	SBC-1-98				79 +/- 10
Summerland terrace Loon Point	LP-1-96 LP-2-98		3,990 +/- 40 yr	105 +/- 15	167 +/- 15 <sup>d</sup>

a. Uranium-series and luminescence ages are reported as 1 ka = 1,000 years before present.

b. Radiocarbon samples were submitted to Beta Analytic Laboratory for AMS analysis and ages are designated as radiocarbon years before present (RCYBP).

c. Optically stimulated luminescence age estimates are based on analysis of quartz and K-feldspar grains (Spencer and Owen, 1999).

d. Results are considered maximum ages and the date (336 +/- 64 ka) at Santa Barbara Point and the date (167 +/- 15) at Loon Point are considered unlikely because: 1) the first emergent terrace at Santa Barbara City College has a U-series age of 70 +/- 2 ka, and 2) first emergent terraces throughout the Santa Barbara-Ventura region (when dated) are no older than 125 ka.

Table 5. Selected examples of southern California earthquakes.

Earthquake	Approximate Magnitude	Location Relative To San Andreas Fault	Direction of Lateral Propagation of Rupture	Aftershock Locations	Lateral Component of Displacement	Supports Hypothesis? YES (Y) NO (N)	Comments References
1925 Santa Barbara	6.3	south	west (?)	not known	probably left-oblique		many uncertainties
1952 Kern Co.	7.5	north	northeast	all northeast	left-oblique	Y (displacement)	Oakeshott, 1955
1971 San Fernando	6.6	south	probably to southeast	mostly southeast	left-oblique	Y (displacement) N (propagation)	left-lateral component of slip apparently increases east to west (Palmer and Henyey, 1971)
1978 Santa Barbara	5.9	south	northwest	northwest	left-oblique	Y	Corbett & Johnson, 1982; Yeats & Olson, 1984
1994 Northridge	6.7	south	northwest	mostly northwest	not known	Y	USGS, 1996

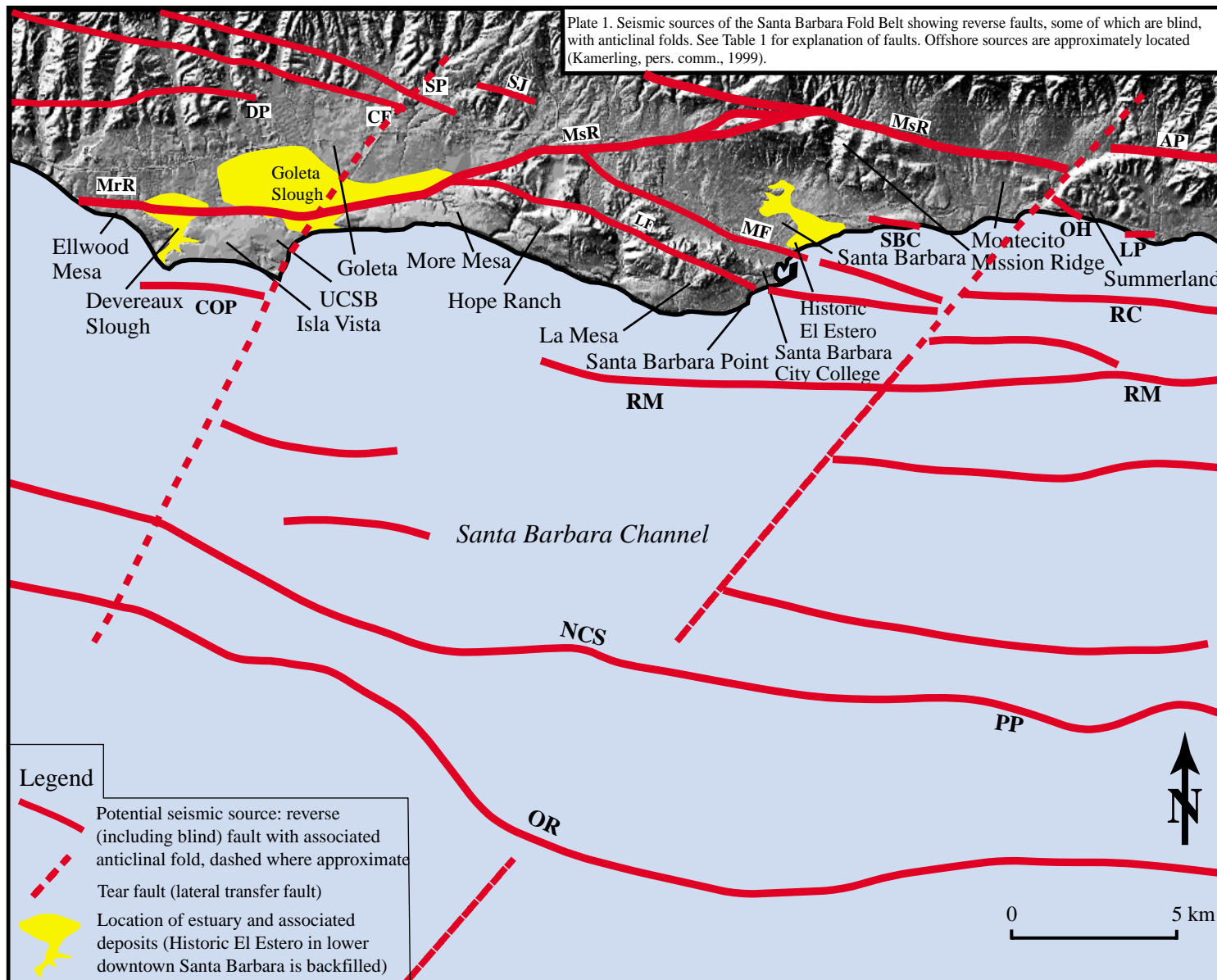


Figure 1. Seismic sources of the Santa Barbara Fold Belt showing reverse faults, some of which are blind, with anticlinal folds. Offshore sources are approximately located (Kamerling, pers. comm., 1999). The Mission Ridge Fault System is subdivided into the More Ranch (MrR), the Mission Ridge (MsR), and the Arroyo Parida (AP) segments. Additional onshore seismic sources include the Dos Pueblos (DP), the Carneros (CF), the San Jose (SJ), the San Pedro (SP), the Lavigia (LF), the Mesa (MF), the Santa Barbara Cemetery, the Ortega Hill (OH), and the Loon Point (LP) faults.

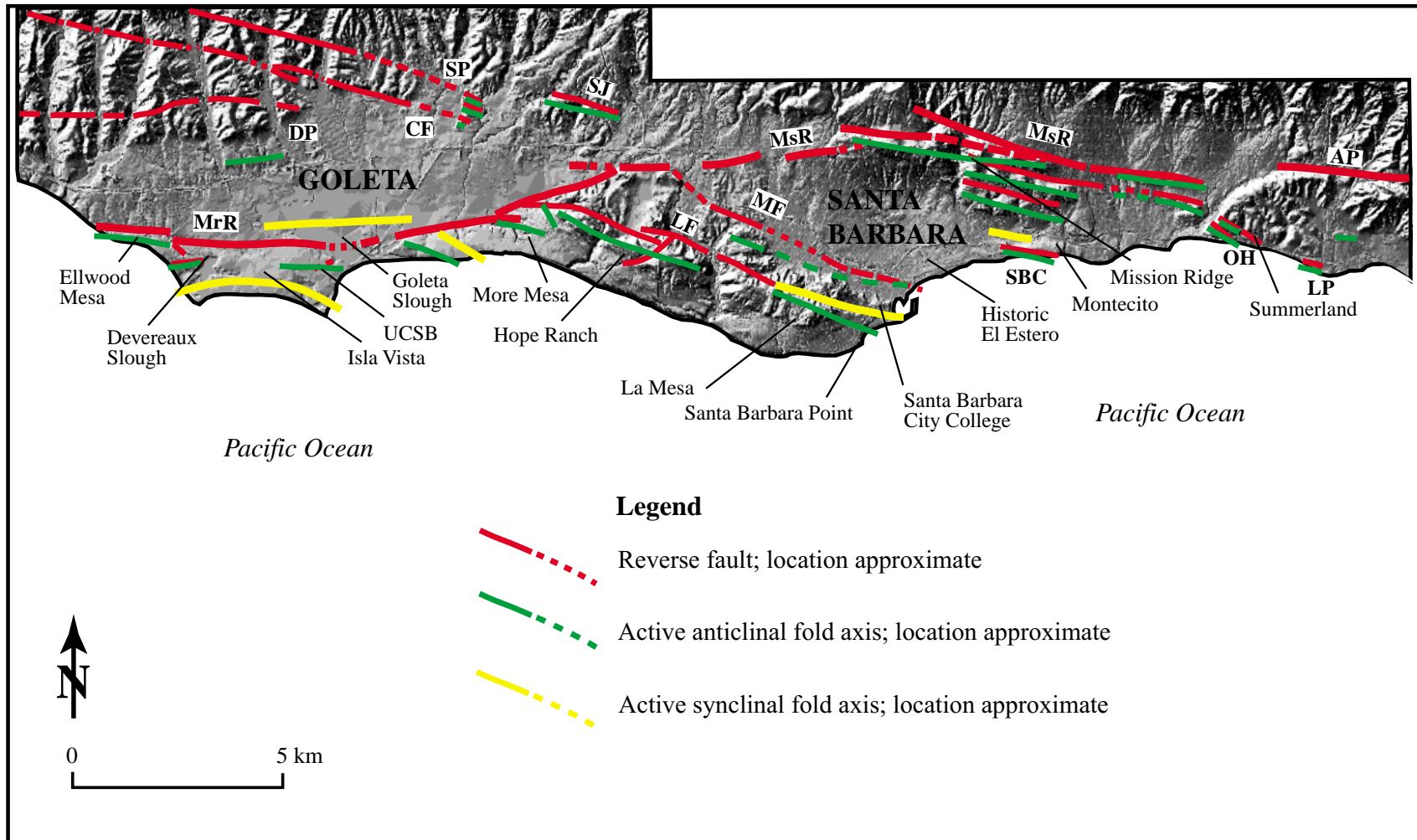
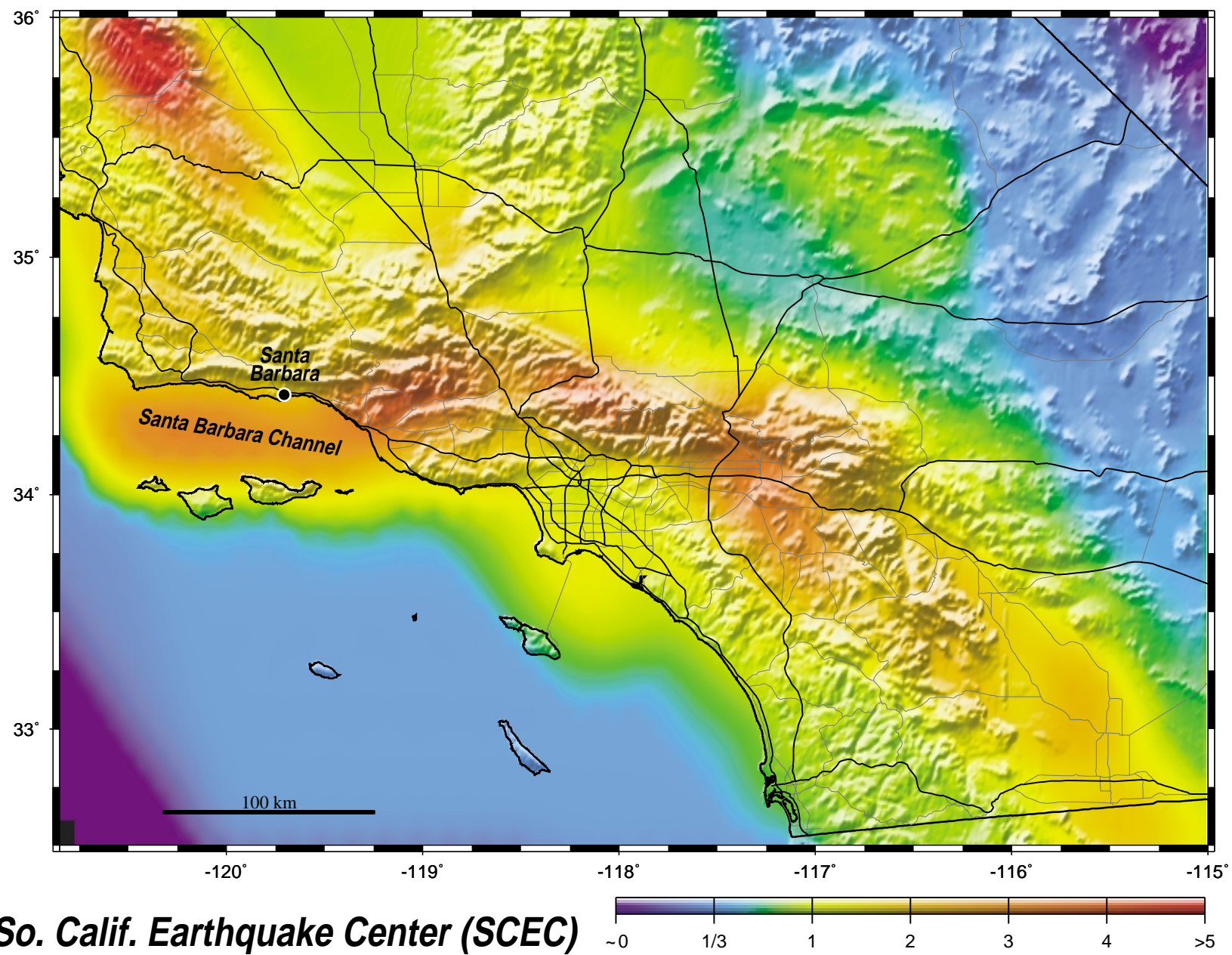


Figure 2. Seismic sources of the onshore Santa Barbara Fold Belt showing south-dipping, reverse faults, some of which are blind, with associated north-verging, hanging wall anticlines and footwall synclines. The Mission Ridge Fault System is subdivided into the More Ranch (MrR), the Mission Ridge (MsR), and the Arroyo Parida (AP) segments. Additional onshore reverse faults include the Dos Pueblos (DP), the Carneros (CF), the San Jose (SJ), the San Pedro (SP), the Lavigia (LF), the Mesa (MF), the Santa Barbara Cemetery (SBC), the Ortega Hill (OH), and the Loon Point (LP) faults.



**So. Calif. Earthquake Center (SCEC)**

GMT Feb 2 13:06

Computer graphics by Ken Hudnut (USGS - Pasadena)

Figure 3. Relative seismic hazard for southern California (SCEC, 1995).

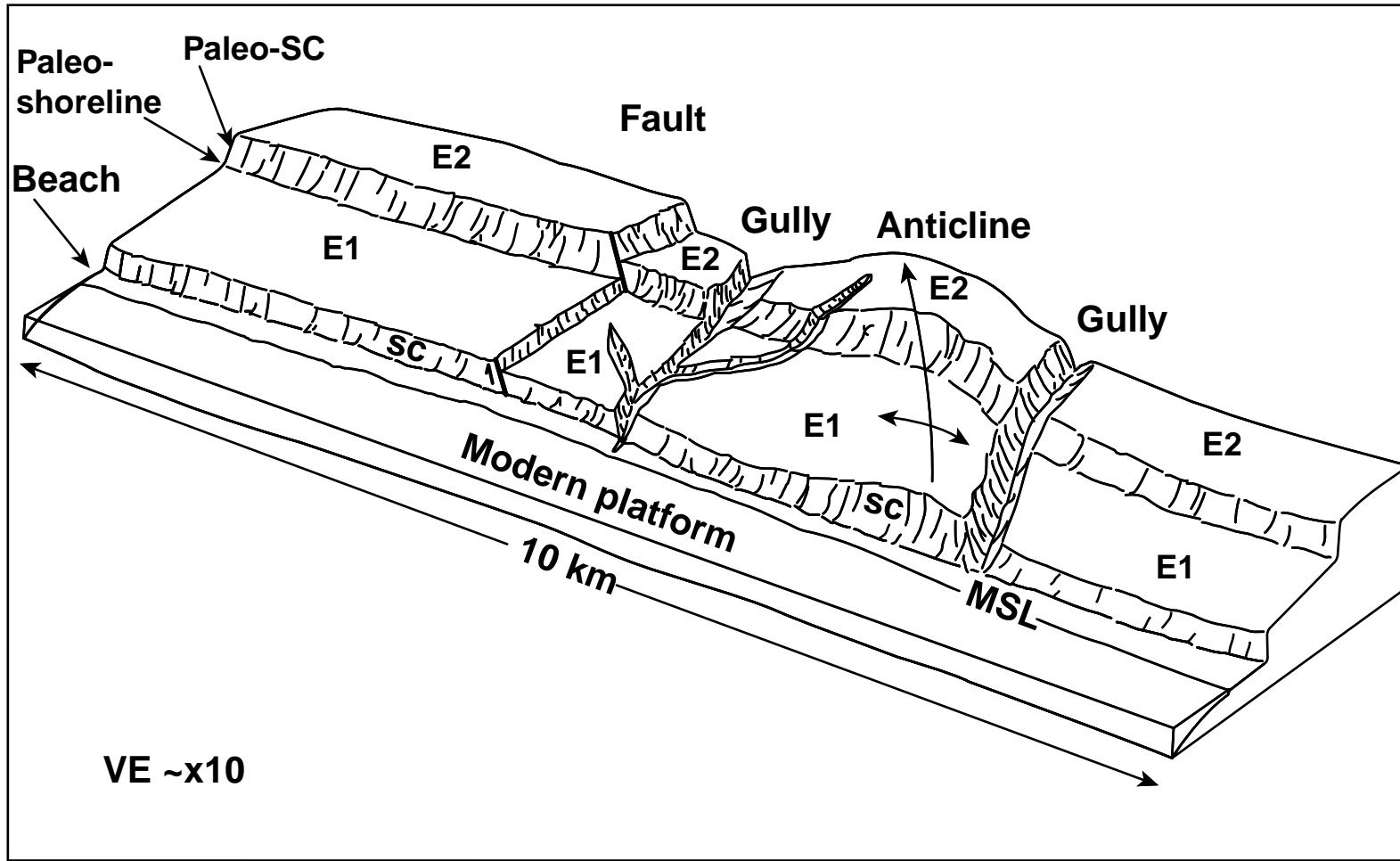


Figure 4. Idealized diagram of a modern wave-cut platform and associated sea cliff (SC) and relation to uplifted marine terraces and associated morphology. The first emergent marine terrace is (E1) and the second emergent terrace (E2) is the next higher terrace. The elevation of the buried marine platform and the associated paleo-sea cliff (Paleo-SC) defines the terrace shoreline angle. The elevation of the terrace shoreline angle is measured in order to calculate total amount of vertical surface uplift. Note that uplifted marine terraces are discontinuous □ and folded, complicating their correlation (modified after Trecker et al., 1998).

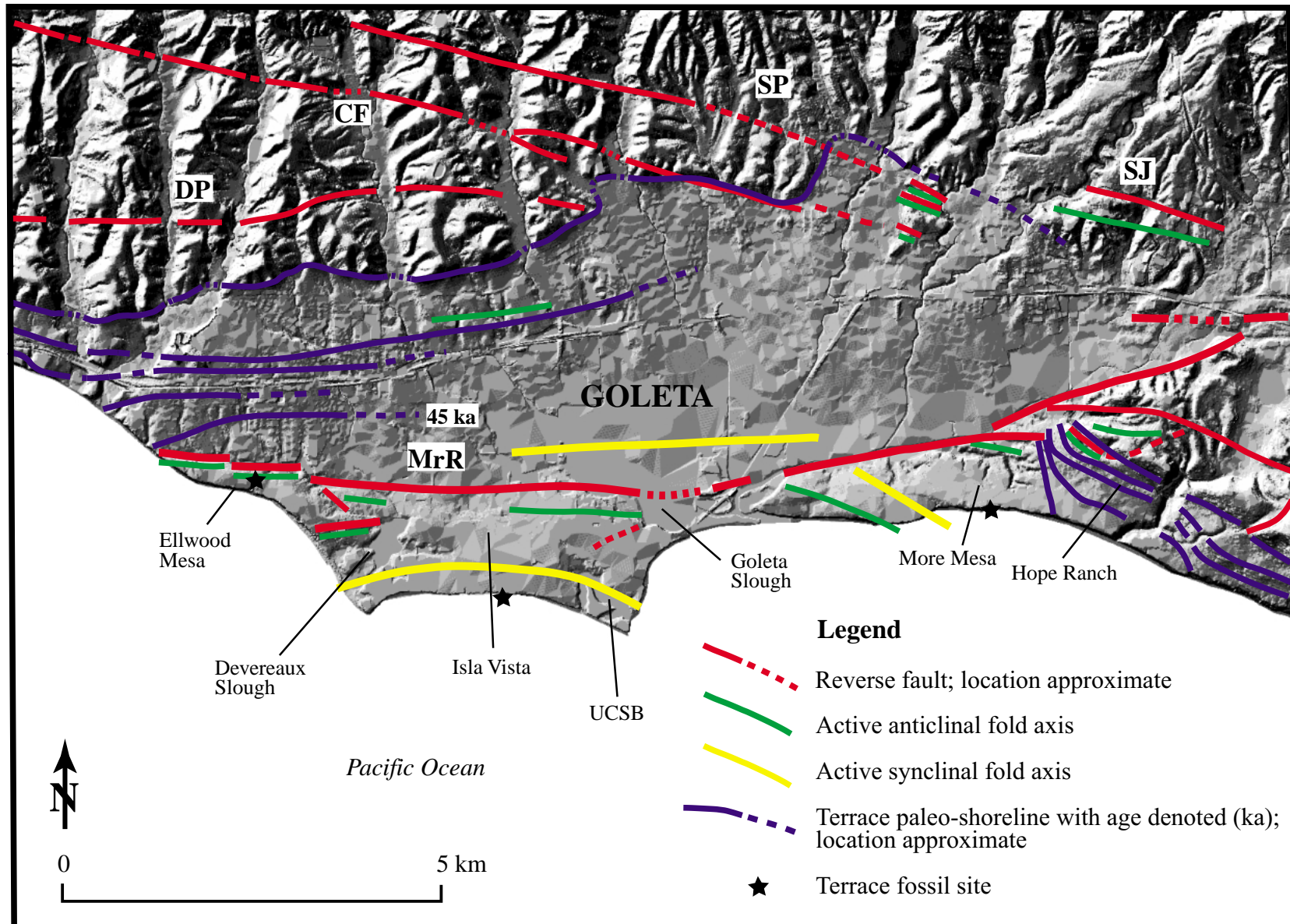


Figure 5. Geomorphic map of the Ellwood and UC Santa Barbara campus area showing shoreline angle and the positions of the associated paleo-shorelines. Note that the paleo-shorelines are discontinuous at drainages and eroded across the More Ranch fault (MrR). Other faults include the Carneros (CF), the Dos Pueblos (DP), the San Jose (SJ), and the San Pedro (SP) faults.

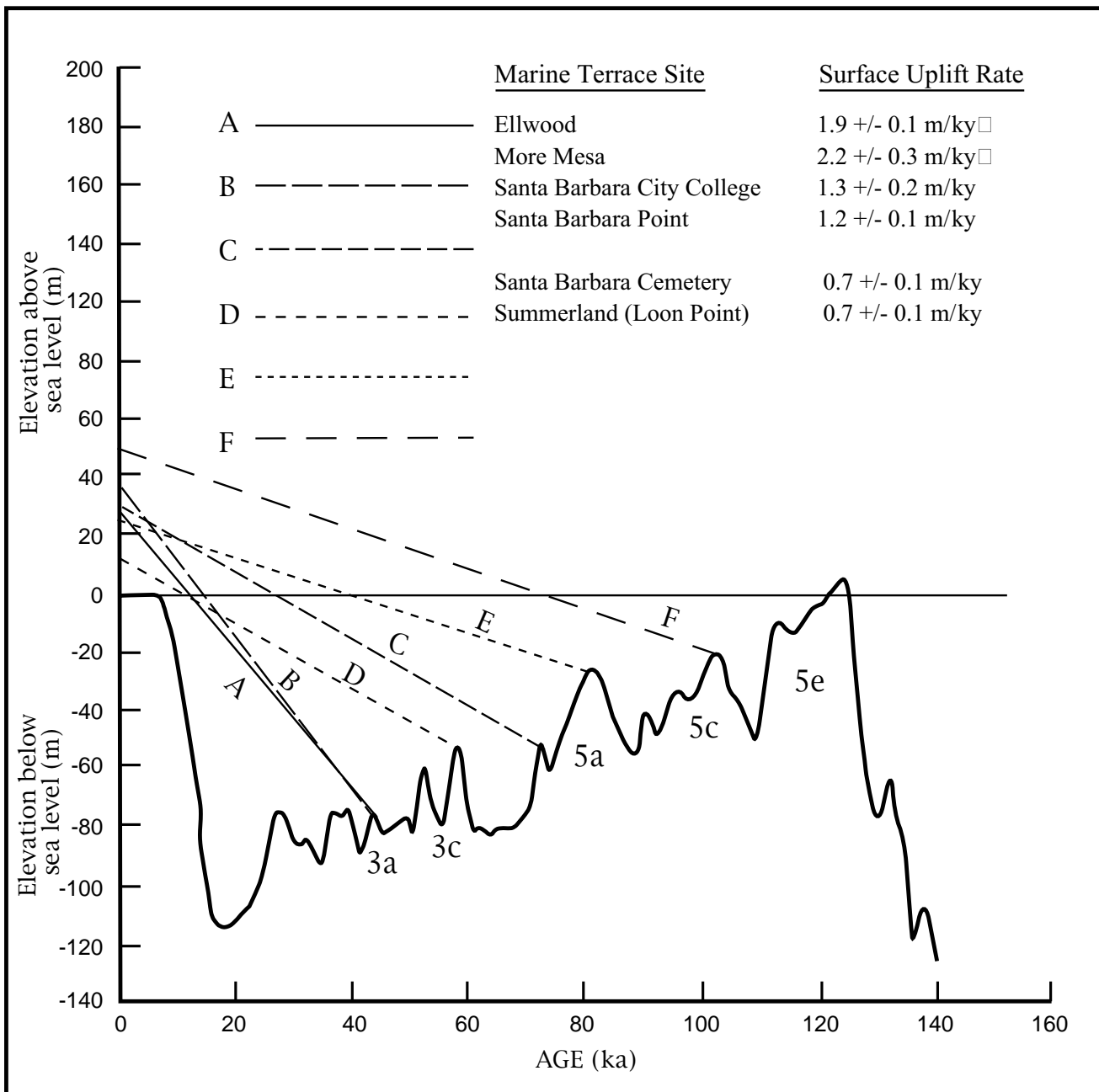


Figure 6. Graph of the late Pleistocene sea level curve (Chappell and others, 1996) with the elevations of the shoreline angles of the first emergent terraces in the SBFB. The elevations and ages of the first emergent terraces are plotted, and the slope of the resultant line is the rate of surface uplift (m/ky) for that terrace.

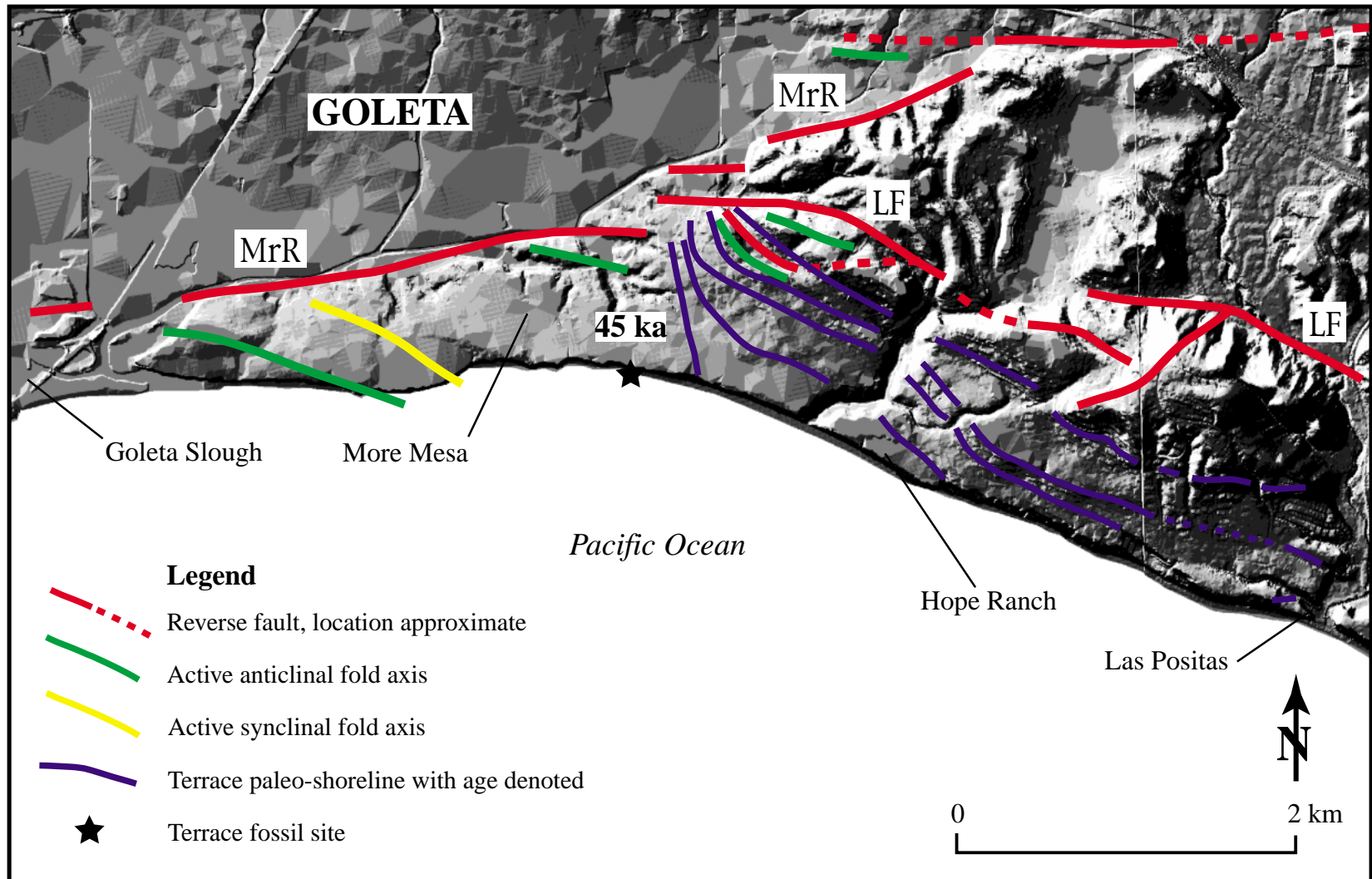


Figure 7. Geomorphic map of More Mesa marine terraces on the hangwing wall of the More Ranch (MrR) and Lavigia (LF) faults. The position of the five emergent terraces and associated paleo-shorelines are shown. The first emergent terrace is age-dated at approximately 42 ka and correlated to isotope substage 3a and yields a surface uplift rate of  $2.2 \pm 0.2$  m/ky.

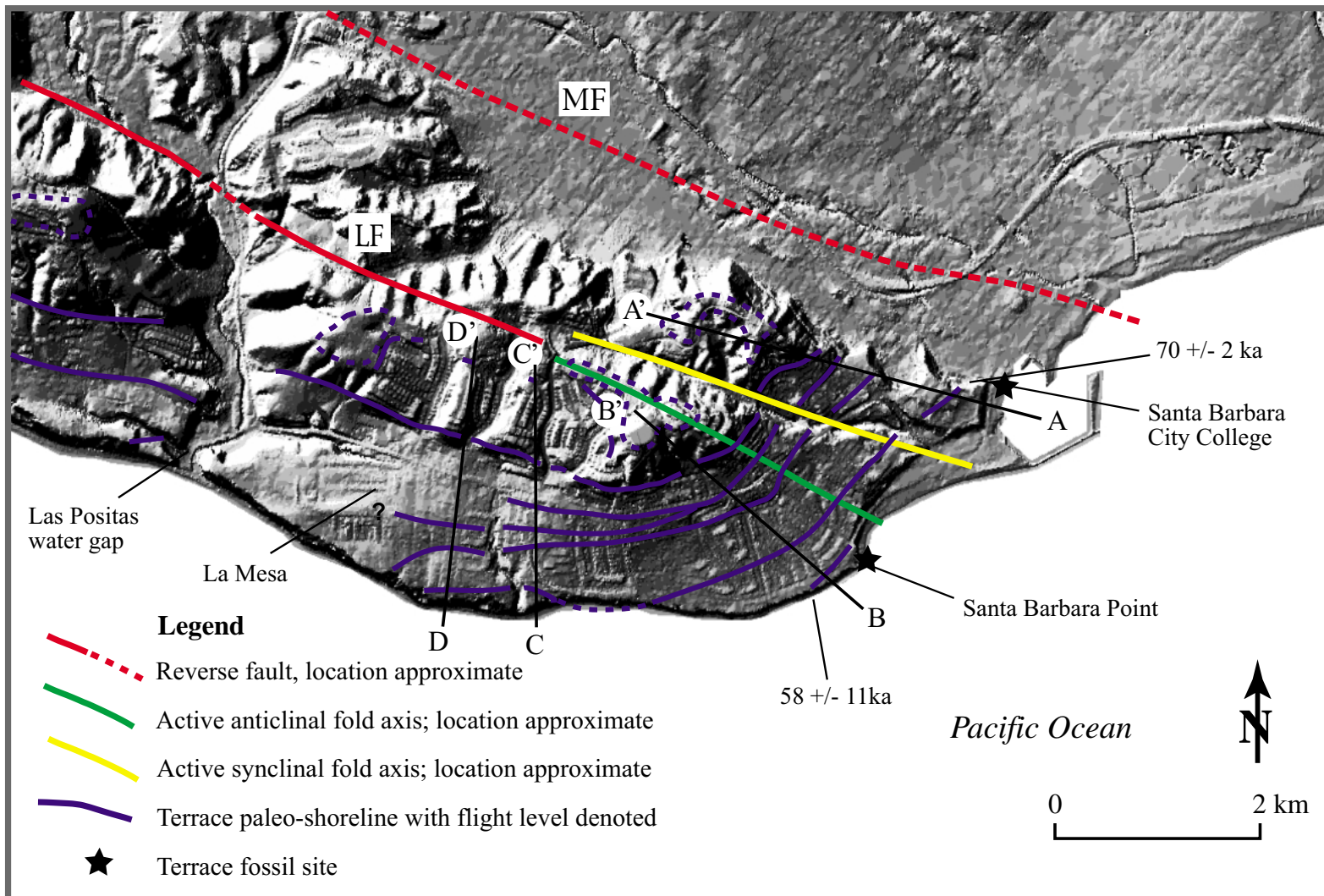


Figure 8. Geomorphic map of the La Mesa anticline and uplifted, marine terraces: (La Mesa fault (MF) and Lavigia fault (LF)). Flights of marine terraces (denoted 1, 2, 3, etc.) are preserved on the south flank and the nose of the east-plunging La Mesa anticline. Sites where u-series and OSL age-dates are labelled and are correlated across the Las Positas water gap. They are truncated by the blind, south-dipping MF. The LF forms a well-expressed fold scarp east of the Las Positas water gap and is expressed as an anticlinal-synclinal fold sequence to the west.

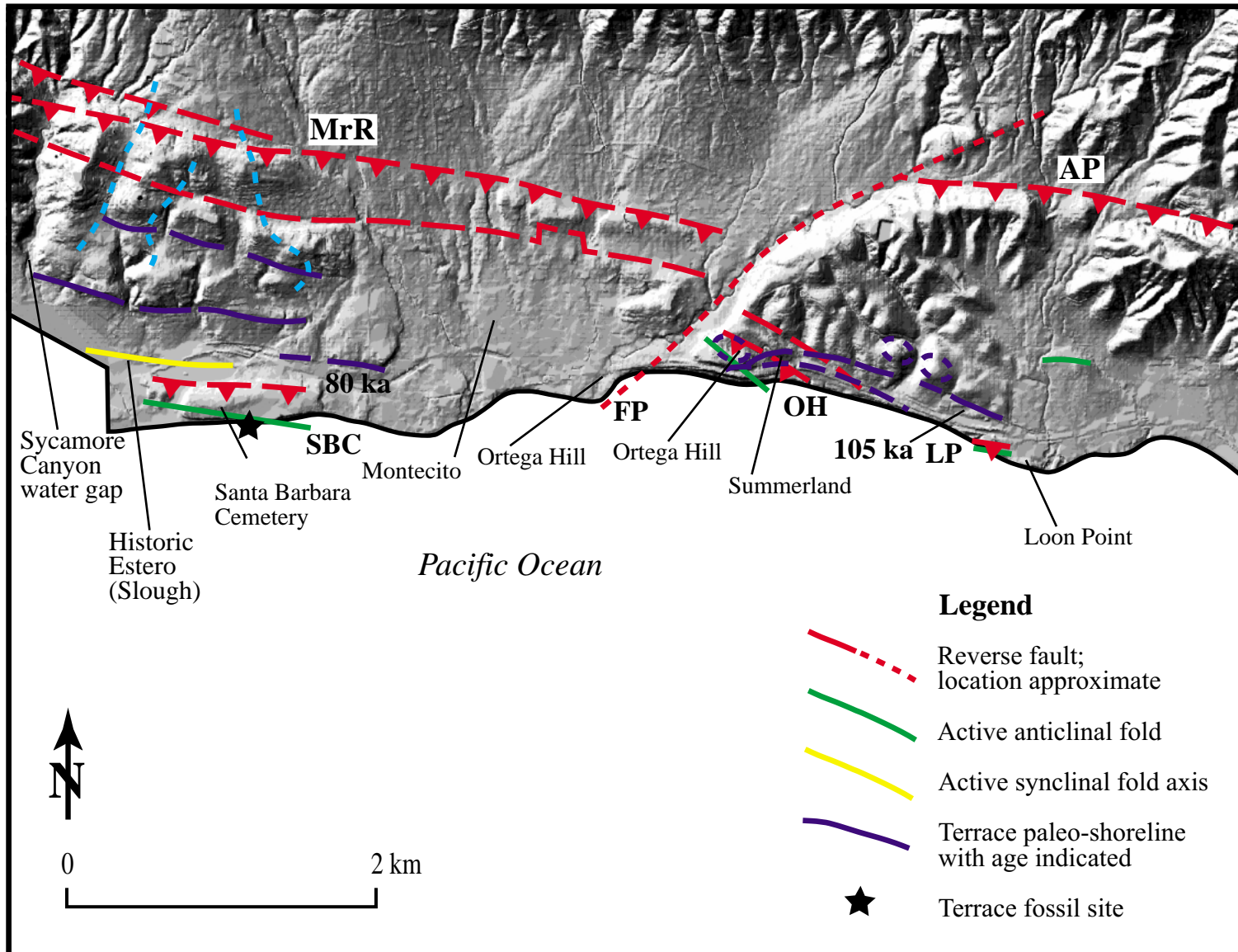


Figure 9. Geomorphic map of the eastern SBFB from Santa Barbara eastward to Summerland. Uplifted marine terraces and the associated paleo-shorelines are shown. The Mission Ridge (MrR), the Fernald Point (FP), the Arroyo Parida (AP), the Santa Barbara Cemetery (SBC), the Ortega Hill (OH), and the Loon Point (LP) faults are shown.

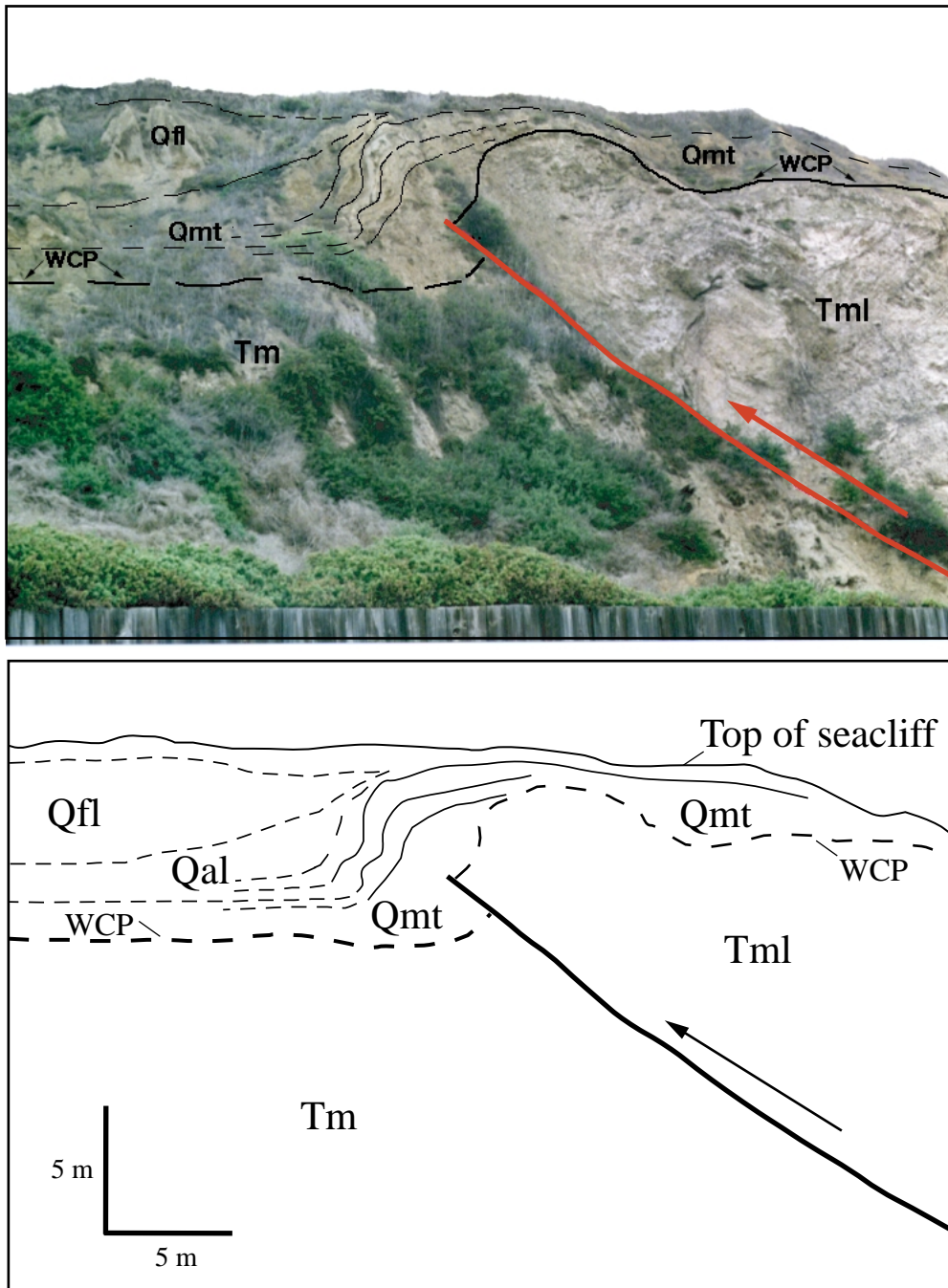


Figure 10. Photograph and sketch of the More Ranch fault seacliff exposure at Ellwood. The drape anticline folds Quaternary marine terrace (Qmt), alluvial (Qal) and fluvial (Qfl) sediments. The wave-cut platform (WCP) on top of Tertiary Monterey Formation (Tm and Tml-lower member) is vertically offset about 6 m.

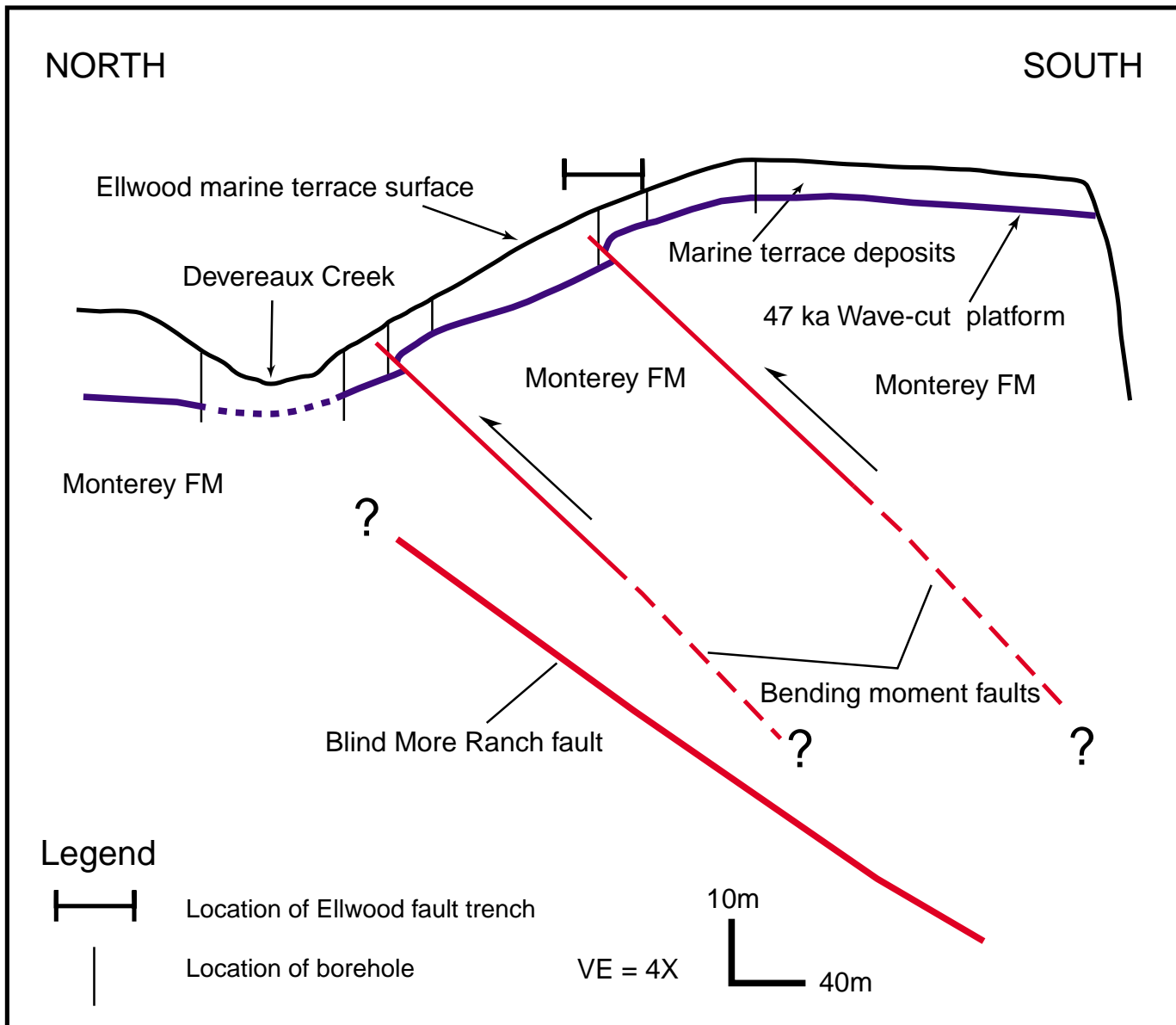


Figure 11. Subsurface profile of the Ellwood wave-cut platform and terrace based on shallow, continuous-core sampling of small-diameter boreholes and surface elevation surveys. The borehole data is supplemented with data from previous geotechnical and environmental excavations. The subsurface profile shows the relationship of bending moment faults to the blind trace of the More Ranch segment.

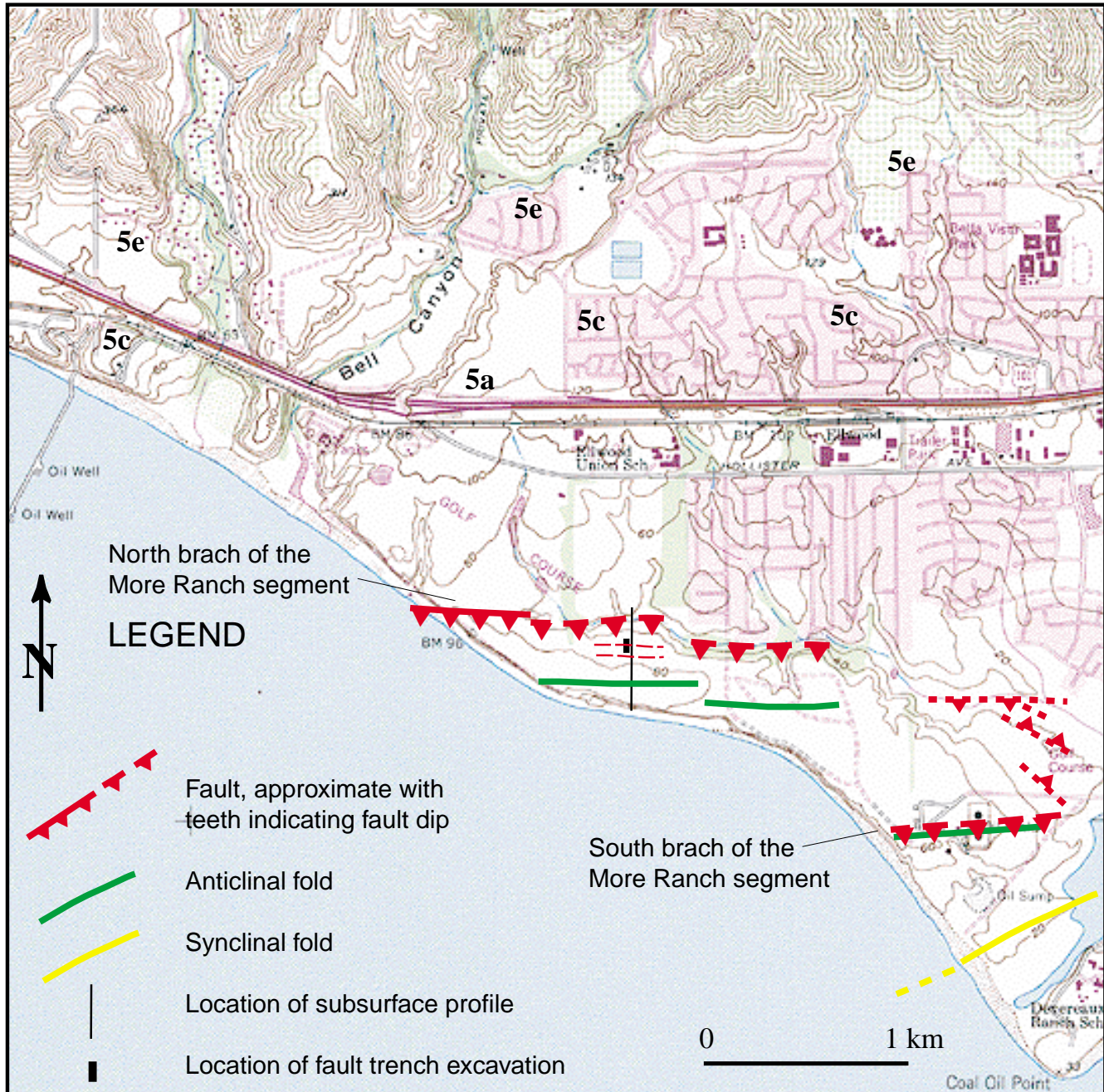


Figure 12. Map of the Ellwood Beach area showing the locations of the north and south branches of the More Ranch fault and location of fault trench. The north branch of the More Ranch fault is exposed at its western extent, however the fault is blind east of the sea cliff exposure and mapped based on the projection of the fault plane to the surface. A north-south profile (Figure 11) of the wave-cut platform and terrace is constructed across bending moments formed on the forelimb of the Ellwood anticline.

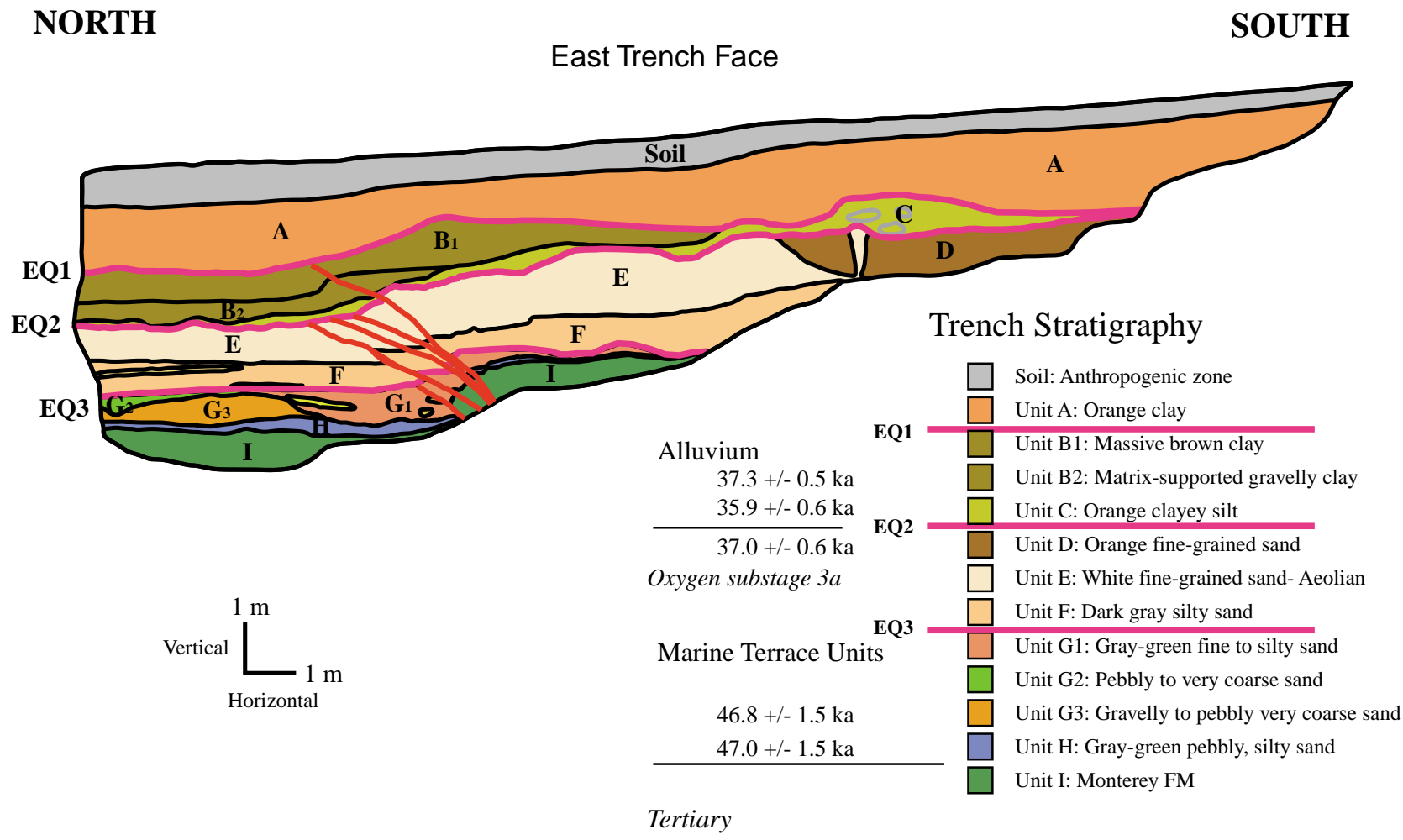
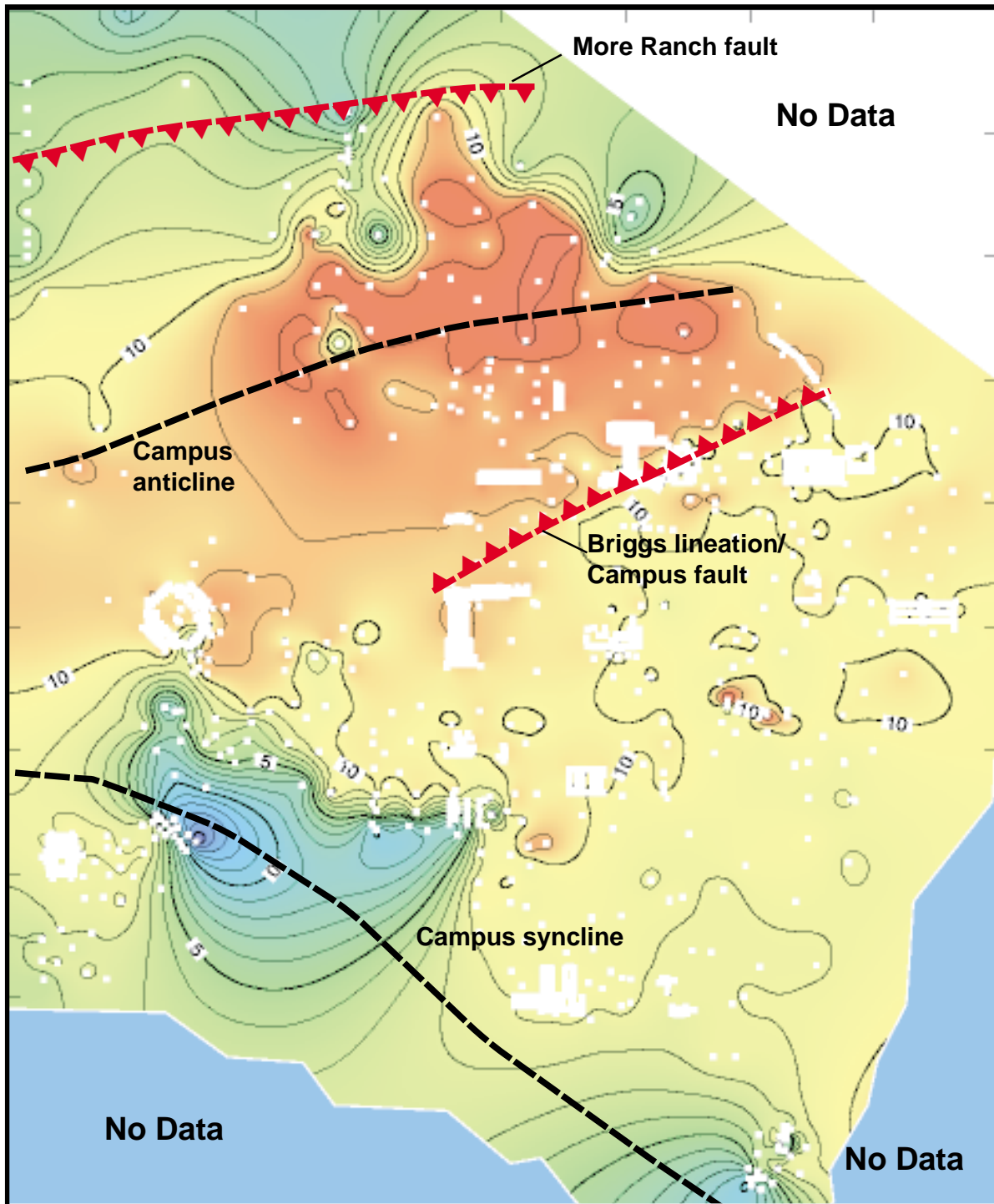
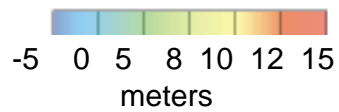


Figure 13. Trench log of the east trench face of the More Ranch fault folding and faulting oxygen isotope substage 3a marine terrace. The wave-cut platform (contact between units I and H) is vertically offset a total of approximately 1.2 m. The trench stratigraphy reveals three paleoearthquakes denoted EQ1, EQ2, and EQ3. EQ2 and EQ3 occurred approximately about 37 ka and between 47 ka and 37 ka respectively. The most recent earthquake (EQ1) occurred since 36 ka, however a minimum age of faulting has not been established.



Contour Interval = 1.0 meter



Horizontal Scale



Figure 14. Subsurface topographic map of the 45 ka UCSB marine platform showing fault and fold features related to the More Ranch segment. A south-facing scarp (Briggs lineation) is believed to have formed as the result of uplift due to a north-dipping fault termed the Campus fault.

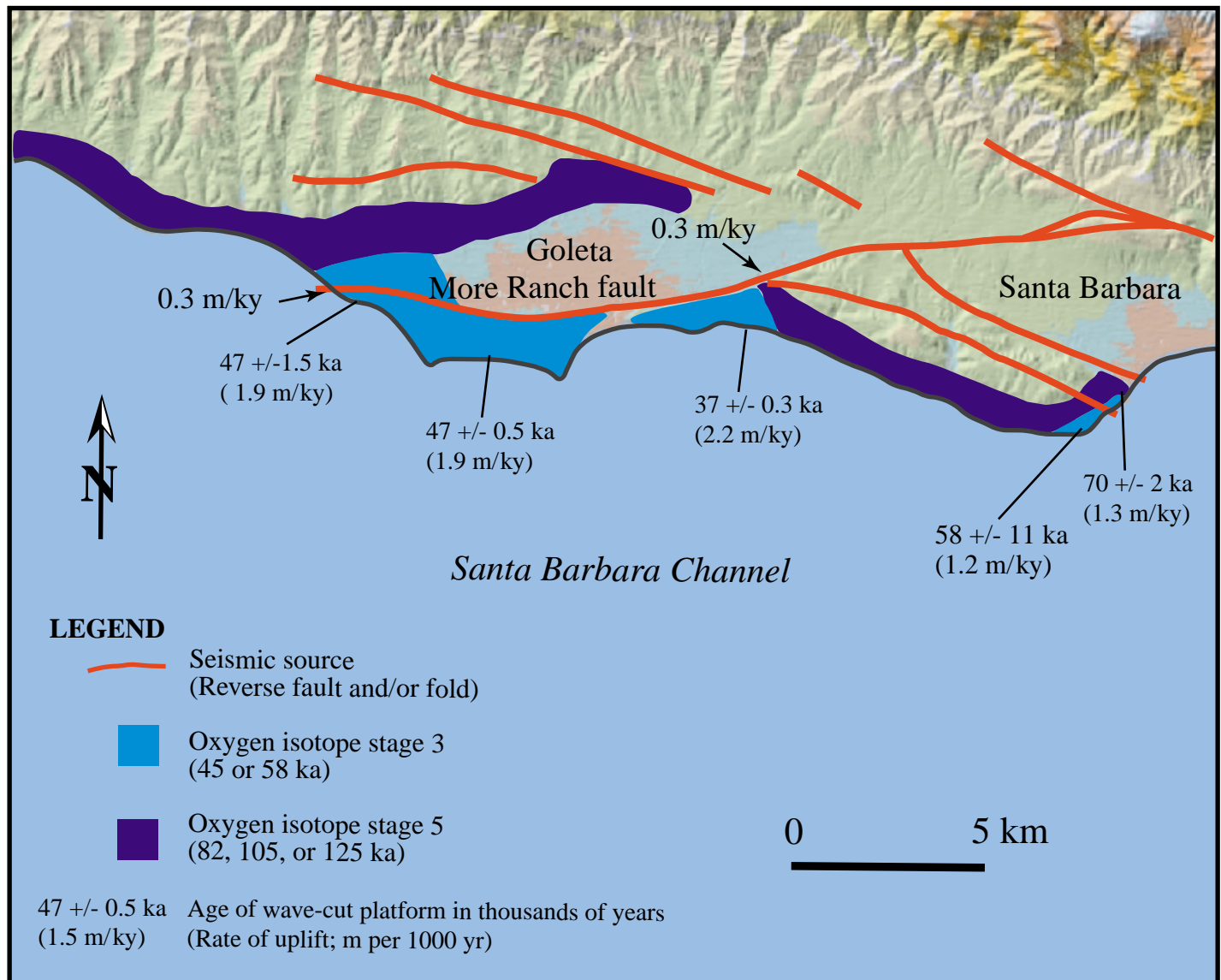
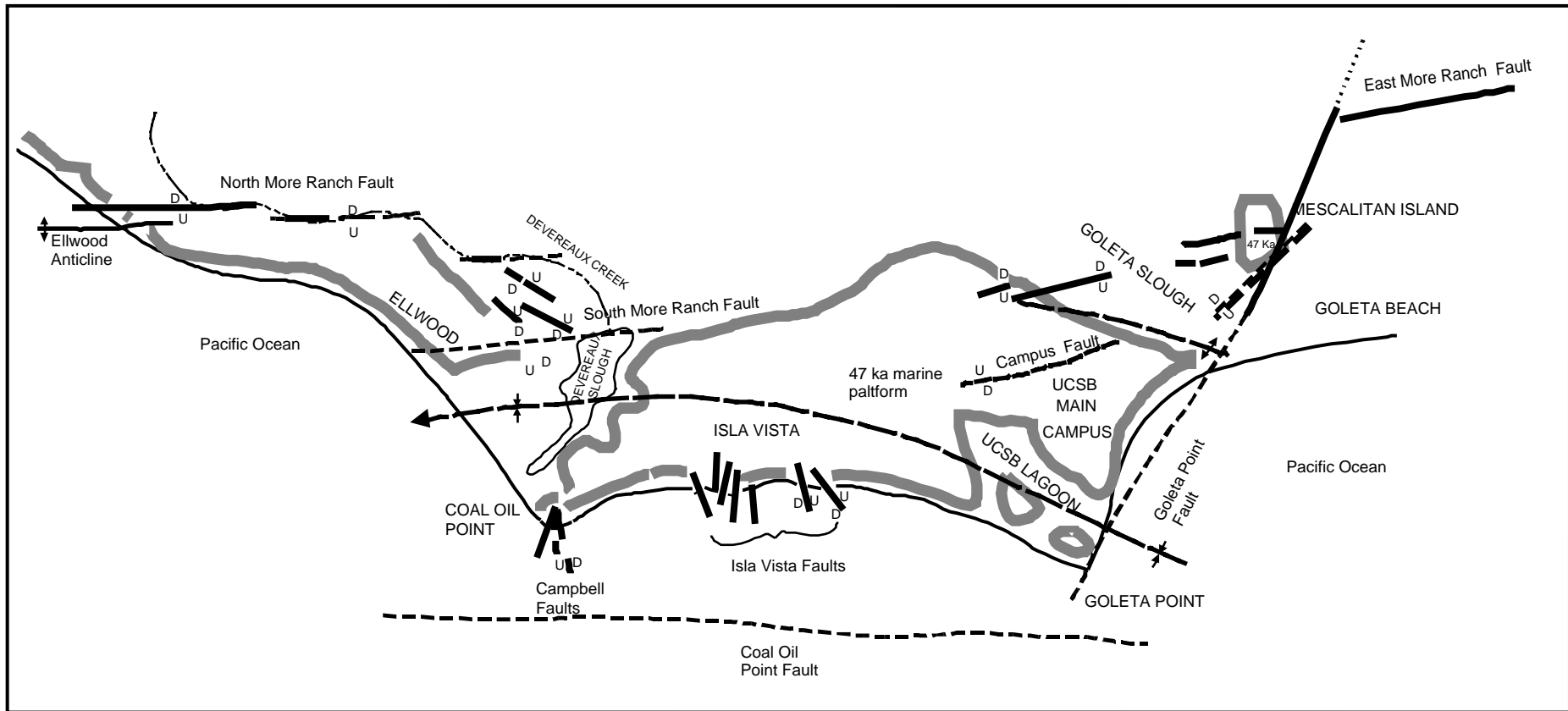


Figure 15. Late Pleistocene marine terraces of the western Santa Barbara Fold Belt. Uranium series ages of fossil terrace corals and radiocarbon ( $^{14}\text{C}$ ) ages of terrace charcoal and a fossil pholad sampled are shown. Vertical surface uplift rates are shown as are faulting rates for the More Ranch fault where oxygen isotope stages 3 and 5 are vertically displaced.



#### Symbols

- Fault:** Dashed where approximately located; showing relative sense of displacement and dip direction.
- Anticline:** Approximately located; showing direction of plunge.
- Syncline:** Approximately located; showing direction of plunge.
- Edge of elevated coastal mesa:** Shaded gray wavy line.

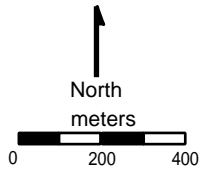


Figure 16. Local fault map and associated geomorphology of the UCSB campus area.

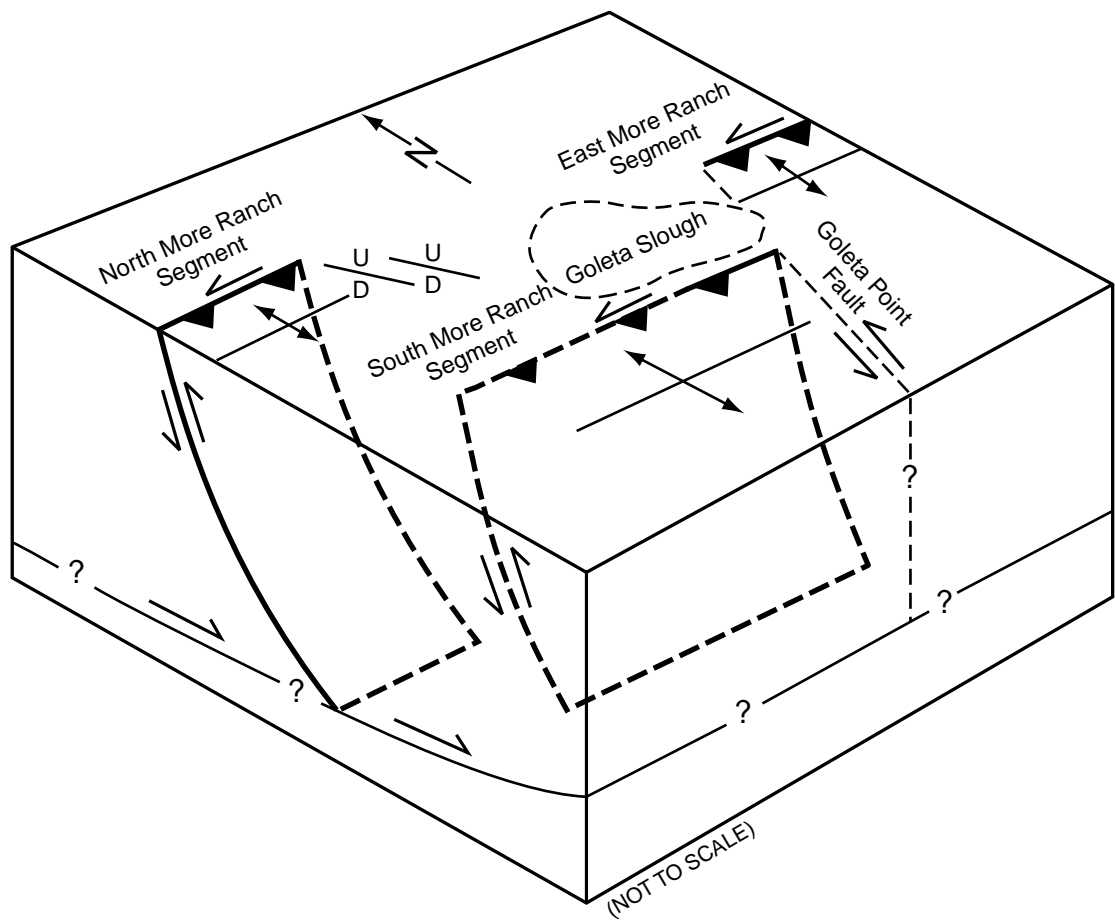


Figure 17. Tectonic geomorphology associated with oblique slip along the More Ranch segment and the relationship to northeast and northwest-striking cross faults.

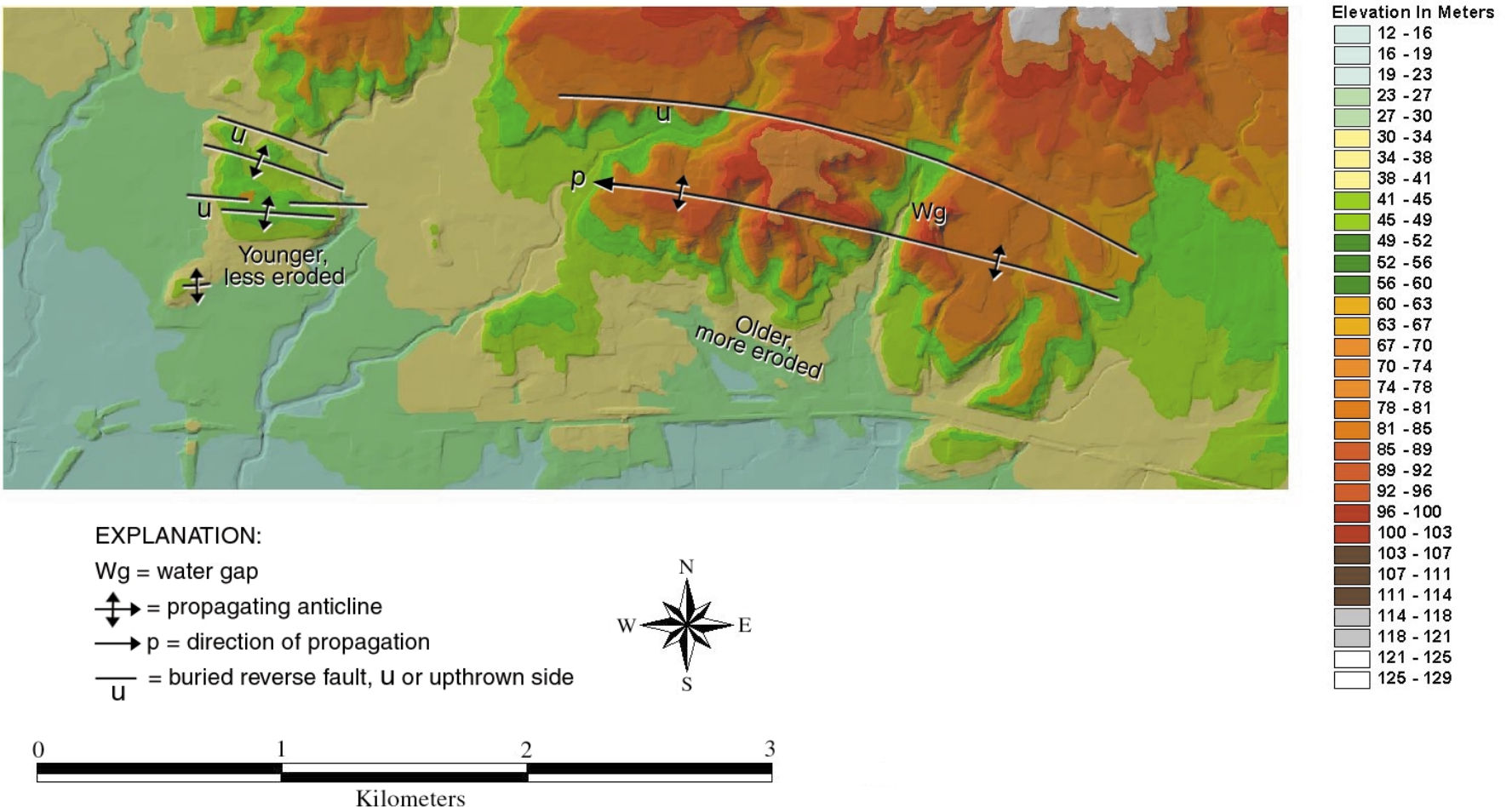


Figure 18. Image of the Goleta Valley anticline which apparently is propagating westward. Evidence for this includes the fact that the eastern portion of the fold is more eroded and probably represents older topography than the less eroded and presumably younger topography to the west.

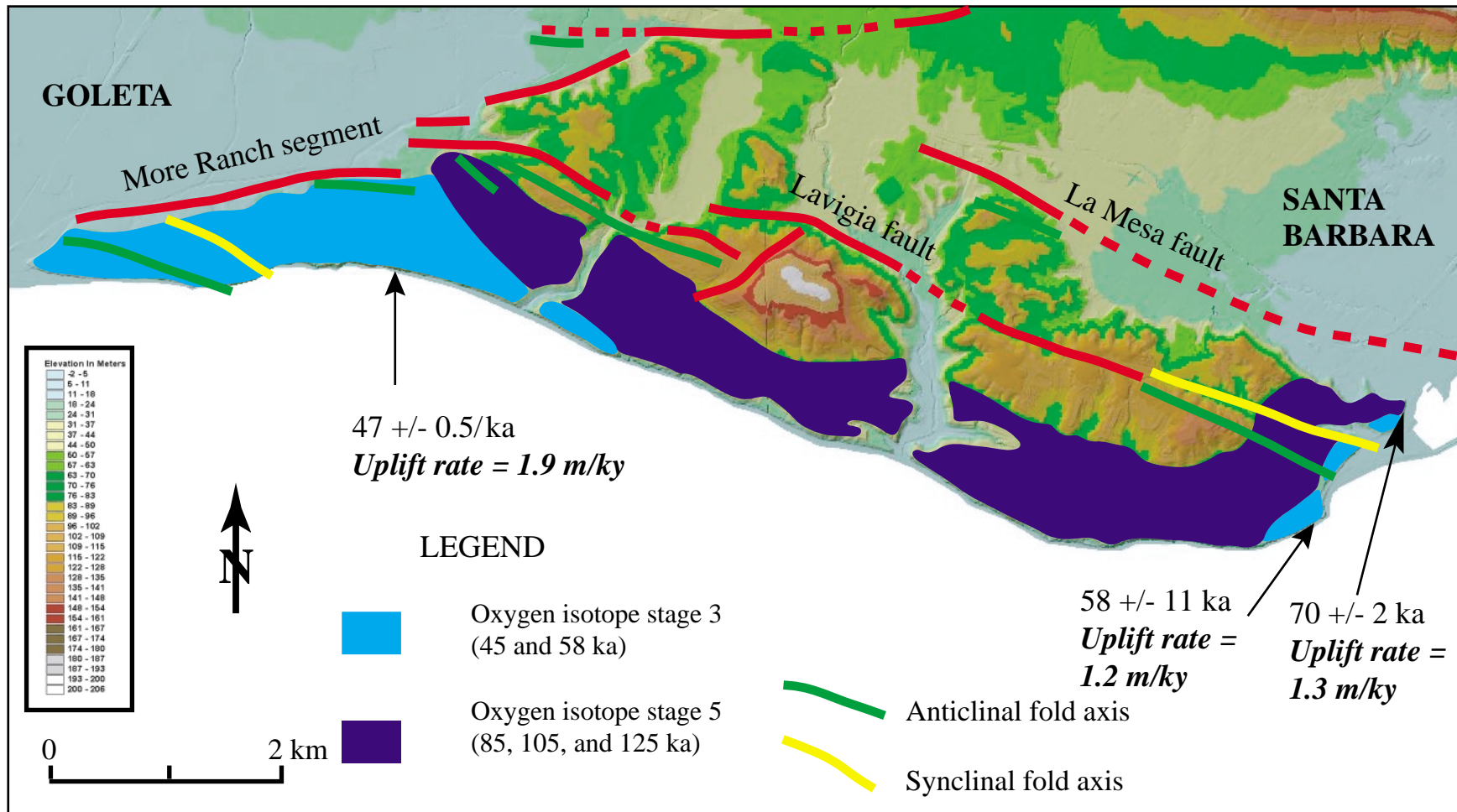


Figure 19. La Mesa to Hope Ranch area showing rates of surface uplift based upon first emergent marine platforms of oxygen-isotope stages 3 and 5.

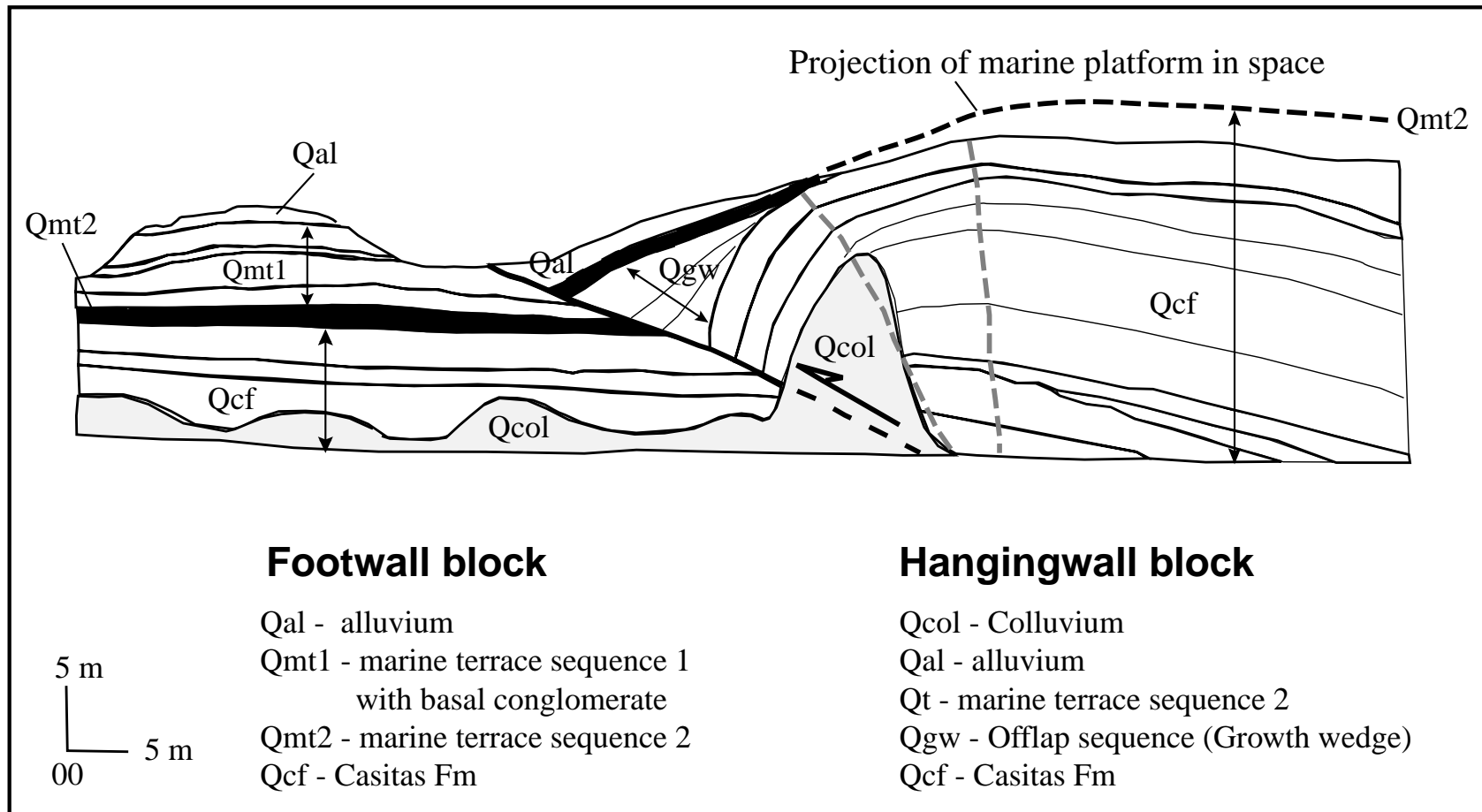


Figure 20. Quaternary stratigraphy of the seacliff exposure (oblique to the fault) of the Loon Point fault-propagation fold. Note the geometry of the growth wedge on the hanging wall fold and that overlying units are rotated into the fault to a lesser degree. Marine terrace sequence 2 projects into space (dashed line) as the result of folding and subsequent erosion. Active axial surfaces (gray dashed lines) are shown.

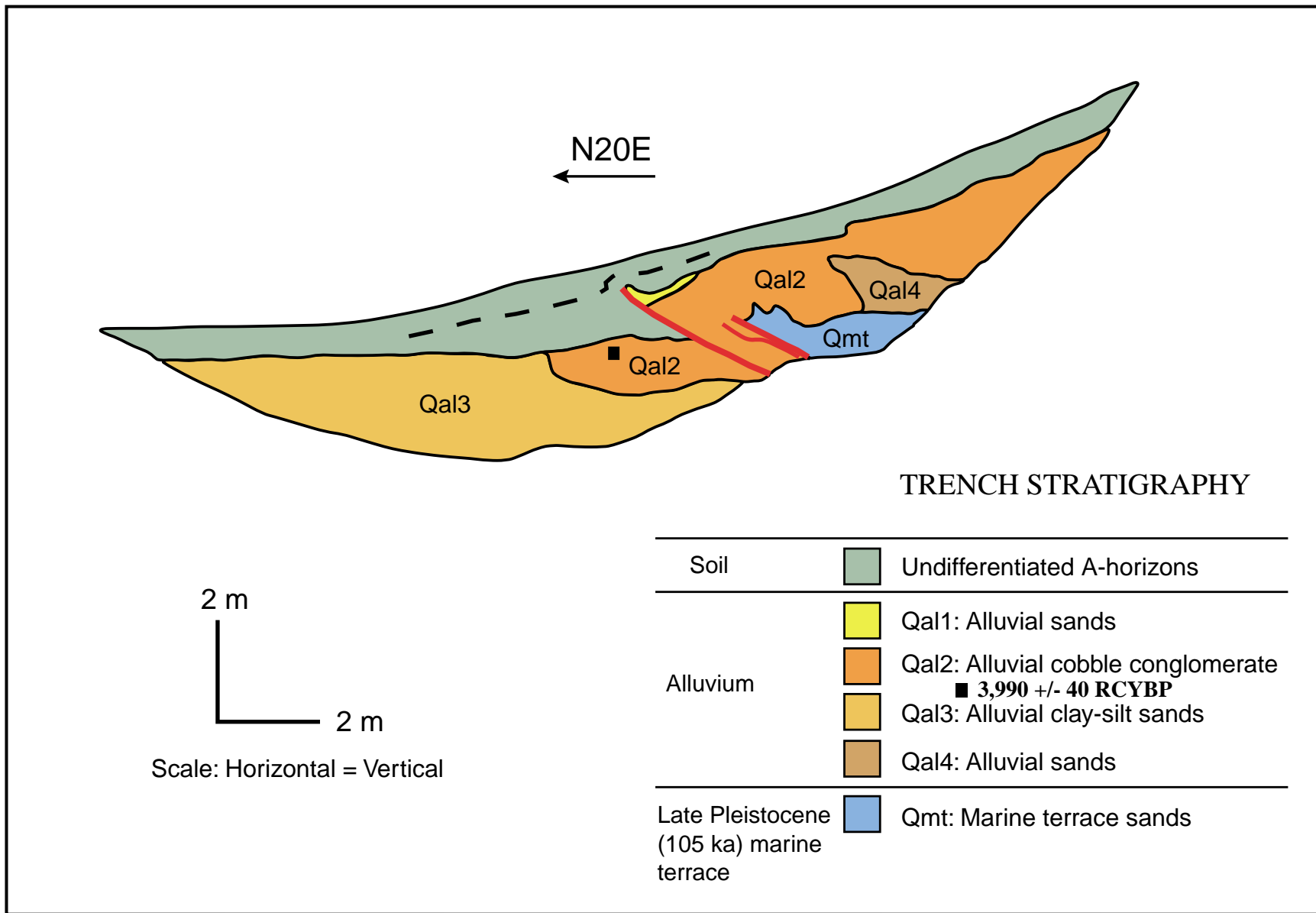


Figure 21. Log of the east trench face of the Loon Point fault, Summerland, California. The top of unit Qa12 is vertically displaced nearly 1 m and radiocarbon analysis of detrital charcoal yields a maximum 14C age of about 4 ka, therefore the fault is determined to be active.

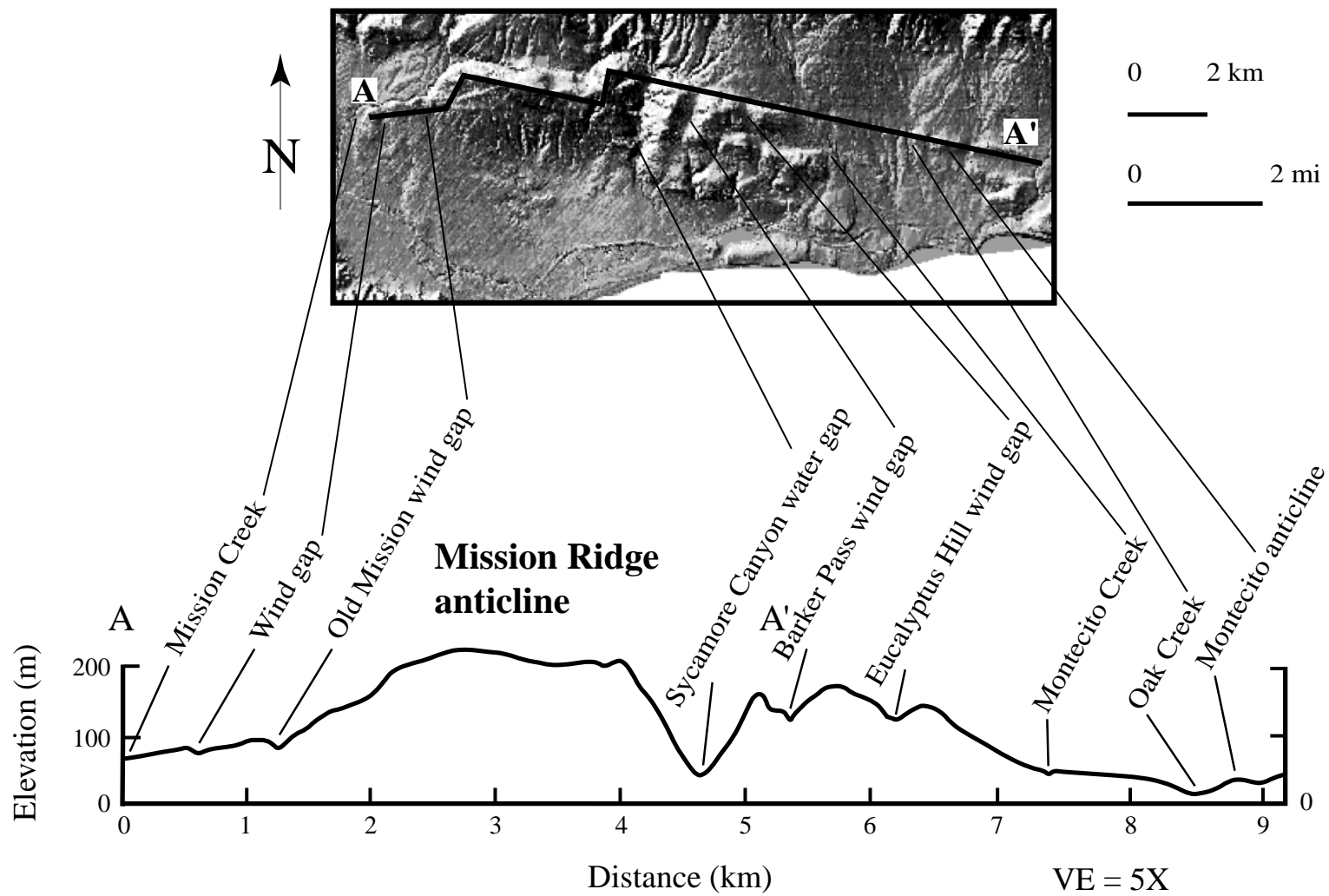


Figure 22. Longitudinal profile of the Mission Ridge anticline showing tectonic geomorphology from Santa Barbara to Montecito. Note the topographic expressions of water and wind (air) gaps as well as the decrease in elevation westward and eastward.

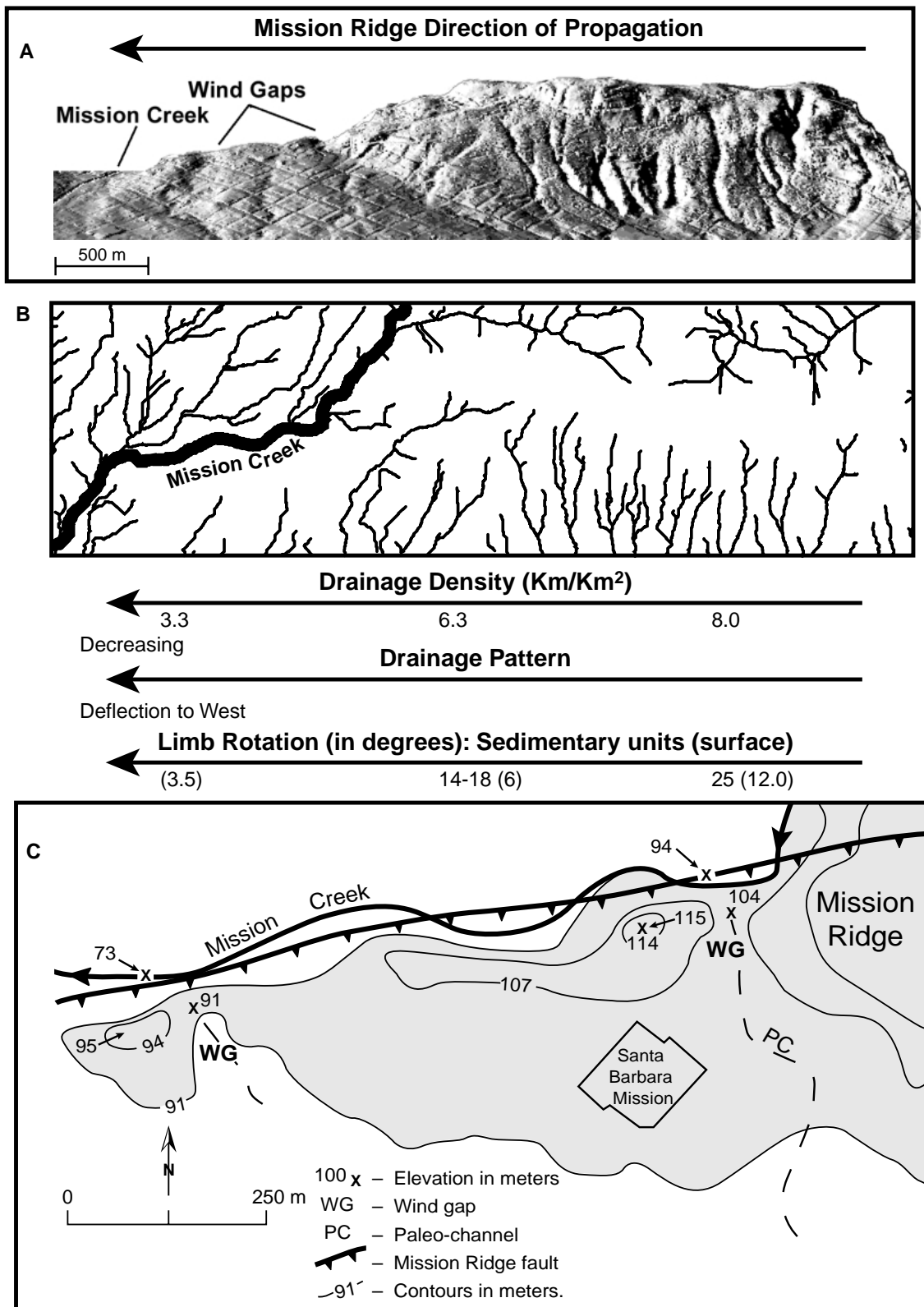


Figure 23. Diagrams of western Mission Ridge showing westward propagation of the Mission Ridge fold (Keller and others, 1999). The location of wind (air) gaps on the  $3 \text{ m}^2$  DEM is shown in A; decrease in drainage density, drainage pattern deflection to the west, and decrease of limb rotation to the west are shown on B; and decrease in wind gap elevations and the locations of associated paleochannels are shown on C.

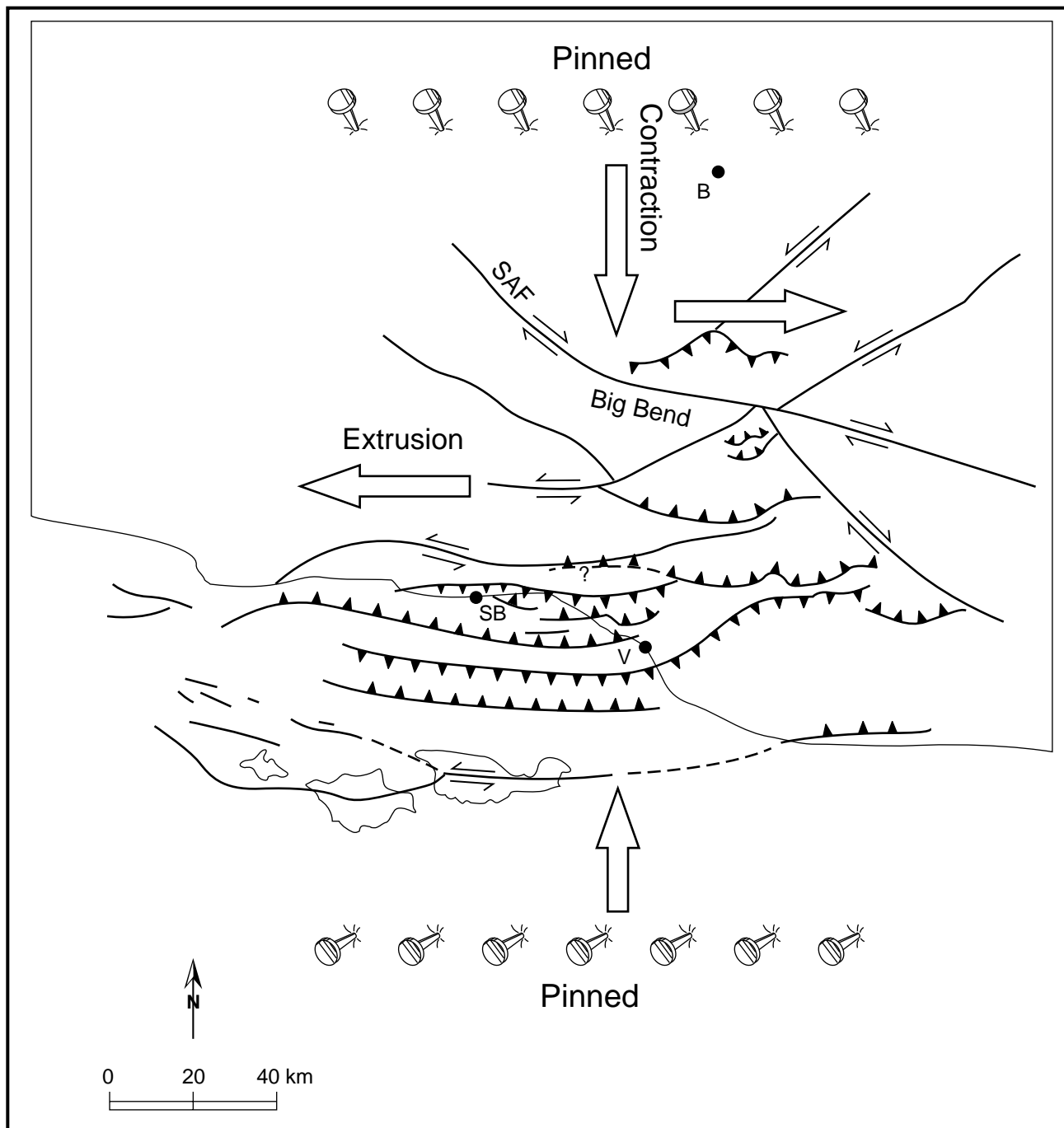
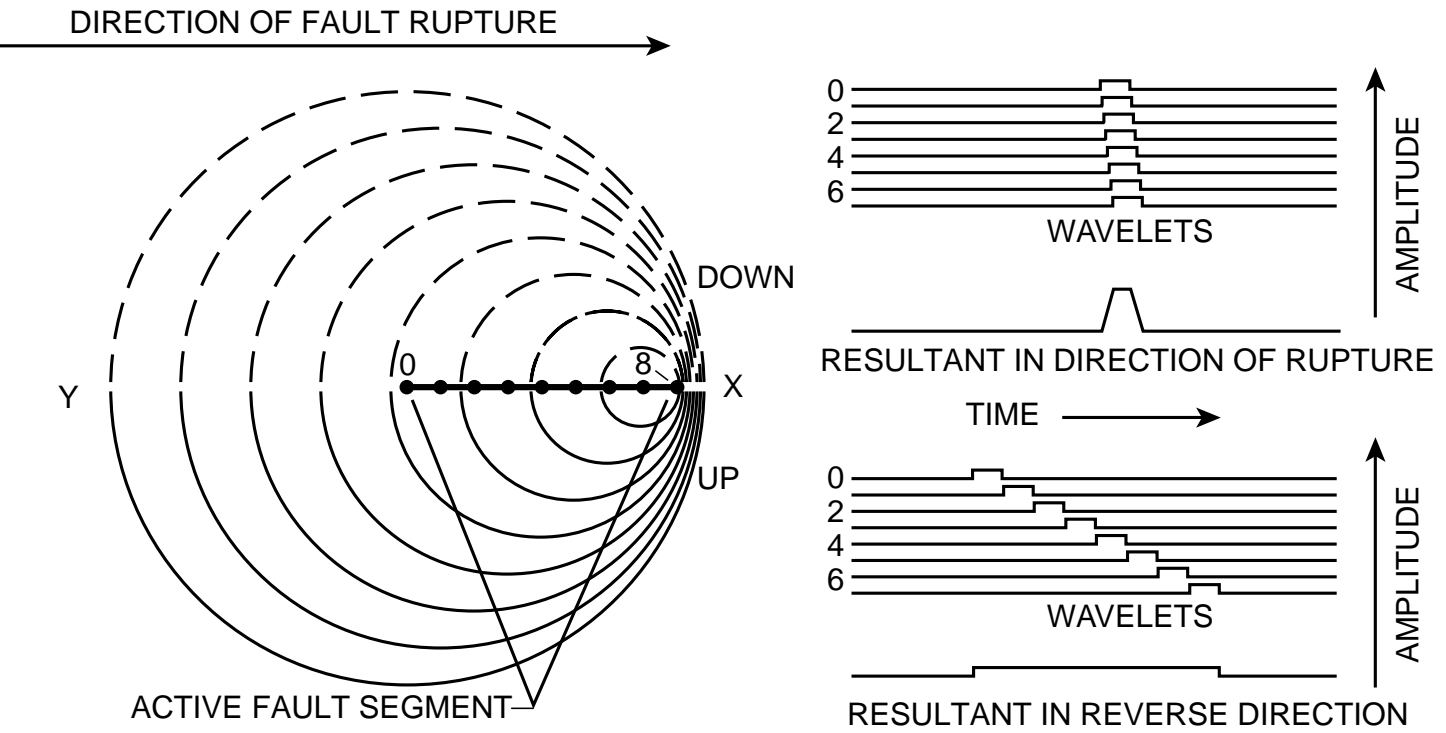


Figure 24. Tectonic model of westward extrusion south of the San Andreas Fault and eastward extrusion north of the San Andreas fault (Modified after Wallace, 1990). SB = Santa Barbara and V = Ventura.



*After H. Benioff, 1955*

Figure 25. Concept of directivity increasing the amplitude of seismic waves in the direction that a rupture propagates. After Benioff, 1955.